Zeolites: Structural Properties and Benchmarks of Feasibility

by

Colby Dawson

A Dissertation Presented in Partial Fulfillment
of the Requirements for the Degree
Doctor of Philosophy

Approved April 2013 by the
Graduate Supervisory Committee:

Michael Treacy, Chair
Michael O'Keeffe
Michael Thorpe
Peter Rez
Peter Bennett

ARIZONA STATE UNIVERSITY

May 2013

ABSTRACT

Zeolites are a class of microporous materials that are immensely useful as molecular sieves and catalysts. While there exist millions of hypothetical zeolite topologies, only 206 have been recognized to exist in nature, and the question remains: What distinguishes known zeolite topologies from their hypothetical counterparts? It has been found that *all* 206 of the known zeolites can be represented as networks of rigid perfect tetrahedra that hinge freely at the connected corners. The range of configurations over which the corresponding geometric constraints can be met has been termed the "flexibility window". Only a small percentage of hypothetical types exhibit a flexibility window, and it is thus proposed that this simple geometric property, the existence of a flexibility window, provides a reliable benchmark for distinguishing potentially realizable hypothetical structures from their infeasible counterparts. As a first approximation of the behavior of real zeolite materials, the flexibility window provides additional useful insights into structure and composition.

In this thesis, various methods for locating and exploring the flexibility window are discussed. Also examined is the assumption that the tetrahedral corners are force-free. This is a reasonable approximation in silicates for Si-O-Si angles above ~135°. However, the approximation is poor for germanates, where Ge-O-Ge angles are constrained to the range ~120°–145°. Lastly, a class of interesting low-density hypothetical zeolites is evaluated based on the feasibility criteria introduced.

ACKNOWLEDGMENTS

I'd like to thank the members of my committee, most of whom have collaborated directly on various parts of this work (Mike Thorpe on zeolite flexibility and feasibility, Peter Rez on the T-O-T angle calculation, and Mike O'Keeffe on the T-O-T angle calculation and double-layer silica zeolites). I've particularly enjoyed the weekly Netpicker's meetings with Mike O'Keeffe, which have been sometimes rumored to consist of at least as much storytelling and cashews/coffee/milk as science.

In addition, I'd like to thank the many people who have laid the groundwork for what is presented in this thesis, including Asel Sartbaeva and Stephen Wells who did pioneering work on the flexibility window in zeolites and developed the GASP program, Martin Foster who worked extensively on the development of the hypothetical zeolite database, and especially Vitaliy Kapko (developer of the ZeNuSpEx program, among other things) with whom I have worked closely for much of the duration of my PhD. Lastly, I'd like to thank my advisor Mike Treacy whose support, guidance, and example have been invaluable not only in my development as a scientist, but also as an individual. My years as a PhD student have truly been a pleasure, due in a large part to these many wonderful associations.

This work has been sponsored by National Science Foundation Grants No. DMR-0703973 and DMS-0714953.

TABLE OF CONTENTS

Page

CHAPTER Page

APPENDIX Page

LIST OF TABLES

LIST OF FIGURES

LIST OF SYMBOLS

Symbol Page

Chapter 1

INTRODUCTION

Zeolites are an important class of microporous tectosilicate materials used extensively in the petrochemical and fine-chemical industries as catalysts and molecular sieves. Related to quartz, the basic structural unit in zeolites is a TO_4 regular tetrahedron formed of a tetrahedrally-coordinated atom (i.e. a 'T-atom', often silicon) located at the center of four oxygen atoms, which form the vertices of the tetrahedron. The tetrahedra are corner-linked (sharing an oxygen atom) to form elaborate, frequently beautiful, periodic networks, usually displaying channels in one dimension or more (see, for example, Figure 1.1a). To be considered a zeolite, a material must be porous; that is, the channel openings must be large enough to allow reversible passage of water molecules through the framework. Each framework type is uniquely defined by the way the comprising tetrahedra are linked. Mathematically, the periodic linkage pattern, or *topology*, of a zeolite can be represented as a colored (or directed) graph. The graph uniquely defines the framework topology.

There are currently 206 zeolite topologies recognized to exist as real materials, and these will be referred to hereafter as *known framework types*. Each of the known framework types is assigned a boldface three-letter code, by the *Structure Commission* of the *International Zeolite Association* (IZA), that identifies the unique topology, but doesn't necessarily identify any specific material (though in several cases, the code is derived from the name of the first material found to exhibit the framework topology – known as the *type material*). In a database maintained by the (IZA), each known framework type is represented as a pure silicate in the highest symmetry in which it can

be realized as a regular tetrahedral-coordinated structure, using a simple distance least squares optimization procedure.[6] In practice, however, many diverse compositions are represented among the ~200 approved zeolite framework types. In fact, only about 20% of the known zeolite framework types (to date) have been synthesized as pure-silicates,[7] and a significant number have been synthesized with no silicon at all. Silicon atoms are often replaced by aluminum, germanium, phosphorous, or boron atoms (among others), which act chemically as tetrahedrally-coordinated substitute atoms. These substitutions have significant consequences for our simple geometric model as will be discussed later.

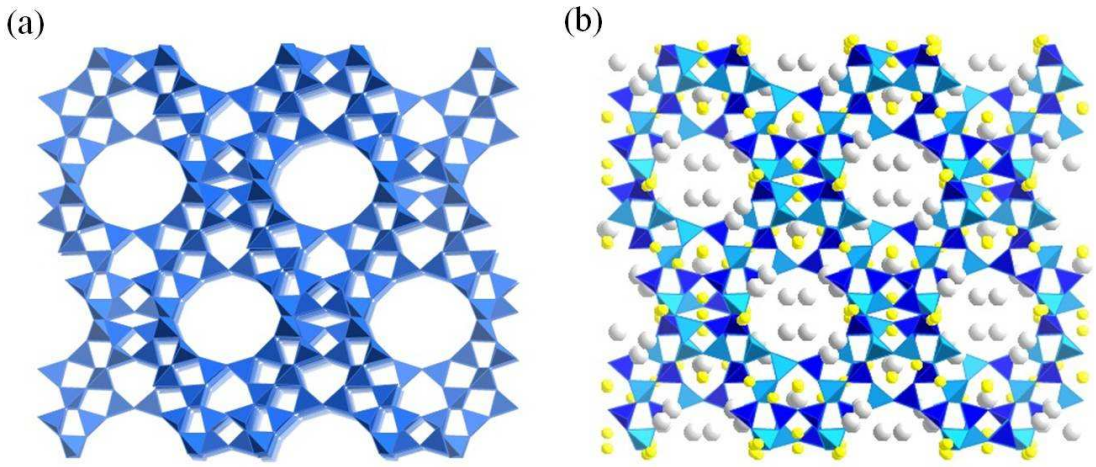

Figure 1.1: (a) An idealization of the zeolite framework **FAU** represented as a network of corner-connected tetrahedral units. (b) A representation of the material faujasite with both silicon (dark tetrahedra) and aluminum (light tetrahedra) tetrahedral atoms. Filling the channels are the extra-framework cations (small spheres), which balance the electronegative AlO_2 units, and water molecules (large spheres).

Many canonical zeolites exist as aluminosilicates, which are electronegative and require extra-framework cations to maintain charge neutrality. These cations are responsible for the catalytic and ion-exchanging properties for which zeolites are known.

When the charge-balancing cations are protons (H^+), zeolites exhibit Brønsted acidity (i.e. a proton-donor; a Lewis acid, such as sulfuric acid, is an electron acceptor). This Brønsted acidity plays an important role in hydrocarbon reforming, where large waxy hydrocarbons are 'cracked' by protons into smaller hydrocarbon chains, such as those found in gasoline. About 50% of the gasoline consumed in the US has been in contact with the zeolite faujasite (Figure 1.1b). The IZA 3-letter framework type code for the faujasite topology is **FAU** (Figure 1.1a).

Due to a wide range of applications and the relative abundance of silica, there is an ongoing search for useful, new zeolite materials. However, while millions of hypothetical zeolite structures have been enumerated,[8-11] only a small number of framework types are currently recognized to exist in nature.[6] The question remains: Why, given the enormous number of possibilities, does nature seem to prefer only a small subset of the mathematically-possible topologies?

The fundamental principles guiding zeolite nucleation and crystallization are not well understood, and the effort to synthesize new materials is still largely a heuristic process. Consequently, the possibility of systematic rational design of zeolites and other similar inorganic materials remains a distant goal. It becomes important to identify those characteristics of hypothetical structures that lead to synthetic feasibility, and several efforts have been made to develop benchmarks for sifting out unsuitable structures.[12-15]

Here we introduce the *ideal zeolite model* whereby zeolites are considered as comprising rigid, regular tetrahedra connected at the vertices by force-free spherical joints. When represented this way, all known zeolite framework types as well as all dense silicates studied thus far are flexible, meaning they can accommodate a wide range of

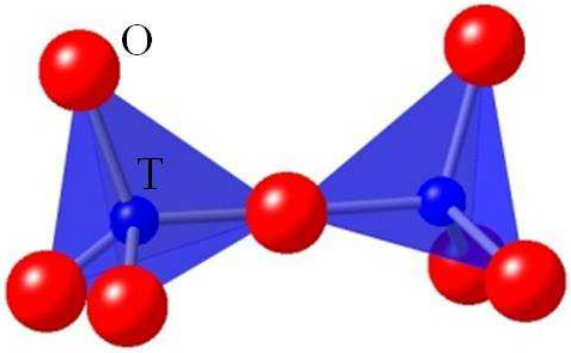

Figure 1.2: The T_2O_7 unit on which zeolites are based, with T-atoms (small spheres) at the tetrahedral centers and oxygen atoms (large spheres) at the vertices. In zeolite materials, the T-atom can be one of a number of elements, including silicon, aluminum, phosphorous, germanium, gallium, beryllium, boron, zinc, and others.

configurations over which the corner-connected tetrahedra remain structurally perfect, even as adjacent tetrahedra are allowed to flex and rotate relative to one another (Figure 1.2). The configuration space over which a framework type can be represented with perfectly regular tetrahedra has been termed the *flexibility window*,[16,17] and while it has long been known that some zeolites are flexible in the rigid tetrahedra representation, it has only recently been discovered that this property is universal for all of the realized framework types.

When represented as ideal structures, zeolites are *locally isostatic*, meaning that the local number of degrees of freedom is equal to the local number of constraints. However, an excess number of degrees of freedom arise due to symmetry. Essentially, symmetry imposes degenerate constraints, and reduces some degrees of freedom. However, more constraints are removed than are degrees of freedom, rendering the frameworks locally *hypo-static* (i.e. more degrees of freedom than constraints).

Additionally, for periodic structures at least three infinitesimal degrees of freedom are embedded in the unit cell parameters.[18] By infinitesimal, it is meant that even a rigid framework can distort by a small strain. In these modes, the strain energy in the framework grows (at the worst) as the third power of the strain, whereas in ordinary elastic systems the strain energy grows as the second power of the strain. Thus, small displacements induce negligible restoring forces, and if symmetry is maintained, constraints are rendered redundant, leading to framework floppiness (i.e. flexibility).[17,19] The flexibility window represents a special case where the rigid units (tetrahedra) are structurally perfect, and the large-amplitude cooperative motions of tetrahedra that give rise to the flexibility window are related to the rigid unit modes (RUMs) of Dove and colleagues,[20,21] which in turn are based on the floppy modes of Thorpe.[22] RUM theory has been used to describe displacive phase transitions in quartz and other dense silicates, where to a good approximation, alpha to beta transitions (and vice-versa) follow folding modes that preserve tetrahedrality.[23] Sartbaeva, Wells, and Gatta found that the flexibility window governs pressure induced phase transitions in various materials of the analcime framework **ANA**,[24,25] and framework flexibility has been linked to other properties in zeolites including pressure-induced amorphization,[26] adsorption,[27] and thermal expansion.[28,29]

For practical purposes, a framework type is considered "flexible" if it can be realized with (1) all O-T-O bond angles equal to 109.471±0.001°. Possible additional constraints include (2) uniform T-O bond lengths for each individual tetrahedral atom and (3) an effective oxygen radius of 1.32Å to prevent collisions between adjacent tetrahedra. Once these geometric constraints are met, flexible modes are guaranteed by periodicity,[18]

though these may be infinitesimal. For most zeolite frameworks, all T-O bond lengths can be made the same without any tetrahedral deformation (we typically use 1.610±0.001Å, the standard Si-O bond length in quartz), though a small number of known framework types (**CZP**, **GOO**, **ISV**, **ITR**, **IWS**, and **STW)** can be relaxed only with tetrahedra of varying sizes. In each of these cases, the substitution of tetrahedral sizes that results in relaxation directly reflects T-atom compositions in materials with this framework type. Each of these cases will be discussed later in more detail. One framework type (**RRO**) has such a narrow flexibility window that a small increase of the oxygen radius from 1.32Å to 1.335Å eliminates the window. The radius of 1.32Å is justified by noting that intratetrahedral oxygen distances are actually $\sqrt{\frac{8}{3}} \times 1.610\text{Å} = 2.629\text{Å}$ for perfectly regular SiO_4 tetrahedra. However, it is worthwhile to note that oxygen atoms are not really hard spheres, and so some latitude in the precise value for the radius is acceptable.

The most general flexibility calculations are performed in the triclinic *P*1 space group symmetry. This space group possesses only translation symmetry and no internal symmetries such as mirror planes and rotation axes, thus allowing maximum exploration of the flexibility window. However, the removal of symmetry doesn't necessarily ensure comprehensive sampling since the flexibility space also depends on the choice of cell, or supercell. Some framework types require cell doubling from the maximum symmetry representation to be relaxed with regular tetrahedra. The reason is that such cell-doubling removes some of the translation-symmetry constraints, potentially increasing the excess of degrees of freedom over constraints.

As is observed in several known zeolite frameworks, variable tetrahedral size offers an additional degree of freedom that leads to flexibility in some framework types that cannot be relaxed with uniformly sized tetrahedra. A physical connection can be made by noting variations in tetrahedral size based on the comprising T-atom and its average T-O bond distance. As an example, the preferred Al-O bond length is approximately 1.735Å, compared to the Si-O bond length of 1.610Å noted earlier, thus leading to larger tetrahedra. In practice, substituting different types of T-atoms for silicon leads to a new set of geometric constraints that must be satisfied within the flexibility window. However, the location of such tetrahedra provides additional degrees of freedom which, on occasion, introduce flexibility that is not possible in a pure silicate.

From a physical perspective, there is a possibility that in some cases the criteria for declaring a framework type flexible are overly strict since real materials tend to tolerate small strains within the tetrahedra. At least two framework types that have been reported in pure-silica composition (**ISV** [30] and **STW** [31]) cannot be relaxed without substituting some larger tetrahedra, and it is possible that guest-host interactions can sometimes stabilize small tetrahedral deformations. Nevertheless, in the case of **ISV**, Sastre and Corma reported that the addition of germanium sped up the synthesis by about a factor of ten.[5] While some cases have been found where a framework type couldn't be perfectly relaxed in one of its realized material compositions, no case has been found where the tetrahedra can't be brought to be almost regular. It is possible that a further distinction of "quasi-flexible" is necessary to take into account the cases where the tetrahedra don't quite meet the strict flexibility criteria, but are still regular within a small margin of error.

Many zeolite materials include two or more types of T-atoms, and in the majority of cases studied thus far, frameworks can be made to have perfectly regular tetrahedra when T-O bond lengths reflect realized material compositions. It is conjectured that framework types that can accommodate a wide range of tetrahedral sizes are more likely to be synthesized in diverse compositions, and preliminary attempts to quantify and compare the adaptability of different framework types validate this hypothesis.

The flexibility model can provide possible insight into the sites occupied by various T-atoms in frameworks where this information has not been experimentally determined, i.e. frameworks will be able to be relaxed when the T-atoms (and corresponding T-O constraints) reflect realizable compositions. In addition, the flexibility model may allow prediction of the chemical composition necessary for the synthesis of potentially interesting hypothetical frameworks.

Though in *P*1 space group symmetry there are usually an enormous number of possible T-atom combinations to explore, the application of symmetry allows a more tractable search. For aluminosilicates, Löwenstein's rule - that no two aluminum atoms can occupy adjacent tetrahedral sites [32] - also helps to significantly reduce the number of possibilities. For a given framework type, an initial search would involve substituting aluminum or germanium atoms at each of the symmetry related T-sites, and relaxed configurations were found for three known framework types (**ISV**, **ITR**, and **STW**) by this simple method. If searching over a set of hypothetical structures, this approach would be feasible, provided each structure does not have a large number of unique T-atoms.

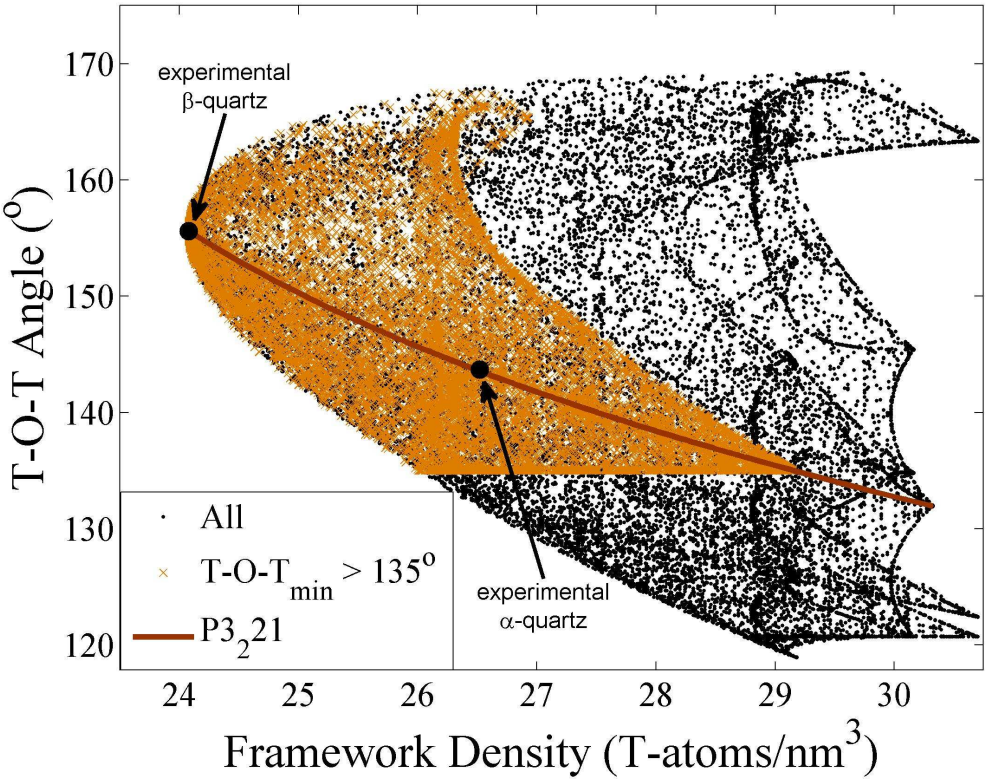

Figure 1.3: Points representing all the T-O-T angles available at each density for quartz structures found in the flexibility window in *P1* (dark points), obtained by random sampling within the window. The light points represent the subset of structures with a minimum T-O-T angle greater than 135º (close to the minimum value allowed in SiO_2). The curve is for structures with *$P3_221$* symmetry retained. In this case, symmetry dictates that all T-O-T angles have the same value. For experimental α-quartz (room temperature), this value is 143.7º,[2] whereas for experimental β-quartz (high temperature), it is 153.0º.[4] The various cusps observed at high density reflect that the structure can follow a number of folding paths to higher density with the densest configurations forming the outer edges of the window.

A simple one-dimensional measure of a framework's flexibility is the *flexibility index*, which is the ratio of the maximum and minimum densities at which the framework can be relaxed with regular tetrahedra. This measure was tabulated for all known zeolites by Kapko et. al.,[17] though ensuing efforts have discovered a wider range of relaxed

configurations for many framework types. While the flexibility index represents an important first step to quantify the flexibility window, additional measures are necessary to fully represent the rich flexibility behavior of many framework types. By placing constraints on the unit cell parameters or allowed T-O-T angles, it is possible to display a two-dimensional subspace of the flexibility window (Figure 1.3). However, any such representation is necessarily limited, and we continue to develop better methods to quantify and compare the flexibility of different framework types. So far, the greatest link to feasibility appears to be whether or not a framework type can be realized with regular tetrahedra in the first place, rather than the extent of its flexibility window. As an example, the most stable phase of silica is quartz, which has a smaller flexibility window than cristobalite, the next highest energy phase.

Several methods have been used to explore the flexibility window, each based on a slightly different mechanical model. In the case of the GASP (*Geometric Analysis of Structural Polyhedra*) method developed by Wells et. al.,[33] TO_4 units are considered as rigid tetrahedral templates with oxygen atoms connected at the vertices by springs of zero natural length. GASP attempts to locate and explore the flexibility window by incrementally varying unit cell parameters, thereby adjusting cell volume and density, and using the fractional coordinates of the previously-obtained relaxed configuration as an initial guess. The oxygen atoms are then randomly displaced from their initial positions and each tetrahedral template is placed at the geometric center of the four corresponding oxygen atoms. The positions of the atoms and the template are then refined until conditions for relaxation are met (i.e. all O-T-O angles are 109.471±0.001°, all T-O bonds are the prescribed length, and there are no oxygen collisions), or the

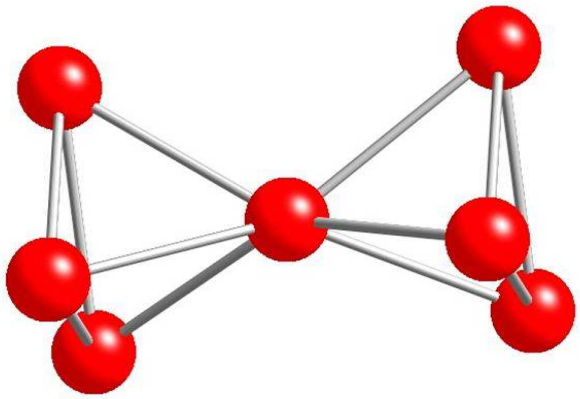

Figure 1.4: The oxygen-only representation of zeolite tetrahedra as used in the ZeNuSpEx method. In this model, distance constraints between oxygen atoms enforce tetrahedral regularity, and the T-atom is implied at the geometric center of the four oxygen atoms forming the tetrahedral vertices.

minimization algorithm fails. This process is repeated numerous times at each given density to determine whether relaxed configurations can be found for a specific set of unit cell parameters. The GASP approach was used to explore the flexibility space of many of the 206 known zeolite framework types,[17] and the GASP computational tool remains the final step in the refinement of relaxed configurations.

The second method of exploring the flexibility window involves following folding paths of zero tetrahedral strain through the flexibility window. This approach was incorporated into the *Zeolite Null Space Explorer* (ZeNuSpEx) program developed by Kapko et. al.[17,34] which models zeolites as frameworks of oxygen atoms at tetrahedral vertices, separated by distance constraints that enforce tetrahedrality (Figure 1.4). Interestingly, when zeolites are considered as oxygen-only frameworks, the oxygen atoms are six-coordinated (octahedral). Silicon atoms are implied as residing at the geometric center of the four oxygen atoms to which they are bonded, but are not a

necessary component of this physical model. Harmonic terms are applied to enforce distance constraints between intratetrahedral oxygen atoms, and relaxed configurations within the flexibility window are found when the sum of these terms is zero. As in the first model, hard sphere constraints prevent oxygen collisions.

ZeNuSpEx is based on a mathematical formulation developed in the field of mechanical engineering for the study of deployable truss systems and involves use of the compatibility matrix **C** [18,35,36] which relates generalized atom displacements (represented by the vector **d**) to elongation of distance constraints between atoms (represented by the vector **e**) by the eigenvalue equation

$$\mathbf{Cd} = \mathbf{e}.$$

Null vectors of the compatibility matrix correspond to stress-free folding modes within the flexibility window. Gram-Schmidt orthonormalization is necessary to ensure that all null vectors (the flexible folding modes) are linearly independent and orthogonal. Any linear combination of null modes then represents a distinct folding path through the flexibility window. To follow a folding path, null vectors are added (with small amplitude) to the atom coordinates, thus representing a first order approximation of a finite fold through the window. A relaxation step is required to remove second order tetrahedral deformations. The process is then repeated with the new, relaxed configuration as the starting point. When adding the null vector results in a configuration that cannot be relaxed, the process is abandoned. Thus, one can find continuous folding paths through the flexibility window, though not all null vectors correspond to finite modes, since infinitesimal modes are also possible.

When moving to supercells (thus reducing periodicity constraints), we find that the number of folding modes almost always increases. For a certain class of known framework types, this proliferation of flexible modes grows linearly with the volume of the supercell. For others, the number of flexible modes increases in proportion to the surface of the supercell, and still others gain flexible modes as the cell edges are elongated. Although these surface and edge mechanisms are not extensive (i.e their number does not grow linearly with system size), it is conjectured that they are likely important during the nucleation phase of zeolite synthesis, when kinetic effects dominate, and when nuclei are mostly surfaces anyway.[34]

The fact that known zeolite framework types all share the flexibility property allows for striking comparisons with sets of hypothetical zeolites. A recent query of the database of Treacy et. al.[8] found that only about 10% of low-energy hypothetical zeolites were flexible compared to 80% of known zeolites found therein.[37] While the simple flexibility calculation used to search the database left some territory unexplored, it demonstrated that flexibility is an effective filtering criterion for evaluating the feasibility of hypothetical framework types. This study will be discussed later in greater detail.

The last 30 years have seen the development of a number of empirical interatomic potentials used to model silica.[38-40] One example is the Sanders-Leslie-Catlow (SLC) potential,[41,42] which has successfully reproduced energy orderings in silica polymorphs,[43] and low SLC energies have been shown to correlate strongly with framework feasibility in high-silica materials.[14,37] Due to its simplicity and relative accuracy, this potential form has also proven useful in calculations on large databases of hypothetical structures.[8,10] A detailed accounting of the SLC potential is found in Appendix A.

The main limitation of the SLC model is that it can only be considered accurate in evaluating the framework energy for pure-silica compositions. As a result, feasibility comparisons based on SLC energy alone are likely to fail in detecting structures that can be realized only in mixed compositions, or non-silica compositions, and there are several examples of realized zeolite framework types with high SLC energy. Since real zeolite materials are usually made up of varied tetrahedral atoms, often with accompanying extra-framework cations and an entourage of water molecules (all of which contribute significantly to the framework energy), the SLC potential is of limited utility when evaluating and comparing many zeolite materials in their naturally occurring compositions. The flexibility criterion is thus proposed as a universal tool for evaluating the feasibility of hypothetical zeolite frameworks, independent of an accurately-computed framework energy. In fact, regardless of chemical composition, flexibility confers an energetic advantage in that flexible framework types are more likely to be able to access low-energy configurations that optimally balance framework electrostatics and T-O-T angle preferences, without being subject to the high-energy penalties that come with deforming the framework tetrahedra.

A central conjecture of this work can thus be stated as:

Flexibility = Feasibility.

Based on empirical evidence, that *all* of the known zeolite frameworks exhibit a flexibility window, we believe that we have resolved the so-called “zeolite conundrum” – why are there so many hypothetical frameworks, but so few realized frameworks? It is because many low energy hypothetical frameworks lack flexibility.

In real materials, T-O-T angle preferences place an additional constraint on the flexibility window. For example, in silicates and aluminosilicates the T-O-T angles tend to be greater than about 135º,[44] whereas the angles in germanates can range from about 120-145°.[3,5] Studies of the energy dependence of the T-O-T angle (discussed later) demonstrate that silicates have a much wider available range of T-O-T angles than do germanates, and this versatility provides some physical justification for the ideal zeolite model where T-O-T angle preferences are ignored. This also might help explain why there exist many more silicates than germanates. By examining the range of T-O-T angles available within the flexibility window, it may be possible to gain additional insight into the compositions available for a given framework type. Framework types that can occupy a wide range of T-O-T distributions likely exhibit enhanced realizability in a wider range of material compositions.

There is a continuing effort to synthesize new zeolite materials with ever-increasing pore size and decreasing density. Nevertheless, to date, most of the lowest density zeolites have been characterized by exotic compositions, leading to limited industrial potential. Indeed, no one has yet synthesized an industrially scalable, high-silica material that rivals the most prodigiously useful zeolite faujasite (framework type code **FAU**) in terms of accessible volume, pore size, and thermal stability.[45]

Possible zeolite frameworks of arbitrarily low density were suggested earlier by Smith and Dytrych and in fact their structures had pores lined by silica double layers although they did not use this description.[1] Even earlier, Barrer and Villiger introduced a hypothetical structure, with large 24-ring channels, as a possible candidate for the 12-ring-channel zeolite L structure.[46] Its channel walls had a bi-layer structure, but they did

not comment on the fact that it was one member of a structural family of arbitrarily low-density zeolite structures.

Families of low-density hypothetical zeolites have been identified based on double-layer silica sheets. The sheets form the pore walls in these *double-layer silicate* (DLS) zeolites and can be extended to form structures with arbitrarily low density and arbitrarily large pore size, even competing favorably with metal-organic framework (MOF) materials. Several such members of the infinite families of DLS zeolite frameworks are in the *Atlas of Prospective Zeolite Structures* (APZS) [47] and were examined previously by Zwijnenburg and Bell.[48] A number of these families have been explored and it has been found that many of them have low framework energy and exhibit extensive flexibility. This leads to the conjecture that DLS zeolites are synthetically feasible, and recent reports of experimentally observed double-layer silica sheets [49-51] bring us ever closer to the possibility that these materials will someday be synthesized.

This thesis is primarily concerned with the flexibility of zeolites. Chapters 2 and 3 describe the methods that were used, and developed, to locate and explore the flexibility window of zeolite frameworks. In chapter 4, framework flexibility is used to identify potentially feasible hypothetical zeolite frameworks from a large sample set. Chapter 5 details a study of the energy dependence of the T-O-T angle in silicates and germanates, and chapter 6 describes the evaluation of hypothetical DLS zeolites based on the feasibility criteria proposed.

Chapter 2

FINDING THE FLEXIBILITY WINDOW

The procedure for finding initial relaxed configurations within the flexibility window involves several steps, the series of which may vary between framework types. This chapter will focus on the most advanced methods for relaxing structures with perfect tetrahedra, as well as specific cases where the flexibility model provides insight into the structure of real zeolite materials

The ideal zeolite cost function

A general first approach to finding relaxed configurations is an optimization in the *General Utility Lattice Program* (GULP)[30] using the *ideal zeolite cost function*, which imposes large energy penalties for even small deviations from perfectly regular TO_4 tetrahedra. Harmonic terms are included between bonded atoms, with a natural spring length corresponding to the appropriate T-O bond distance (in Ångstroms) and a harmonic constant of 100.0 eV/Å^2. An additional harmonic term enforces O-T-O bond angles of 109.471° with a harmonic constant of 100.0 eV/ rad^2. Overlaps between intertetrahedral oxygen atoms are penalized by a harmonic term (with harmonic constant of 1000.0 eV/Å^2) that is activated at the onset of steric clashes (i.e. oxygen atoms overlapping). The cost function can thus be expressed as

$$U_{ideal} = \sum_{All\ TO} \frac{1}{2} k_1 (L - L_0)^2 + \sum_{All\ \angle OTO} \frac{1}{2} k_2 (\theta - \theta_0)^2 + \sum_{All\ overlapping\ OO} \frac{1}{2} k_3 (R - R_0)^2 \quad (2.1)$$

where L is the T-O bond distance, L_0 is the prescribed T-O bond distance, θ is the O-T-O angle, R is the O-O distance, $k_1 = 100.0$ eV/Å^2, $k_2 = 100.0$ eV/rad^2, $k_3 = 1000.0$ eV/Å^2, $\theta_0 = 109.471°$, and $R_0 = 2.64$ Å..

A configuration is relaxed when the cost function is effectively zero, which is when there are negligible violations from the ideal zeolite condition (i.e. all O-T-O angles are 109.471±0.001°, all T-O bond lengths are the prescribed values, and there are no oxygen overlaps). The relative strength of the harmonic constants can be varied, and is somewhat arbitrary. In some difficult cases, it has proved beneficial to increase the strength of the T-O and O-T-O terms to speed up the migration of the configuration from flat energy surfaces, though in most cases, relaxation is possible with no modification of the terms.

Optimization routines in GULP

The default optimization algorithm in GULP is based on the Newton-Raphson method with the Broyden-Fletcher-Goldfarb-Shanno (BFGS) algorithm employed for update of the Hessian matrix.[52] Useful information about how these algorithms are implemented in GULP can be found on pages 33-37 of the online GULP manual.[53] To accelerate the optimization process, GULP updates the Hessian occasionally rather than after each optimization step. This approach is effective for bringing about relaxation in most cases, but for more difficult cases, the Rational Functional Optimisation (RFO) update technique [54] is usually preferable (GULP keyword 'rfo'). In the RFO technique, optimization steps are taken in such a way as to prevent imaginary eigenvalues for the

Hessian matrix, which can occur at saddle points on the energy surface. Additional details about the RFO method can be found in Appendix A.

The disadvantage of the RFO technique is that it is sometimes not stable far from minima, and thus must be employed with relative care when operating on a large number of structures. However, absent instability, the RFO technique is generally the method of choice for speed and effectiveness. In fact, several framework types that were previously thought non-flexible, were finally relaxed using RFO, including **EUO**, **IWV**, **MVY**, **OSO**, **-PAR**, and **PUN**.

When searching for flexibility in a given set of structures, it has proven effective to use the RFO optimization method as the first approach. For structures that fail to properly minimize, the BFGS method can be used instead to reach a more stable point on the energy surface, after which the update algorithm can be switched to RFO. Generally this switch can take place when the gradient norm reaches a certain stable value (by default the optimization routine terminates when the gradient norm falls below 10^{-6} eV/Å), although it is possible to program the switch point based on the number of optimization steps or the value of the cost function. Structures that have reached a cost function value close to zero can be entered into the GASP program for final verification of relaxation since GULP does not always offer the necessary degree of precision. This final step is necessary to ensure complete agreement with previous work on zeolite flexibility.[17] Once a relaxed configuration is found, it is possible to probe the flexibility window by the various techniques to be described in full later.

In all cases, it is necessary to monitor the final phonon frequencies for occurrence of imaginary values. Phonon frequencies are reported by using the ‘phonon’ keyword in

the GULP input file. GULP reports the squares of the phonon frequencies, and thus imaginary frequencies correspond to negative values in the output. If imaginary frequencies are present, the structure has reached a saddle point, and the relaxation is thus not complete, although the gradient norm will have reached the required value. Imaginary frequencies usually appear in cases where symmetry constraints have prevented a structure from reaching a true minimum. The RFO technique generally avoids saddle points, although this is not always the case. Some framework types exhibit a tortured energy space in the ideal zeolite potential, and navigation through the space is not always straightforward, even using advanced minimization techniques. The optimization process sometimes stalls when the local energy surface becomes too flat or in some cases conditions for optimization are not met even though no lower energy point can be found. Because it updates the Hessian after every minimization step, the RFO technique is especially inefficient for large systems, and in these cases it is often preferable to start with the BFGS updating scheme to reach a reasonable starting point for RFO.

As with any optimization, it is impossible to know if a global minimum has been reached without reaching the lowest possible value of the cost function (zero in the case of the ideal zeolite field). As such, it is always possible that more advanced searches or better starting coordinates may find relaxed configurations for framework types currently thought to be non-flexible. GULP features an optimization algorithm that searches for transition states (GULP keyword ‘trans’), and although it has proven thus far ineffective in relaxing previously non-relaxable structures, it has sometimes resulted in new, lower-energy minima for strained structures.

In the original studies of zeolite flexibility, the GASP program was used to find initial relaxed configurations. The advantage of using GULP over GASP is primarily the access to more sophisticated optimization routines and versatility in switching between different routines depending on the state of the input coordinates. As noted earlier, the advantage of the GASP program is the increased precision in the final convergence as well as faster optimization speed when close to relaxed states, especially for large structures.

Flexibility of known zeolite frameworks

A convenient measure of tetrahedrality for a given configuration has been derived based on the intratetrahedral oxygen distances and will be referred to as T_2 in the text. The formula for this dimensionless quantity is

$$T_2 = \sum_{m=1}^{5} \sum_{n>m}^{6} \frac{(l_n - l_m)^2}{15\bar{l}^2}$$

where l_n is the length of one of the six oxygen-oxygen distances within the tetrahedron, and $\bar{l}$ is the average of the six distances. For perfectly regular tetrahedra, the value of T_2 is zero. The convenience of this measure is that it is independent of the preferred T-O distance and thus can be applied even when the structure contains tetrahedra of varying size.

Based on the set of flexibility criteria used in previous studies (where a larger oxygen radius of 1.35 Å was used),[16,17] all but one framework type (**RRO**) can be relaxed with perfectly regular tetrahedra. Table 2.1 shows all the known zeolite framework types with their ability to meet the geometric constraints consistent with framework flexibility

CODE	#1	#2	#3	CODE	#1	#2	#3	CODE	#1	#2	#3	CODE	#1	#2	#3	CODE	#1	#2	#3	CODE	#1	#2	#3	CODE	#1	#2	#3
ABW	√	√	√	AWO	√	√	√	DFO	√	√	√	IHW	√	√	√	LTJ	√	√	√	NES	√	√	√	SAO	√	√	√	STT	√	√	√
ACO	√	√	√	AWW	√	√	√	DFT	√	√	√	IMF	√	√	√	LTL	√	√	√	NON	√	√	√	SAS	√	√	√	STW	√	×	√
AEI	√	√	√	BCT	√	√	√	DOH	√	√	√	IRR	√	√	√	LTN	√	√	√	NPO	√	√	√	SAT	√	√	√	SVR	√	√	√
AEL	√	√	√	BEA	√	√	√	DON	√	√	√	ISV	√	×	√	MAR	√	√	√	NPT	√	√	√	SAV	√	√	√	SZR	√	√	√
AEN	√	√	√	BEC	√	√	√	EAB	√	√	√	ITE	√	√	√	MAZ	√	√	√	NSI	√	√	√	SBE	√	√	√	TER	√	√	√
AET	√	√	√	BIK	√	√	√	EDI	√	√	√	ITH	√	√	√	MEI	√	√	√	OBW	√	√	√	SBN	√	√	√	THO	√	√	√
AFG	√	√	√	BOF	√	√	√	EMT	√	√	√	ITR	√	×	√	MEL	√	√	√	OFF	√	√	√	SBS	√	√	√	TOL	√	√	√
AFI	√	√	√	BOG	√	√	√	EON	√	√	√	ITV	√	√	√	MEP	√	√	√	OSI	√	√	√	SBT	√	√	√	TON	√	√	√
AFN	√	√	√	BPH	√	√	√	EPI	√	√	√	ITW	√	√	√	MER	√	√	√	OSO	√	√	√	SFE	√	√	√	tri	√	√	√
AFO	√	√	√	BRE	√	√	√	ERI	√	√	√	IWR	√	√	√	MFI	√	√	√	OWE	√	√	√	SFF	√	√	√	TSC	√	√	√
AFR	√	√	√	BSV	√	√	√	ESV	√	√	√	IWS	√	×	√	MFS	√	√	√	PAR	√	√	√	SFG	√	√	√	TUN	√	√	√
AFS	√	√	√	CAN	√	√	√	ETR	√	√	√	IWV	√	√	√	mog	√	√	√	PAU	√	√	√	SFH	√	√	√	UEI	√	√	√
AFT	√	√	√	CAS	√	√	√	EUO	√	√	√	IWW	√	√	√	MON	√	√	√	PHI	√	√	√	SFN	√	√	√	UFI	√	√	√
AFX	√	√	√	CDO	√	√	√	EZT	√	√	√	JBW	√	√	√	MOR	√	√	√	PON	√	√	√	SFO	√	√	√	UOS	√	√	√
AFY	√	√	√	CFI	√	√	√	FAR	√	√	√	JRY	√	√	√	MOZ	√	√	√	PUN	√	√	√	SFS	√	√	√	UOZ	√	√	√
AHT	√	√	√	CGF	√	√	√	FAU	√	√	√	JST	√	√	√	MRE	√	√	√	qtz	√	√	√	SFV	√	√	√	USI	√	√	√
ANA	√	√	√	CGS	√	√	√	fel	√	√	√	kea	√	√	√	MSE	√	√	√	RHO	√	√	√	SGT	√	√	√	UTL	√	√	√
APC	√	√	√	CHA	√	√	√	FER	√	√	√	KFI	√	√	√	MSO	√	√	√	RON	√	√	√	SIV	√	√	√	UWY	√	√	√
APD	√	√	√	CHI	√	√	√	FRA	√	√	√	LAU	√	√	√	MTF	√	√	√	RRO	√	√	×	SOD	√	√	√	VET	√	√	√
AST	√	√	√	CLO	√	√	√	GIS	√	√	√	LEV	√	√	√	MTN	√	√	√	RSN	√	√	√	SOF	√	√	√	VFI	√	√	√
ASV	√	√	√	coe	√	√	√	GIU	√	√	√	LIO	√	√	√	MTT	√	√	√	RTE	√	√	√	SOS	√	√	√	VNI	√	√	√
ATN	√	√	√	CON	√	√	√	GME	√	√	√	LIT	√	√	√	MTW	√	√	√	RTH	√	√	√	SSF	√	√	√	VSV	√	√	√
ATO	√	√	√	cri	√	√	√	GON	√	√	√	LOS	√	√	√	MVY	√	√	√	RUT	√	√	√	SSY	√	√	√	WEI	√	√	√
ATS	√	√	√	CZP	√	×	√	GOO	√	×	√	LOV	√	√	√	MWW	√	√	√	RWR	√	√	√	STF	√	√	√	WEN	√	√	√
ATT	√	√	√	DAC	√	√	√	HEU	√	√	√	LTA	√	√	√	NAB	√	√	√	RWY	√	√	√	STI	√	√	√	YUG	√	√	√
ATV	√	√	√	DDR	√	√	√	IFR	√	√	√	LTF	√	√	√	NAT	√	√	√	SAF	√	√	√	STO	√	√	√	ZON	√	√	√

Table 2.1: A list of approved zeolite framework types and dense silicates (**coe** is coesite; **cri** is cristobalite; **fel** is feldspar; **kea** is keatite; **mog** is moganite; **qtz** is quartz; **tri** is tridymite) with the ability to meet the three flexibility criteria indicated. Criterion #1 is that all tetrahedra can be made to be perfectly regular with O-T-O angles of 109.471±0.001°. Criterion #2 is that all tetrahedra are of uniform size, i.e. all T-O bond lengths are 1.610±0.001Å. Criterion #3 is that there are no overlaps between intertetrahedral oxygen atoms, i.e. all intertetrahedral oxygen atoms are at least 2.7Å apart (the criterion used in earlier studies). Six framework types can be relaxed only with different sized tetrahedra substituted, and one framework type can only be relaxed when the effective oxygen radius is reduced slightly.

according to the ideal zeolite model. Seven common dense silicates are also included. Each exceptional case will now be discussed in detail.

Frameworks flexible only in mixed compositions

A material with the **CZP** framework type was first synthesized in a zincophosphate composition,[55] and this is the only composition tried thus far where it can be relaxed with perfectly regular tetrahedra. This composition includes a 1:1 ratio of zinc

to phosphorous,[55] although the tetrahedral unit containing zinc is significantly larger than that containing phosphorous (the Zn-O preferred bond length is 1.947Å compared to 1.537Å for P-O). Unlike the material representations of some framework types, the type material composition can be relaxed with its topological symmetry preserved (space group $P6_122$).

Similar to **CZP**, **GOO** (for the mineral goosecreekite) cannot be relaxed with regular tetrahedra when represented as a pure silicate. However, when aluminum atoms are substituted to reflect its experimental type material composition (goosecreekite),[56] it can be relaxed. Although the framework **GOO** has orthorhombic topological symmetry ($C222_1$), goosecreekite is reported experimentally in monoclinic symmetry ($P12_11$) with a smaller unit cell.[56] **GOO** is thus an example of a framework type that must adopt lower symmetry to satisfy flexibility and energy constraints by our methods.

The type material for the framework **IWS** (ITQ-26) has seven crystallographically distinct T-sites, three of which are occupied by germanium with about a 30% probability.[57] These partial occupancies (which are not observed in the type materials chiral zincophosphate for **CZP** and goosecreekite for **GOO**) significantly complicate the search for flexible T-sites, but relaxed configurations have been found with germanium atoms substituted at site 4 and both sites 2 and 4,[17] which are both reported as partially occupied by germanium in ITQ-26.[57]

In the cases of structures with T-sites of partial occupancy, the experimentally reported chemical compositions are often inconsistent with the symmetry reported. For example, the material faujasite is reported in *Fd*-3*m* with a single unique T-atom that is partially occupied by both silicon and aluminum.[58] However, since aluminum substitution

results in a differently sized tetrahedron, the symmetry is automatically lowered in the mixed composition i.e. it is impossible to map an aluminum atom onto a silicon atom by symmetry operations alone; an additional transmutation operation is needed! Although this issue is unresolved at present, it may be possible to find intermediate symmetry for framework materials with reported partial occupancies, rather than resorting to a computationally expensive search over all possible T-atom combinations in *P*1.

The framework type **ITR** can be relaxed with a germanium atom (Ge-O bond length 1.756Å) substituted at the third T-site (0.13351, 0.24762, 0.18893 – in the type material ITQ-34 [59]), which is curiously not occupied by germanium in the type material. Germanium substitution at either site 4 (0.1360, 0.43127, 0.56281) or 8 (0.00000, 0.04629, 0.18852) result in nearly perfect tetrahedra, but not to the stringent requirements of the ideal zeolite model. Both of these sites are partially occupied by germanium in ITQ-34.[59] The type material of **ITR** (ITQ-34) is an example of incompatible chemical composition and symmetry since the chemical formula reports 11% germanium compositions,[59] but no symmetrically unique T-site produces the necessary number of T-atoms to result in this composition.

ISV can be relaxed with a larger tetrahedron (bond length 1.74Å, close to the preferred Ge-O bond distance) at site 1 (0.1192, 0.1146, 0.06251 – in the type material ITQ-7 [30]). Although ITQ-7 is reported as a pure silicate,[30] no perfectly relaxed configuration has been found in this composition without significant reduction of the effective oxygen radius. As noted earlier, Sastre and Corma reported that the presence of germanium accelerated the synthesis of **ISV** by an order of magnitude compared to pure-silica composition, and this may be accounted for by the enhanced flexibility gained by

the addition of germanium.[5] **ISV** has a moderately low framework energy (0.1698 eV/SiO_2) as calculated using the SLC field of Sanders et. al.,[41] although the optimized structure has somewhat distorted tetrahedra (T_2 = 0.0096). It appears that these distortions are necessary to force the structure into the appropriate range of T-O-T angles for silicates (>135°).

STW can be relaxed with a germanium atom substituted at either site 1 (0.70471, 0.38082, 0.03344 – in the type material SU-32 [60]) or site 3 (0.29888, 0.39598, -0.14961). It can also be relaxed with two germanium atoms substituted at sites 1 and 4 (0.2461, 0.33482, -0.04819) as well as sites 2 (0.52888, 0.4169, -0.03266) and 3. Each of these relaxations can occur with symmetry retained ($P6_122$). All five symmetrically unique sites are partially occupied by germanium in the SU-32,[60] and it can be predicted that the flexibility of certain T-atom combinations enhances their realizability in the real material. The chemical composition of SU-32 includes an approximately 1:1 ratio of germanium and silicon that is incommensurate with the symmetry,[60] though a wide range of chemical ratios may be feasible based on the flexibility analysis. It is also possible that individual cells in germanium-containing **STW** materials may contain different compositions and germanium occupancies. As in the previous cases, no relaxed configurations have been found in pure-silica composition, although it should be noted that **STW** has recently been reported as a pure silicate.[31] When optimized in the SLC potential, **STW** has a reasonably low energy value (0.2066 eV/SiO_2) but with significantly distorted tetrahedra (T_2 = 0.0110) compared to other zeolite framework types. As a reference, the mean value for all known framework types optimized in the

SLC field is T_2 = 0.0088. This sample set does not include **CZP**, **PUN**, or **RWY** which are extreme outliers and almost certainly unfeasible in pure or high-silica compositions.

Flexibility with cell modifications

At least two known framework types require larger unit cells to exhibit framework flexibility. The first, **GOO** cannot be relaxed with regular tetrahedra in the unit cell dictated by its topological symmetry (orthorhombic), but must be represented in the monoclinic cell of its type material goosecreekeite [56] with aluminum atoms substituted to reflect the material composition for full relaxation to occur. It is possible that the enhanced flexibility of the experimental composition and cell representation impart an energetic advantage that drives the structure toward lower symmetry.

As with **GOO**, **VNI** must be represented in the supercell version of its experimental type material VPI-5 [61] to be realized with regular tetrahedra, thus dropping from the topological rhombohedral symmetry to tetragonal symmetry. Although in the experimental composition 20% of the T-sites are occupied by zinc,[61] **VNI** can be relaxed as a pure silicate in this cell representation without reducing symmetry to *P1*. However, no fully relaxed configurations have yet been found for **VNI** in mixed compositions, including that of its experimental type material, leading to unclear conclusions about the link between flexibility and feasibility in this particular case.

Relaxation in high symmetry

While the flexibility results presented in Table 2.1 were all done with symmetry lowered to *P*1, it is instructive to examine framework flexibility with symmetry retained.

The symmetry presented for a given framework in the Database of Zeolite Structures maintained by the IZA generally corresponds to the maximum topological symmetry of the framework, although symmetry is lowered in cases where maximum symmetry results in unrealizable configurations with planar tetrahedra. Relaxed, pure-silica configurations have been found in the IZA symmetry for 147 out of 206 known framework types. For the other 59 framework types, it is necessary to lower the symmetry, substitute T-atoms, or adjust the cell dimensions for full relaxation with perfectly regular tetrahedra.

Starting with relaxed configurations in *P*1, configurations with higher symmetry can be found within the flexibility window either by modifying the ideal zeolite cost function or comprehensively sampling the low-density region of the window. It is possible to add an inverse volume term (or less ideally, a coulombic term) to the ideal zeolite cost function to inflate the structure from higher density configurations (where they usually exist in *P*1 symmetry) to minimum density. We thus take advantage of the fact that in virtually all cases, the minimum density configuration in the flexibility window also corresponds to the maximum symmetry configuration in which a given framework type can be realized with perfectly regular tetrahedra. If the flexibility window has been well-sampled, we can also search for symmetry in the minimum density configuration found. We use the FINDSYM program of Stokes et. al.[62] to detect symmetry in structures represented in *P*1.

Flexibility in intermediate symmetry

Framework flexibility can provide insights into the symmetry preference of real zeolite materials. As an example, the experimentally reported structure for pure-silica

MTN at room temperature resides in tetragonal symmetry rather than its topologically cubic symmetry,[63] corresponding to flexibility calculations that show that **MTN** must drop to tetragonal symmetry for all of the tetrahedra to be made regular. **MTN** can also be made to have regular tetrahedra in rhombohedral symmetry, though no known material has been reported in this symmetry. A closely related case is **MEP**, which can also be made to have regular tetrahedra in rhombohedral symmetry, but not in its topologically cubic symmetry. As with **MTN**, **MEP** occupies tetragonal symmetry at room temperature,[64] but becomes cubic at high temperature.

The type material for **EUO** (EU-1) has been reported as a pure silicate in its topological symmetry (orthorhombic),[65] although the framework cannot be relaxed with regular tetrahedra in this symmetry. However, full relaxation is possible for **EUO** in monoclinic symmetry, and this same symmetry yields lower energy configurations in the SLC field. This raises the possibility that EU-1 has been wrongly reported in the higher symmetry, and in fact exists as a monoclinic structure.

Conclusion

In this chapter, the various computational methods for identifying and exploring the flexibility window of zeolite frameworks have been described. After much trial-and-error, it has been discovered that *all* of the known zeolite framework types possess a flexibility window. Inconsistencies have been observed between some reported compositions and our attempts to relax those particular frameworks with the variously sized tetrahedra required by the composition. Although such discrepancies may be indicating the limits of our flexibility hypothesis, it is also possible that the converse is

true; that our analysis may be highlighting experimental limits in the crystallographic determination of compositions (as opposed to the structures – that is, the atom locations.) The scattering factors of Si^{4+} and Al^{3} atoms are almost identical, and thus framework compositions are inferred indirectly from other experimental measures.

Hints that this latter, optimistic, interpretation may have merit were encountered several times during this study. For example, we were aware that the **MTN** framework could not possibly relax under its full cubic topological symmetry. Analysis of the **MTN** framework under various subgroups revealed symmetries where it did relax. It was only after this analysis was performed that we then found a report describing this very structure for **MTN**.[63] Additional insights are gained as the entire flexibility window is sampled, as will be demonstrated in the following chapter.

Chapter 3

EXPLORING THE FLEXIBILITY WINDOW

Once a structure is relaxed with regular tetrahedra, it is possible to search for additional relaxed configurations within the flexibility window. Several methods have been developed for this purpose and will be detailed as follows.

Geometric Analysis of Structural Polyhedra (GASP)

Earlier studies of zeolite flexibility [16,17,37] have been largely based on results obtained using the GASP computational tool, which was developed by Wells et. al.[33] In the GASP model, frameworks are treated as periodic networks of rigid, corner-connected tetrahedral units formed by a T-atom at the center and four oxygen atoms at the regular tetrahedral vertices. To find relaxed atom configurations satisfying constraints that are consistent with rigid tetrahedra, GASP attempts to match oxygen atom positions to a template (represented by the appropriate number of regular tetrahedra with an implied T-atom at the center) within the unit cell. Periodic boundary conditions are applied, but no further symmetry constraints are included in order to allow maximal exploration of the configurational space i.e. relaxation is carried out in *P*1 symmetry.

In GASP, each oxygen atom is tethered to two corresponding template tetrahedra by a fictitious harmonic spring with a natural length of zero. A cost function is used that penalizes both the bending and stretching of the springs, as well as any intertetrahedral oxygen atom overlaps. This cost function includes many terms and is based on geometric algebra techniques. The interested reader can refer to Wells et. al.[33] for additional

information about the GASP model and cost function. An updated treatise is also available with helpful figures.[66]

GASP uses the limited memory Broyden–Fletcher–Goldfarb–Shanno (BFGS) algorithm,[52] which is a quasi-Newton method,[67] to minimize its cost function. A configuration is considered relaxed when all T–O bond lengths have reached 1.61±0.001 Å and all O–T–O bond angles have reached 109.471±0.001º with no oxygen overlaps. GASP attempts to explore the flexibility window by incrementally varying unit cell parameters, thereby adjusting cell volume and density, and using the fractional coordinates of the previously-obtained relaxed configuration as an initial guess. The oxygen atoms are then moved a small distance (typically, 0.01 nm or less) from their initial positions and each tetrahedral template is placed at the geometric center of the four corresponding oxygen atoms. The positions of the atoms and the template are then refined until conditions for relaxation are met or the minimization algorithm fails. This process is repeated numerous times at each given density to determine whether relaxed configurations can be found for a specific set of unit cell parameters.

Zeolite Null Space Explorer (ZeNuSpEx)

The flexibility window has also been explored in previous studies [17,19,34] using an approach from rigidity theory where zeolite frameworks are considered as periodic truss systems. The O-O edges of tetrahedra are treated as bars of ideal length L=0.263 nm, and the six-coordinated oxygen atoms behave as force-free spherical joints.[14,31] Si atoms are ‘‘carried’’ inside the rigid tetrahedra and are ignored. The compatibility matrix $\mathbf{C}$ describes the $3N$ rigid constraints that maintain the bar lengths with N oxygen atoms per

unit cell. The vector of infinitesimal displacements of the oxygen atoms, $\mathbf{d}$, is related to the vector of O-O edge extensions, $\mathbf{e}$, via

$$\mathbf{Cd} = \mathbf{e}. \tag{3.1}$$

The condition $\boldsymbol{e} = 0$ describes a rigid framework. $\boldsymbol{C}$ is a $3N \times 3N$ matrix whose elements are $\widetilde{x_{ij}} = \frac{x_j - x_i}{L}$, y_{ij}, z_{ij}, etc., with appropriate adjustments for periodic continuity. The column vector $\mathbf{d}$ is $3 \times 3N$ with elements $\widetilde{\delta x_{ij}} = \frac{\delta x_j - \delta x_i}{L}$, δy_{ij}, δz_{ij}. If we admit unit cell degrees of freedom, $\mathbf{d}$ acquires six additional components representing small changes in the unit cell dimensions: $\delta a, \delta b, \delta c, \delta\alpha, \delta\beta$, and $\delta\gamma$.[31] $\mathbf{C}$ is now a $3N \times (3N + 6)$ matrix embodying $3N + 6$ degrees of freedom and $3N$ constraints. With compatible initial coordinates that satisfy $\mathbf{e} = 0$, $\mathbf{Cd} = 0$ can be interpreted as an eigenvector problem with eigenvalues equal to zero. $\mathbf{C}$ is rank deficient by 6, yielding a null space containing at least six null solutions $\boldsymbol{d}$ (mechanisms), three of which will be the trivial rigid-body translations.[31] The other three null solutions *are not* the trivial rigid-body rotations, because such rotations would immediately violate the alignment of the structure with the underlying lattice. Instead they represent internal shear modes, which do not necessarily contribute to the flexibility window since the modes may have infinitesimal amplitude only. The null eigenvectors are the modes of the framework that do not strain the O-O linkages. As the framework folds, the $\mathbf{e} = 0$ condition holds to first order between each step, but $\mathbf{C}$ must be continually updated when finite mechanisms explore their range.

Framework symmetry typically renders additional constraints degenerate, resulting in more than three null eigenvectors to the compatibility matrix, or in other words, providing additional "internal folding mechanisms". Most relevant here are the

finite-amplitude null eigenvectors that define the flexibility window. The program ZeNuSpEx (Zeolite Null Space Explorer) uses singular value decomposition (SVD) methods to find non-trivial null vectors of the compatibility matrix.[68] These null vectors can be added, with small amplitude, to the original coordinate vector space to produce a new, nearly-relaxed configuration. This configuration is then relaxed again by energy minimization (to eliminate second and third order deformations), resulting in a unique set of relaxed coordinates that neighbors the original set. Exploration of the flexibility window by following the null eigenvectors in this way offers a potentially more systematic alternative to the stochastic methods used by e.g. GASP.

A related function performed by the ZeNuSpEx program is counting the number of geometry-preserving internal folding mechanisms available at any given configuration, corresponding to the number of null eigenvalues of the compatibility matrix. Zeolites can be folded along multiple paths starting from their highest symmetry configuration, which typically occurs at the lowest possible density within the flexibility window. However, once symmetry is broken, many folding mechanisms are no longer accessible without returning to the maximum symmetry configuration. In a number of cases (e.g. quartz, cristobalite, tridymite, **SOD**, **ANA**, and **LTA**), the framework can be relaxed with regular tetrahedra at a single configuration in maximum symmetry. In these cases, following any fold through the flexibility window results in lowered symmetry. In other cases (e.g. keatite, **FAU**, **EMT**, and **RHO**), maximum symmetry can be maintained by following a symmetry-preserving fold through the flexibility window. However, symmetry-preserving modes are a special case, as the majority of folds result in lower symmetry (generally *P*1). The number of available folding modes is exquisitely sensitive to

framework symmetry, and a small displacement of the coordinates from high symmetry generally results in a drop in the number of internal mechanisms. For configurations with P*1* symmetry, the number of null modes is almost always three (the minimum, and these may be of infinitesimal amplitude).

Counting null modes using Bloch-wave formulation

Of particular interest is the way the number of folding mechanisms (or null modes) evolves for supercells of a given framework type containing N_C unit cells. Depending on the framework, the folding mechanisms will grow as ${N_C}^{n/3}$ where $0 \leq n \leq 3$. When $n = 3$, the growth in null modes is extensive, i.e. the number grows linearly with volume. If the calculation is done in real space, the computational effort of counting the null modes increases approximately with the cube of the volume explored, i.e. $\sim {N_C}^3$. To speed up computation, Bloch's theorem can be applied $\boldsymbol{d}(\boldsymbol{r} + \boldsymbol{R}) = \boldsymbol{d}(\boldsymbol{r})\exp(2\pi i \boldsymbol{K} \cdot \boldsymbol{R})$ to a single unit cell to explore the long-wavelength null mode states within the Brillouin zone and not just those at $\boldsymbol{K} = 0$.[36] $\boldsymbol{R}$ is the position vector of a neighboring cell. The wave vector $\boldsymbol{K}$ has components that are multiples of $(1/(pa), 1/(qb), 1/(rc))$, where p, q, and r are the supercell repeats along the a, b, and c axes, respectively (thus, $N_C = pqr$). Because of loss of periodicity, Bloch's theorem cannot be used to follow a mechanism to finite amplitude. It is used to identify mechanisms that can then, in principle, be followed as modes at the Γ point ($\boldsymbol{K} = 0$) in the p; q; r-expanded cell. In practice, the number of null modes is counted by adding the number of null eigenvalues of the *K*-space representation of the compatibility matrix with the zero cutoff set at 10^{-10}.

By counting the number of null modes at an irrational-index *K*-point for the maximum symmetry configurations, it has been found that 25 of the 197 known zeolite frameworks exhibit extensive flexibility, i.e. the number of folding modes increases linearly with the number of unit cells, N_C (Table 3.1).[64] For other framework types, the number of folding modes scales as ${N_C}^{2/3}$ or ${N_C}^{1/3}$, and these surface and edge mechanisms of the flexibility window could play an important role at the nucleation and growth stage of zeolite synthesis where N_C is small.

ACO-	4	EMT-	2	LTA-	4	OFF-	1	SSF-	2
AST-	12	ERI-	2	LTL-	3	PAU-	24[a]	TSC-	25
ASV-	2	FAU-	16	MER-	2	RHO-	4	UFI-	2
DFO-	4	KFI-	6	MOZ-	2	SAS-	2	UOS-	2
EAB-	1	LEV-	3	MTN-	2[a]	SOD-	2	UOZ-	4

Table 3.1: The 25 extensively flexible zeolite frameworks. The number of folding mechanisms at a general reciprocal lattice point is given. The frameworks **PAU** and **MTN** (marked by an "a") cannot be relaxed with regular tetrahedra in their topological symmetry, although they still exhibit extensive flexibility.

No zeolite structure is truly triclininc, and so we have not found a system whose modes grow as ${N_C}^{0}$, that is, the number of modes does not grow at all with supercell size.

Exploring the flexibility window by random steps

The third method of exploring the flexibility window involves iterative random displacements of the atom coordinates and unit cell parameters. In order to find relaxed configurations within the flexibility window, the ideal zeolite cost function is used (Equation 2.1). Starting from the initial configuration, coordinates and cell parameters are randomly displaced by a small amount and a constant volume optimization is then undertaken, followed by a constant pressure optimization which results in a fully relaxed

configuration within the flexibility window. The process is then repeated with the previously relaxed configuration used as a starting point. Since GULP is able to perform calculations with symmetry maintained, it is possible to search for ideal configurations in space groups other than *P*1. This method has proven effective in exploring previously unknown regions of the flexibility windows of some framework types, particularly at high density. This method was used to obtain randomly sampled points within the flexibility window of quartz as displayed in Figure 1.3.

The flexibility index

The *flexibility index* (the ratio of the maximum and minimum densities within the flexibility window, ρ_{max}/ρ_{min}) has been used to compare the relative flexibility of different framework types. Using a combination of the GASP, ZeNuSpEx, and GULP methods the flexibility index has been tabulated for all of the known framework types as well as the frameworks of several dense silicate materials (Table 3.2). A histogram of all the flexibility index values contained in Table 3.2 is found in Appendix A (Figure A.1). Since the flexibility windows of many framework types have not been fully explored, these results will almost certainly be subject to future updates, but they represent an important starting point.

CODE	ρ_{min}	ρ_{max}	F_O	CODE	ρ_{min}	ρ_{max}	F_O	CODE	ρ_{min}	ρ_{max}	F_O	CODE	ρ_{min}	ρ_{max}	F_O
ABW	17.49	34.91	2.00	**DON**	16.18	23.18	1.43	**MAZ**	16.63	18.65	1.12	**SBT**	13.67	15.63	1.14
ACO	16.40	25.89	1.58	**EAB**	15.84	18.82	1.19	**MEI**	14.56	16.02	1.10	**SFE**	16.85	23.08	1.37
AEI	14.97	18.41	1.23	**EDI**	16.26	19.24	1.18	**MEL**	16.94	20.66	1.22	**SFF**	16.89	20.04	1.19
AEL	18.03	24.45	1.36	**EMT**	13.13	16.83	1.28	**MEP**	18.41	21.15	1.15	**SFG**	17.44	19.38	1.11
AEN	20.88	22.36	1.07	**EON**	16.78	18.74	1.12	**MER**	16.08	25.29	1.57	**SFH**	16.33	18.14	1.11
AET	17.49	22.79	1.30	**EPI**	18.21	22.11	1.21	**MFI**	16.94	21.21	1.25	**SFN**	16.30	20.99	1.29
AFG	16.69	26.17	1.57	**ERI**	15.92	18.80	1.18	**MFS**	17.66	20.18	1.14	**SFO**	15.02	18.09	1.20
AFI	16.67	21.53	1.29	**ESV**	16.37	21.99	1.34	**MON**	17.60	23.33	1.33	**SFS**	16.27	18.62	1.14
AFN	17.80	20.36	1.14	**ETR**	15.69	18.20	1.16	**MOR**	16.94	20.41	1.20	***SFV**	17.13	18.71	1.09
AFO	18.19	24.44	1.34	**EUO**	18.81	20.07	1.07	**MOZ**	17.00	18.66	1.10	**SGT**	17.58	19.38	1.10
AFR	14.99	18.31	1.22	**EZT**	16.90	20.28	1.20	***MRE**	18.27	26.41	1.45	**SIV**	16.09	24.49	1.52
AFS	14.49	16.99	1.17	**FAR**	16.82	26.12	1.55	**MSE**	16.17	17.91	1.11	**SOD**	16.59	31.20	1.88
AFT	14.76	17.58	1.19	**FAU**	13.13	16.85	1.28	**MSO**	17.74	22.64	1.28	**SOF**	16.99	17.41	1.02
AFX	15.00	18.10	1.21	**FER**	17.51	22.64	1.29	**MTF**	20.22	22.61	1.12	**SOS**	16.58	21.39	1.29
AFY	14.45	16.06	1.11	**FRA**	16.63	25.66	1.54	**MTN**	18.18	20.87	1.15	**SSF**	16.36	21.23	1.30
AHT	19.38	28.26	1.46	**GIS**	16.08	27.04	1.68	**MTT**	18.17	22.81	1.26	**SSY**	16.85	22.00	1.31
ANA	19.20	27.01	1.41	**GIU**	16.84	27.79	1.65	**MTW**	17.60	22.16	1.26	**STF**	16.89	21.32	1.26
APC	17.49	22.47	1.28	**GME**	15.02	17.46	1.16	**MVY**	21.41	24.97	1.17	**STI**	16.63	20.54	1.24
APD	17.93	27.69	1.54	**GON**	17.67	24.37	1.38	**MWW**	16.30	17.33	1.06	***STO**	17.95	21.86	1.22
AST	15.78	27.38	1.74	**GOO**	18.76	19.79	1.05†	**NAB**	16.25	25.15	1.55	**STT**	17.67	17.97	1.02
ASV	19.80	21.58	1.09	**HEU**	17.03	21.21	1.25	**NAT**	16.86	19.00	1.13	**STW**	16.59	16.94	1.02†
ATN	17.38	29.94	1.72	**IFR**	16.71	20.65	1.24	**NES**	17.78	19.06	1.07	**-SVR**	16.48	18.43	1.12
ATO	18.46	24.77	1.34	**IHW**	18.59	20.31	1.09	**NON**	18.87	19.93	1.06	**SZR**	17.45	24.08	1.38
ATS	15.91	26.85	1.69	**IMF**	17.42	19.76	1.13	**NPO**	16.02	24.18	1.51	**TER**	17.02	20.77	1.22
ATT	16.86	27.64	1.64	**IRR**	12.37	13.32	1.08	**NPT**	13.68	15.07	1.10	**THO**	16.27	19.22	1.18
ATV	18.81	25.06	1.33	**ISV**	14.96	15.07	1.01†	**NSI**	18.71	25.86	1.38	**TOL**	16.73	24.36	1.46
AWO	18.15	22.25	1.23	**ITE**	15.78	21.08	1.34	**OBW**	12.97	17.19	1.33	**TON**	18.08	24.29	1.34
AWW	16.52	25.60	1.55	**ITH**	17.78	19.18	1.08	**OFF**	15.96	18.68	1.17	**TSC**	13.15	16.17	1.23
BCT	18.89	36.82	1.95	**ITR**	14.02	15.02	1.07†	**OSI**	17.86	25.44	1.42	**TUN**	17.38	19.69	1.13
***BEA**	15.27	16.36	1.07	**-ITV**	10.69	11.07	1.04	**OSO**	17.32	17.74	1.02	**UEI**	18.18	21.47	1.18
BEC	16.03	17.13	1.07	**ITW**	17.49	19.59	1.12	**OWE**	17.03	19.43	1.14	**UFI**	15.03	18.00	1.20
BIK	18.61	34.97	1.88	**IWR**	15.52	18.35	1.18	**-PAR**	16.87	22.29	1.32	**UOS**	17.23	19.59	1.14
BOF	17.69	26.06	1.47	**IWS**	10.06	11.27	1.12†	**PAU**	15.81	17.64	1.12	**UOZ**	19.74	22.98	1.16
BOG	15.46	18.24	1.18	**IWV**	16.03	16.55	1.03	**PCR**	18.46	20.37	1.10	**USI**	15.92	18.91	1.19
BOZ	13.20	17.10	1.30	**IWW**	16.49	18.39	1.12	**PHI**	16.09	24.47	1.52	**UTL**	16.54	16.69	1.01
BPH	14.49	16.82	1.16	**JBW**	18.52	36.19	1.95	**PON**	17.95	20.91	1.16	**UWY**	16.40	18.10	1.10
BRE	17.97	22.90	1.27	**JOZ**	16.08	21.62	1.34	**PUN**	14.79	16.71	1.13	**VET**	21.43	23.12	1.08
BSV	18.68	19.86	1.06	**JRY**	18.70	22.94	1.23	**RHO**	14.30	24.26	1.70	**VFI**	14.80	17.83	1.20
CAN	16.72	24.67	1.48	**JSN**	17.70	20.65	1.17	**-RON**	19.13	21.49	1.12	**VNI**	18.54	19.61	1.06
CAS	18.70	26.42	1.41	**JST**	13.86	18.63	1.34	**RRO**	19.00	19.23	1.01	**VSV**	16.96	22.34	1.32
CDO	20.40	22.17	1.09	**JSW**	18.10	20.06	1.11	**RSN**	16.87	20.40	1.21	**WEI**	16.07	21.73	1.35
CFI	17.44	19.10	1.10	**KFI**	14.93	17.99	1.20	**RTE**	16.73	23.85	1.43	**-WEN**	16.84	20.52	1.22
CGF	18.76	22.77	1.21	**LAU**	17.53	22.13	1.26	**RTH**	15.80	18.73	1.19	**YUG**	17.95	26.21	1.46
CGS	16.49	21.86	1.33	**LEV**	15.90	18.32	1.15	**RUT**	17.39	21.94	1.26	**ZON**	17.53	21.84	1.25
CHA	15.01	17.99	1.20	**LIO**	16.68	22.63	1.36	**RWR**	19.34	23.57	1.22	**coesite**	28.56	31.27	1.09
-CHI	19.90	24.42	1.23	**-LIT**	16.71	26.20	1.57	**RWY**	8.30	14.03	1.69	**cristobalite**	19.45	37.05	1.90
-CLO	10.89	13.69	1.26	**LOS**	16.66	27.15	1.63	**SAF**	17.96	21.70	1.21	**feldspar**	21.24	31.43	1.48
CON	15.85	17.90	1.13	**LOV**	16.84	20.60	1.22	**SAO**	14.20	16.18	1.14	**keatite**	22.98	31.02	1.35
CZP	21.95	26.42	1.20†	**LTA**	13.95	17.33	1.24	**SAS**	15.23	18.69	1.23	**moganite**	22.80	36.17	1.59
DAC	17.43	22.69	1.30	**LTF**	16.86	18.24	1.08	**SAT**	16.33	19.14	1.17	**quartz**	24.08	30.70	1.27
DDR	17.54	18.91	1.08	**LTJ**	18.92	23.51	1.24	**SAV**	15.10	17.38	1.15	**tridymite**	19.45	31.00	1.59
DFO	14.78	16.53	1.12	**LTL**	16.77	19.50	1.16	**SBE**	13.61	16.05	1.18				
DFT	17.57	27.17	1.55	**LTN**	16.49	19.79	1.20	**SBN**	16.25	20.00	1.23				
DOH	17.64	20.76	1.18	**MAR**	16.70	27.51	1.65	**SBS**	13.66	15.64	1.14				

Table 3.2: The minimum (ρ_{min}) and maximum (ρ_{max}) densities found within the flexibility window for the current 206 approved zeolite framework types, as well as several dense silicates. The flexibility index, F_O, is the ratio ρ_{max}/ρ_{min}. † means that flexibility requires a mixed composition, e.g. as an aluminosilicate.

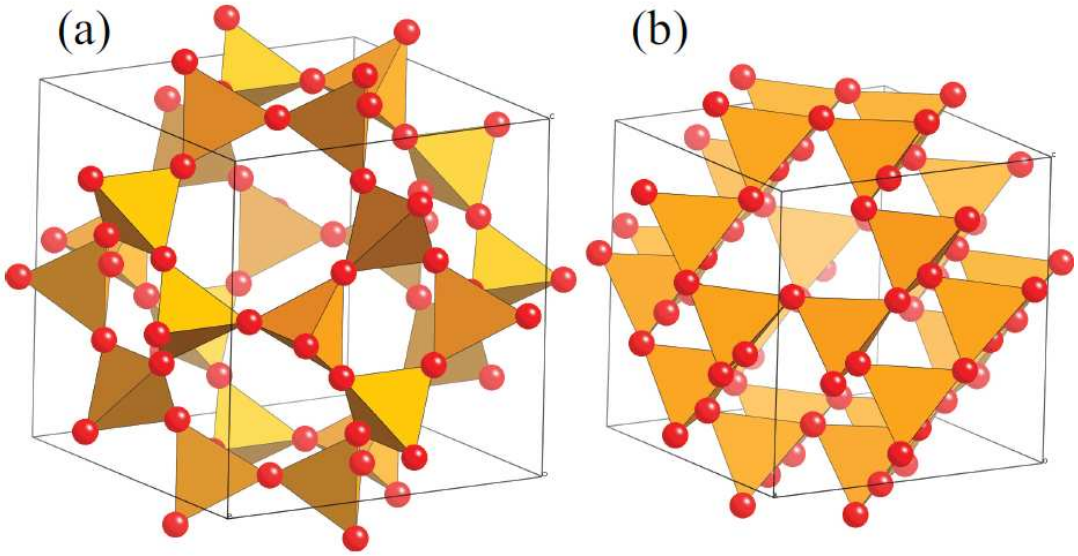

Figure 3.1: Two configurations along a symmetry preserving folding mechanism for the **SOD** framework including (a) maximum volume where the symmetry is *Im-3m* and (b) a folded configuration where the symmetry has become *I*-43*m*. **SOD** exists with regular tetrahedra at a single configuration in *Im*-3*m* whereas in *I*-43*m*, the framework can be folded to high density without deforming the tetrahedra.

Folding with symmetry retained: SOD, LTA, and ABW

Symmetry-preserving folds are found by isotropically adjusting the unit cell parameters by a small amount and then performing a constant volume optimization in GULP using the ideal zeolite potential. This is followed by a constant pressure optimization in which both the coordinates and the unit cell parameters are allowed to vary. By this method, symmetry-preserving folding mechanisms have been explored for several known framework types.

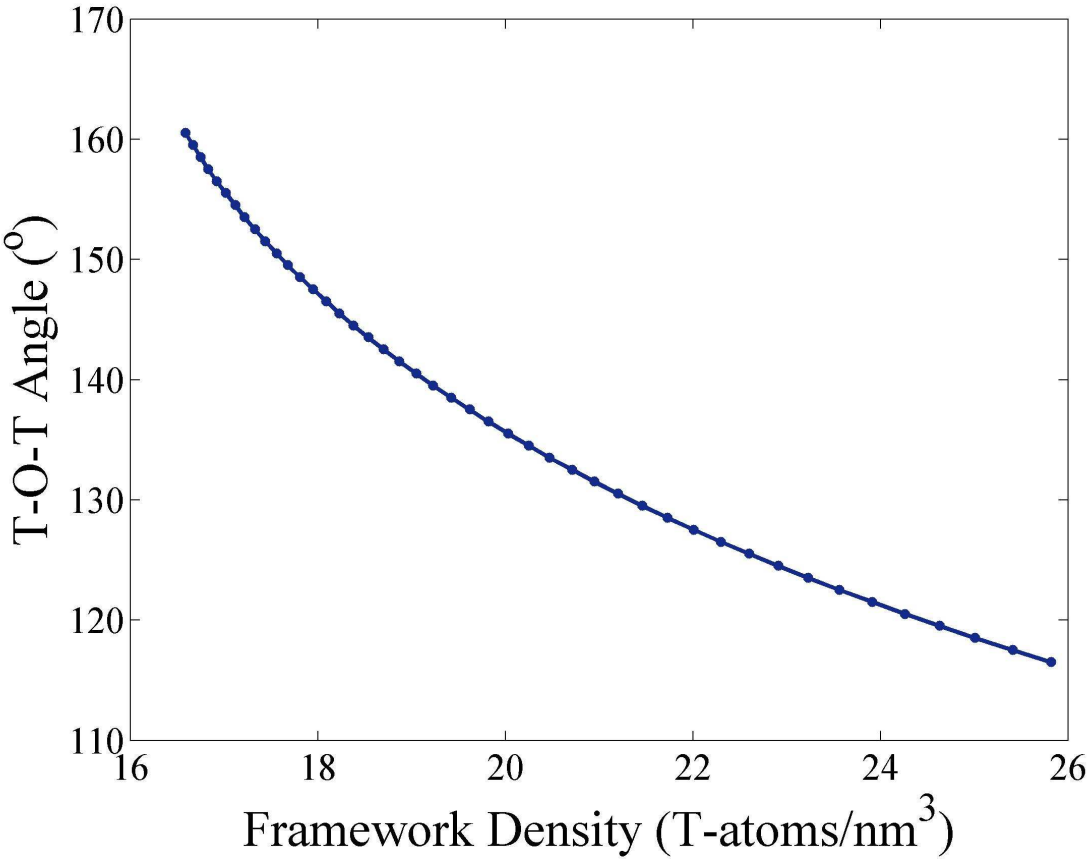

Figure 3.2: A plot of the T-O-T angle against the framework density for **SOD** along a symmetry-preserving fold in *I-43m*. The tetrahedra remain perfectly regular over this fold with a T-O bond length of 1.61Å.

Figure 3.1 shows how the structure of **SOD** (the framework of sodalite) evolves as it is folded from minimum density/maximum symmetry in *Im*-3*m* (Figure 3.1a) to higher density states in *I*-43*m* (Figure 3.1b) without deforming the comprising tetrahedra. Figure 3.2 shows the evolution of the T-O-T angle over this fold. Experimental pure-silica SOD has alternatively reported T-O-T angles of 155.2° [69] and 159.6°,[70] each close to the value of 160.5° expected for perfectly regular tetrahedra at maximum symmetry in *Im*-3*m*. However, the experimentally reported structures reside in *I*-43*m* where they experience enhanced flexibility as ideal structures. It can be surmised that pure-silica

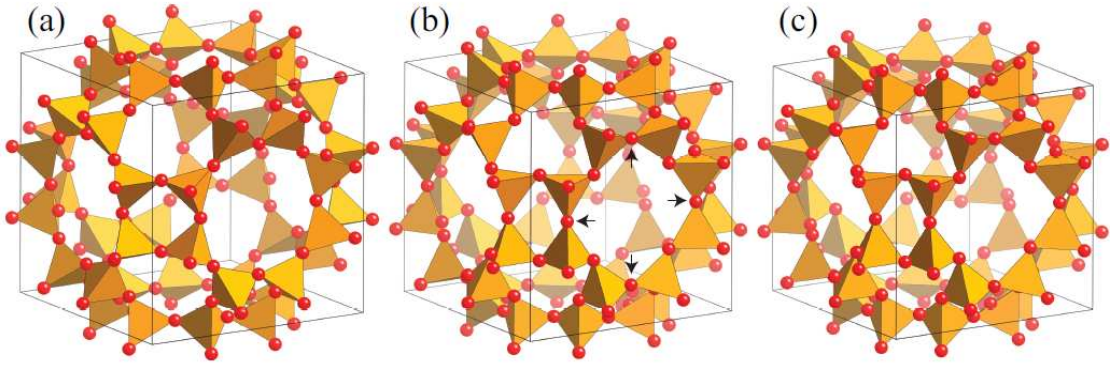

Figure 3.3: Three configurations along a symmetry-preserving fold of **LTA** in *Pm-3m*, including (a) the maximum volume state with a framework density of 13.95 T-atoms/nm^3, (b) an intermediate state (15.88 T-atoms/nm^3) where one of the symmetry-related T-O-T angles reaches a value of 180º (as indicated by the arrows) and (c) a high density state with a framework density of 16.98 T-atoms/nm^3.

SOD will go to maximum symmetry at high temperatures, as observed for e.g. quartz and cristobalite.[71]

The framework for zeolite A (**LTA**) can be folded along a symmetry-preserving mode in *Pm*-3*m*, which is its maximum symmetry representation. Figure 3.3 depicts several confirmations along this fold, and Figure 3.4 shows the evolution of the three unique T-O-T angles over the course of the fold. Experimental pure-silica **LTA** resides close to the low density end with reported T-O-T angles of 149.7º, 151.7º, and 158.5º.[72] As a comparison, **LTA** optimized in the SLC field has T-O-T angles of 146.6º, 148.8º, and 155.7º respectively. It should be noted that pure-silica **LTA** has slightly distorted tetrahedra (T_2= 0.0037) and a smaller mean bond length (1.60Å) than the ideal zeolite model used for this calculation. As the density increases, two of the T-O-T angles diverge considerably from the third into unfeasible ranges for silica (less than about 135º), as was also observed for **SOD** at higher density. Not surprisingly, experimental **LTA** prefers configurations where the T-O-T angles reside close to the preferred silicate value.

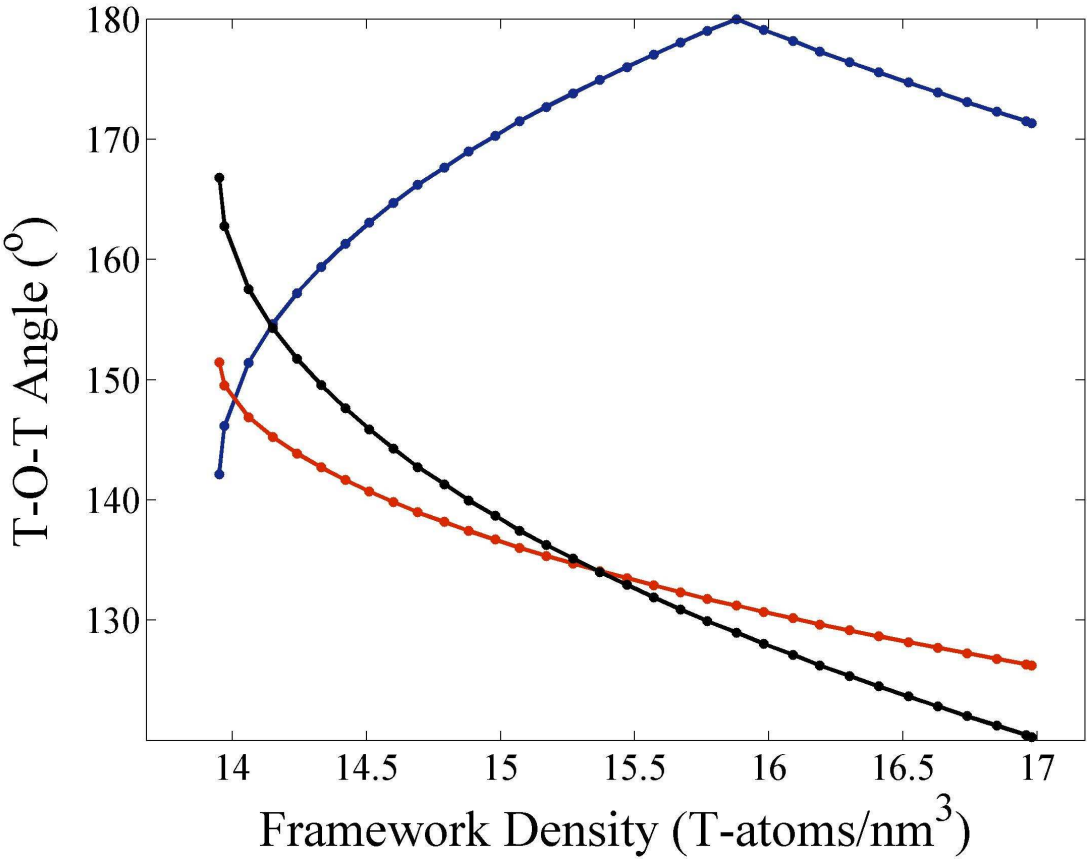

Figure 3.4: A plot of the three unique T-O-T angles against the framework density for **LTA** along a symmetry-preserving fold in *Pm*-3*m*. The tetrahedra remain perfectly regular over this fold with a T-O bond length of 1.61Å. At a density of 15.88 T-atoms/nm^3 one of the T-O-T angles reaches a value of 180º

Unlike the previous two structures, **ABW** has not yet been reported as a pure-silicate, but rather **ABW** materials synthesized up to this point appear to always contain non-homogeneous T-atom compositions.[6] Nevertheless, **ABW** can be folded in maximum symmetry (*Imma*) as depicted in Figure 3.5. As before, the evolution of the T-O-T angles is shown in [Figure]. In *Imma*, one of the T-O-T angles remains fixed at 180º, and while some pure-silicate structures exist with large T-O-T angles (generally at high

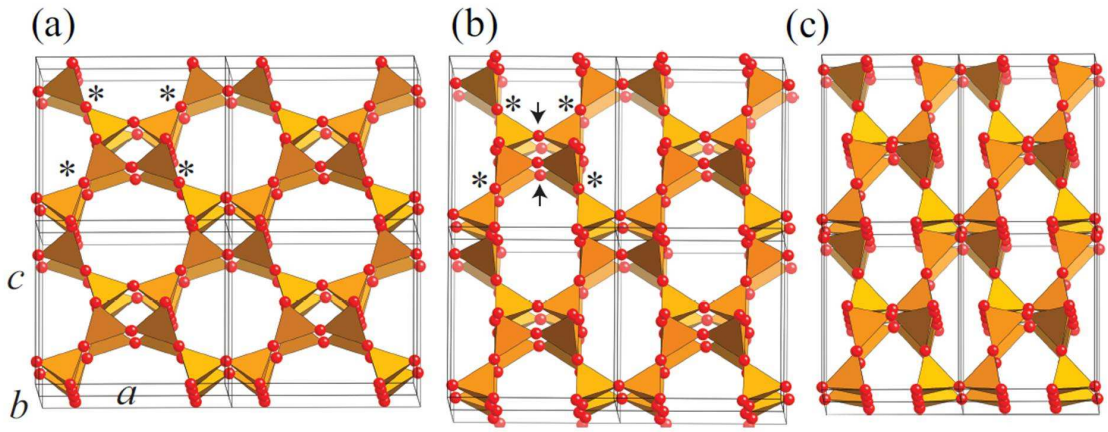

Figure 3.5: Three configurations along a symmetry-preserving fold of **ABW** in *Imma*, including (a) the maximum volume state with a framework density of 17.49 T-atoms/nm^3, (b) an intermediate state (19.38 T-atoms/nm^3) where one of the symmetry-related T-O-T angles reaches a value close to 180º (as indicated by the arrows) and (c) a high density state with a framework density of 23.64 T-atoms/nm^3.

temperatures e.g. beta cristobalite and beta tridymite) there is a small energy penalty for angles in this range (as will be discussed later in detail), and smaller angles are generally preferred at room temperature. In order to obtain a smaller range of angles close to the preferred silicate values, the symmetry must be lowered

ABW cannot be fully relaxed in the SLC field in *Imma* (imaginary phonon frequencies are observed), and the symmetry must be lowered to $P2_1/c$ for full relaxation to occur. In fact, the calculated energy difference (SLC) between the *Imma* and the $P2_1/c$ phases is 0.0193 eV/SiO_2 (as a comparison alpha and beta quartz have a calculated energy difference of 0.06367 eV/SiO_2), and it is conceivable that pure-silica versions of **ABW** could be synthesized in the lower monoclinic symmetry, rather than the topologically orthorhombic symmetry.

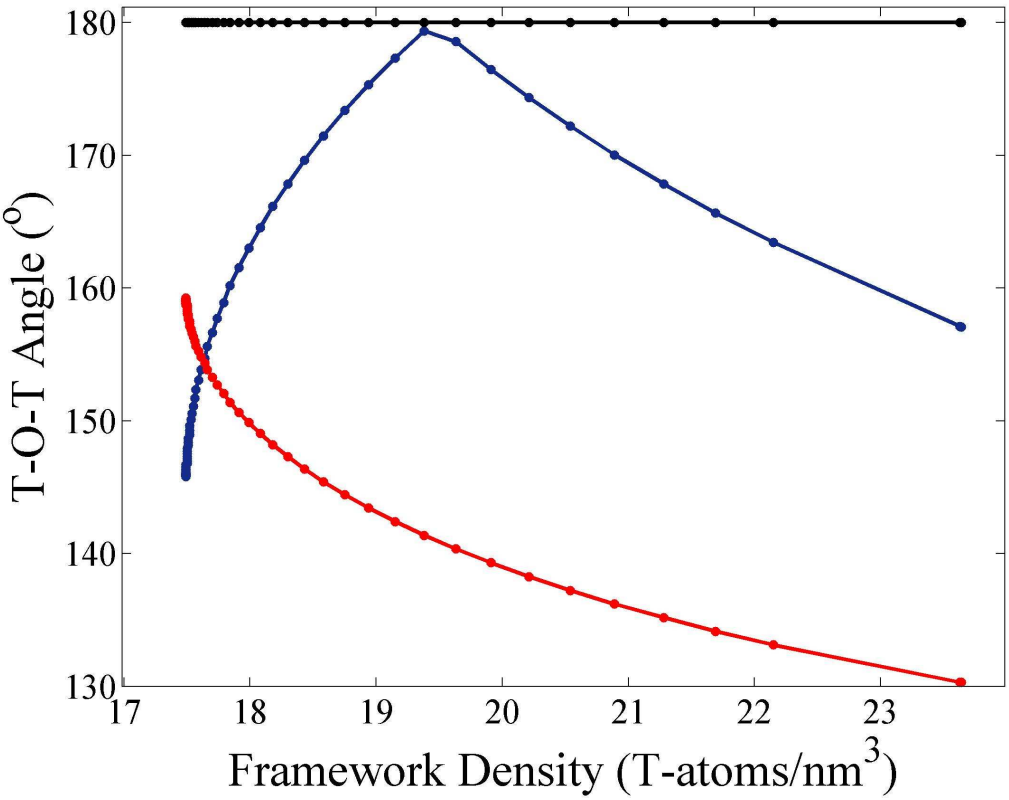

Figure 3.6: A plot of the three unique T-O-T angles against the framework density for **ABW** along a symmetry-preserving fold in *Pm*-3*m*. The tetrahedra remain perfectly regular over this fold with a T-O bond length of 1.61Å.

Conclusion

The comprehensive sampling of the flexibility window helps demonstrate the rich flexibility behavior observed in zeolite frameworks. While additional tools are needed to systematically explore the flexibility window, the methods used thus far represent an important first step. In many ways, flexibility remains a binary (true/false) parameter, and we continue to develop better methods to compare relative flexibility for different framework types. The next chapter will examine the presence of flexibility as a distinguishing feature of viable zeolite frameworks.

Chapter 4

FLEXIBILITY AS A FEASIBILITY BENCHMARK

The database of Treacy et. al.[8] contains over two million topologically unique hypothetical zeolite structures found using a graph enumeration method.[73] The energy requirement [using the modified Boisen-Gibbs-Bukowinski (mBGB) potential, which is based on a pure-silica model [8,74] – see Appendix A for details] for new graph embeddings added to the database was set to be generously inclusive to account for the possibility that certain graphs might be feasible in non-silica compositions. As a result, many structures found in the database are likely unfeasible in high-silica form, and it becomes important to establish an effective vetting process for identifying potentially realizable hypothetical zeolite structures.

In this chapter, we show that framework flexibility is an effective discriminator for finding synthetically feasibility hypothetical zeolite frameworks.

Feasibility criteria

While a large number of empirical potentials have been developed for studying framework oxides and related materials, the widely varying compositions of known zeolite materials makes it extremely difficult to develop universally applicable feasibility criteria based on energetics alone. One of the most successful empirical models (as discussed earlier) is the SLC potential upon which several proposed feasibility criteria are based.[14,75] However, since the SLC potential is based on the assumption of pure-silica composition, feasibility criteria based on SLC energy alone are likely to pass over zeolite frameworks that can be realized only in low-silica or non-silica compositions. At least

eleven known zeolites (**BSV**, **CZP**, **JST**, **NAB**, **NPT**, **OBW**, **OSO**, **PUN**, **RWY**, **SOS** and **WEI**) have SLC energies in excess of 30 kJ/mole SiO_2 (0.311 eV/SiO_2) - the proposed cutoff for feasible zeolites [75] - and another seven (-**CHI**, -**CLO**, -**LIT**, -**PAR**, -**RON**, -**SVR**, -**WEN**) are interrupted frameworks and cannot be represented in the SLC field due to charge imbalances. At the same time well over 16,000 unrealized hypothetical zeolite structures have an energy below 30 kJ/mole (0.311 eV/SiO_2).

A set of feasibility criteria have recently been proposed based on the structure parameters in SLC refinements,[15] but since the search using these criteria was done over a relatively small sample set, it remains unclear whether or not these criteria are too inclusive for practical application. In fact, it is possible that these proposed criteria reflect properties of the SLC potential model rather than intrinsic properties of zeolite framework types, although additional examination is necessary. Another feasibility criterion was recently proposed by Proserpio et. al. based on packings of natural building units, but this was found to account for only 163 out of 201 known framework types.[76]

Finding flexible structures in the database of hypothetical zeolites

A simple search over 117,570 low-energy (mBGB energy less than 0.1 eV/SiO_2) hypothetical frameworks found that only 11,647 exhibited flexibility in a unit cell corresponding to their assigned space group symmetry. These included 78 of the 97 known framework types found in the original set. The flexibility calculation used applied isotropic constraints on the unit cell, i.e. the ratios between the cell lengths *a*, *b*, and *c* remained fixed, and the cell angles α, β, and γ were held constant. The coordinates were allowed to vary freely with no symmetry constraints imposed. This restricted search was

necessary due to the large number of structures to be analyzed, and served as a proof of principle rather than a comprehensive flexibility calculation on all hypothetical zeolites. In fact, all 97 known framework types in the database have been found to be flexible, and an unrestricted search would almost certainly discover additional flexible hypothetical framework types.

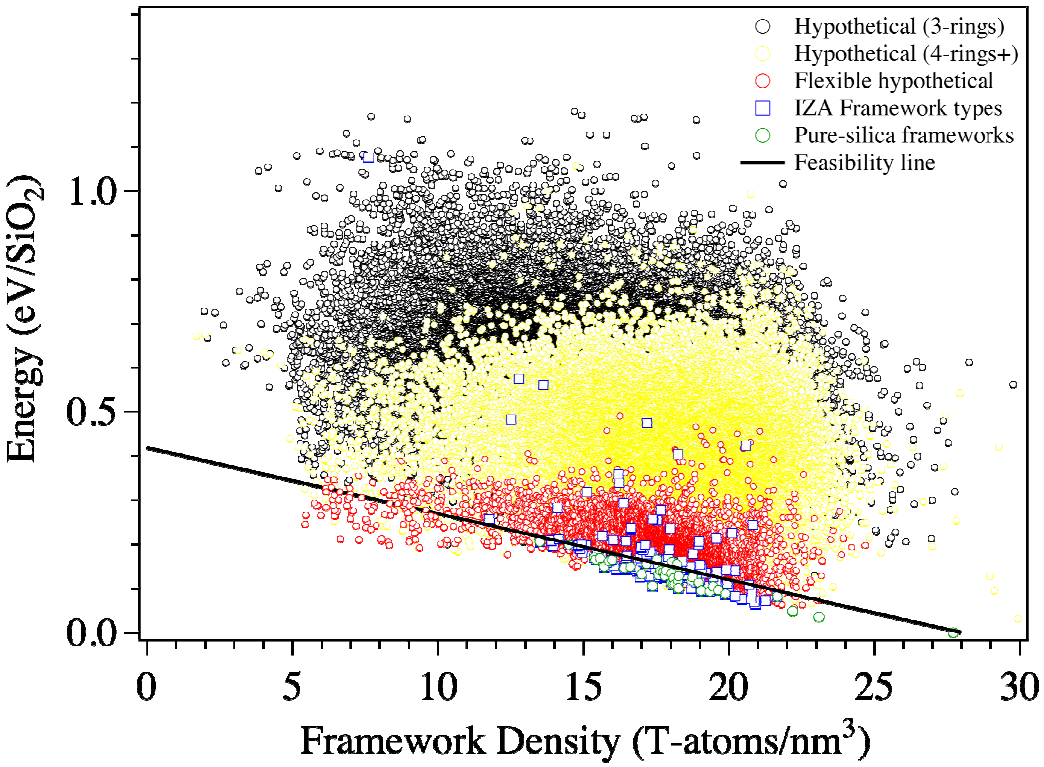

Figure 4.1: Framework energy (relative to quartz, computed with the Sanders-Leslie-Catlow (SLC) potential in GULP) versus framework density. Black points are for all hypothetical frameworks with mBGB energy below 0.01 eV/T-atom. Yellow points are for the subset of hypothetical frameworks that do not have 3-rings. Red points are for the flexible frameworks. Blue points are for the IZA-approved framework types. Green points are for frameworks that can be realized as pure silica. The Points corresponding to IZA approved framework types and pure-silicates are superimposed. Also plotted is the feasibility line of Simperler et. al. Flexible hypothetical frameworks tend to exist closer to the feasibility line.

There is a strong correlation between low SLC energy and framework flexibility as shown in Figure 4.1. In fact, the majority of flexible hypothetical structures (red points) have an energy less than 30 kJ/mole (0.311 eV/SiO_2), although several lie in the high-energy region, including a number of known framework types (the blue hollow points). As expected, hypothetical structures containing 3-ring formations tend to have

higher SLC energies, though the presence of 3-rings does not necessarily present a disadvantage from a flexibility perspective. For this reason, the flexibility criterion may be the preferable measure for evaluating the feasibility of frameworks that contain 3-rings.

Comparison with energy-based criteria

It is instructive to compare results based on SLC energy calculations and the flexibility criterion. A total of 16,317 structures in the starting data set of 117,570 have anSLC energy below 30 kJ/mole SiO_2. Of these, 6,962 (43%) were found to be flexible. Most known framework types found in the database (75%) were both found to be flexible and have an SLC energy less than 30 kJ/mole SiO_2. 17% have a low SLC energy, but were not found in our flexible set, while 6% were found to be flexible, but have a high SLC energy. Two framework types (**OSO** and **NAB**) have a high SLC energy, and were missed by the restricted flexibility calculation. We conclude that energetic comparisons and flexibility calculations are complimentary techniques for determining the realizability of a given hypothetical framework type.

In addition to low-energy framework types, the flexibility criterion seems to also identify framework types that have been realized only in exotic compositions (for which it is often difficult to accurately compute the framework energy). As a case in point, the recently approved framework types **JST** (205_2_60908) and **NPT** (200_2_571), with high SLC energies of ~0.56 eV/SiO_2 and ~0.43 eV/SiO_2 respectively, were each found in the set of 11,647 flexible hypothetical structures before their discovery as real materials.

Both of these structures contain 3-rings, which as noted earlier, likely makes the flexibility criterion the preferable measure for feasibility in these cases.

Structural characteristics of flexible hypothetical zeolites

A useful measure of framework porosity is the diameter of the largest sphere that can either occupy the empty regions of the zeolite structure (the "maximum included sphere diameter") or diffuse freely throughout the network channel openings (the "maximum free sphere diameter"). These quantities are calculated using a Delaunay triangulation technique outlined in previous studies.[77] Currently, the calculation is applied on a large supercell of the structure in question, but another implementation is being developed that accounts for periodicity.

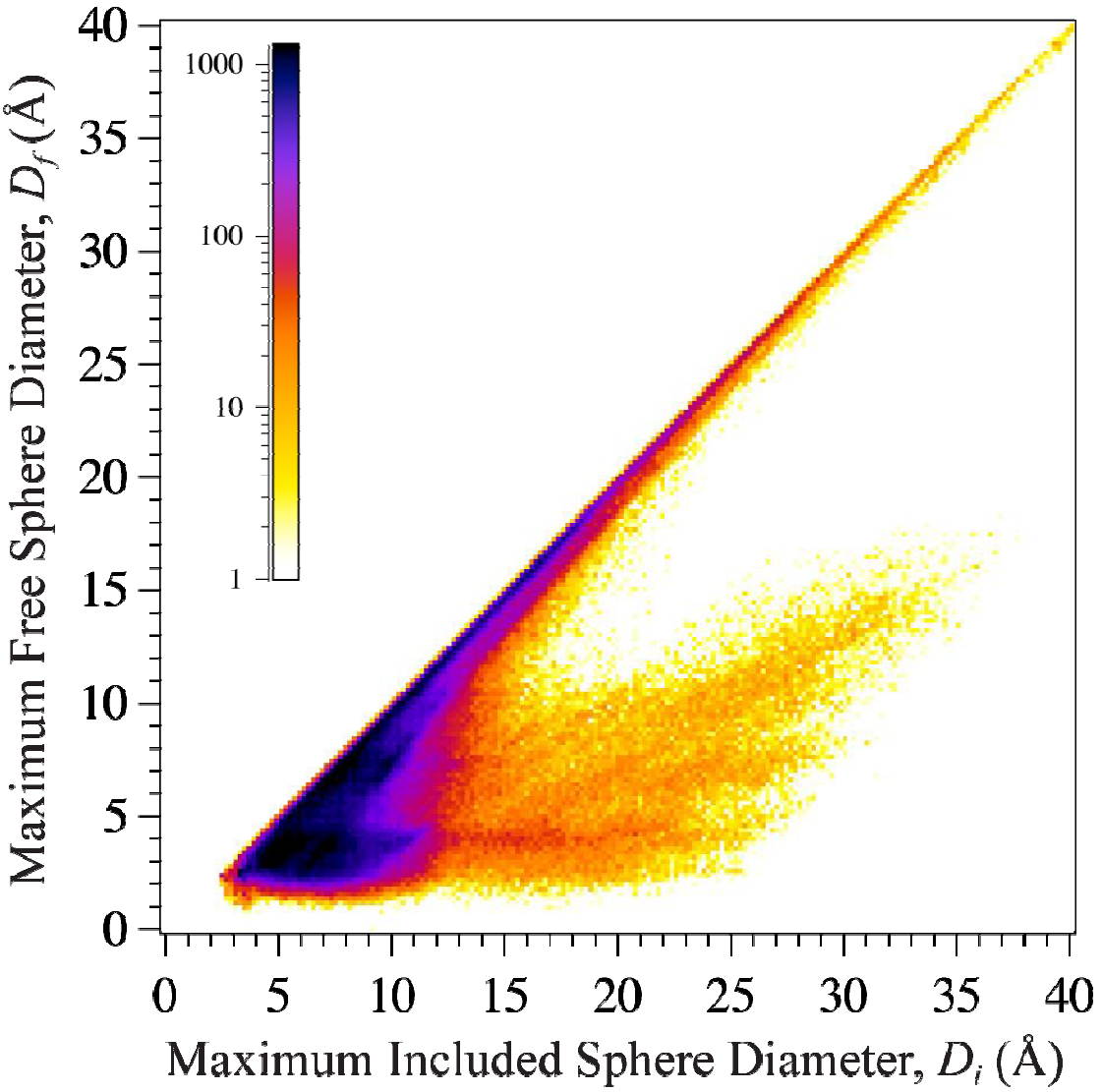

Figure 4.2: Comparison of the maximum freesphere diameter, D_f, against the maximum included sphere diameter, D_i, for the full set of low-energy hypothetical zeolite frameworks (117,570). The intensity scale is logarithmic, and the pixilation is in 0.2 Å increments. Most of the frameworks are concentrated in the range $3\text{Å} \le D_i \le 12\text{Å}$. The strong diagonal line represents straight-walled channel frameworks where $D_f \approx D_i$. The region $D_f < D_i$ represents those nodular frameworks with cavities significantly larger than the openings into them.

Figure 4.2 shows the maximum included sphere diameter, D_i, plotted against the maximum free sphere diameter, D_f, for all 117,570 low-energy hypothetical zeolites.

Although most frameworks lie in the region $D_f < D_i$, the strong diagonal trend, where $D_f \approx D_i$, represents those frameworks that have straight-walled channels. There are two horizontal bands appearing on this plot (and especially visible in Figure 4.3) that correlate with those frameworks whose minimum restricting apertures are dominated by 6-rings, 8-rings and elliptical 10-rings (freespheres of ~3–4 Å diameter), and 12-rings (freespheres of ~7Å diameter).

Similar data for a subset of 5,824 flexible hypothetical structures with only 4 member rings and greater is presented in Figure 4.3a as a set of contour lines, over a smaller range of diameters. Data points for 197 approved zeolite structures are superimposed as solid dots. The Framework Type codes for a subset (chosen as representative of the larger data set) are presented in Figure 4.3b, which allows the contour lines to be seen more clearly. The vast majority of flexible hypothetical structures have small pores, although several structures accommodate similar-sized spheres to industrially important zeotypes as indicated in Figure 4.3b.

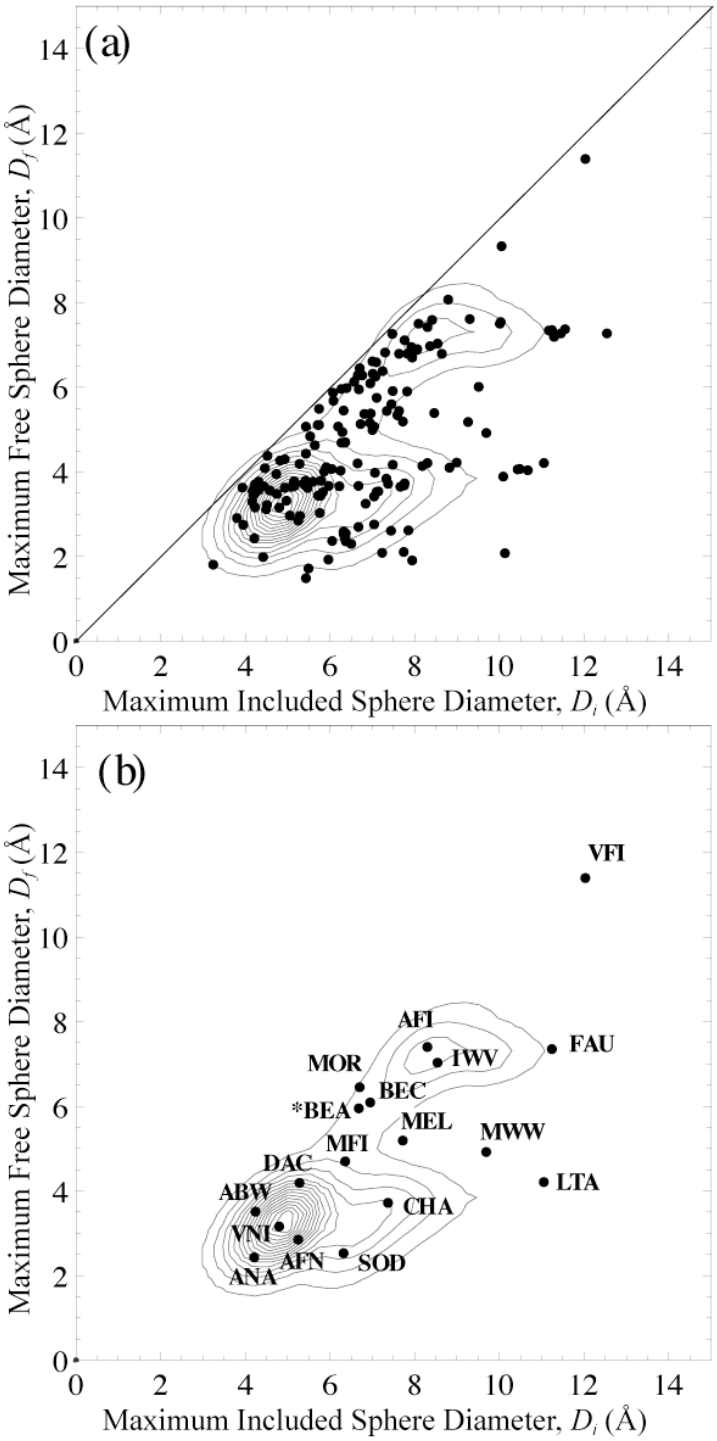

Figure 4.3: A two dimensional histogram of maximum included sphere diameter versus the maximum free sphere diameter for 5,824 flexible hypothetical zeolites with (a) data for experimentally known framework types (assuming pure SiO_2 composition) superimposed as solid dots and (b) with a subset of the approved framework types labeled. The contour lines represent increments of 0.0125 1/Å^2.

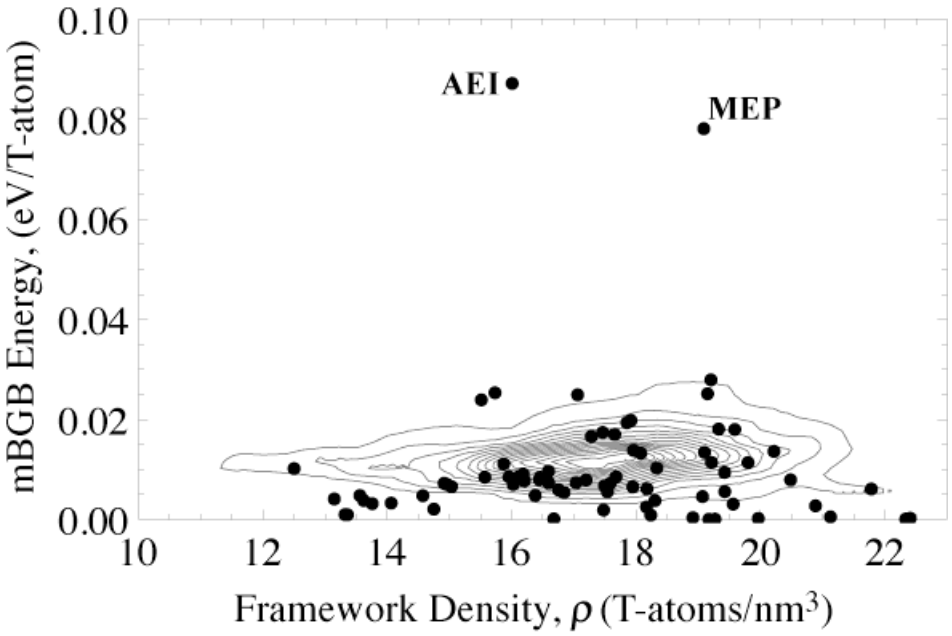

Figure 4.4: Framework density is plotted versus energy (mBGB) for all 5,824 flexible hypothetical structures, shown as a contour plot. The solid dots represent the 78 known flexible framework types found in the database. The contour lines correspond to increments of 1.57 nm^3/eV. The two outliers, **AEI** and **MEP**, have unusually high energies, but are still flexible.

While the mBGB energy cutoff for the original set of 117,570 structures was 0.01 eV/SiO_2, the vast majority of flexible structures had energies less than 0.03 eV/SiO_2, as shown in Figure 4.4, which gives a comparison of energy and density for the flexible subset. This stems from the fact that the mBGB potential is closely related to the ideal zeolite cost function, so structures with low mBGB energy are more likely to be realizable with perfectly regular tetrahedra. However, several known zeolites (e.g. **AEI**, **MEP**, and **RWY**) have an mBGB energy higher than 0.03 eV/SiO_2, although each of these is flexible.

Conclusion

While this set of flexible hypothetical zeolites represents an important starting point, it is clear that a more expansive search is needed to identify additional flexible structures from the larger set. The most advanced approach for relaxing hypothetical structures involves using the ideal zeolite potential in GULP with the RFO optimization method, as described in chapter 2, and this is preferable to the approach used previously. It will be advantageous to begin the search, as before, with the lowest energy hypothetical structures.

We see that flexibility is not only present in all realized zeolite frameworks, but that it can be used to simplify the search for viable hypothetical structures. The flexibility indicator is shown to be neither overly inclusive nor overly exclusive in identifying feasible zeolites, thus rendering it an effective and useful discriminating criterion.

The following chapter will explore the energy profile of the Si-O-Si and Ge-O-Ge angles across the flexibility window of cristobalite, thus demonstrating additional applications of the flexibility model.

Chapter 5

ENERGY DEPENDENCE OF THE T-O-T ANGLE

In the ideal zeolite model used to define the flexibility window, constraints on the T-O-T angle are ignored as the tetrahedral vertices are treated as force-free spherical joints. However, in real zeolite materials, T-O-T angle preferences play a more significant energetic role than was previously thought. Thus, the ideal zeolite model ignores an important, subtle, contribution to the framework energy. While the Si-O-Si angle has been studied extensively, particularly in recent years,[3,5,44,78,79] less work has been done on the Ge-O-Ge angle,[3,5] likely related to the fact that Germania-based zeolite materials are rare in nature. In fact zeolite materials containing germanium are a relatively recent phenomenon, and the first germanium-containing zeolite ASU-7 (**ASV**) was reported in 1998 by Yaghi et. al.[80]

Earlier work used cluster models, i.e. molecules, to study the Si-O-Si and Ge-O-Ge angles [3,5] which represent an idealization of the highly constrained, periodic crystalline networks of real materials. To date, no one has studied the energy dependence of the T-O-T angle using a crystalline model. However, the cristobalite framework is an ideal candidate for such a study as it is the only tetrahedral framework (known or hypothetical) that can maintain perfectly regular tetrahedra through the entire possible range of T-O-T angles, 0°–180°.

The geometry of *I*-42*d* cristobalite and *I*-43*m* SOD

In tetragonal *I*-42*d* symmetry, the cristobalite framework can be realized with perfectly regular tetrahedra over T-O-T angles ranging from 180° down to 0°, where the

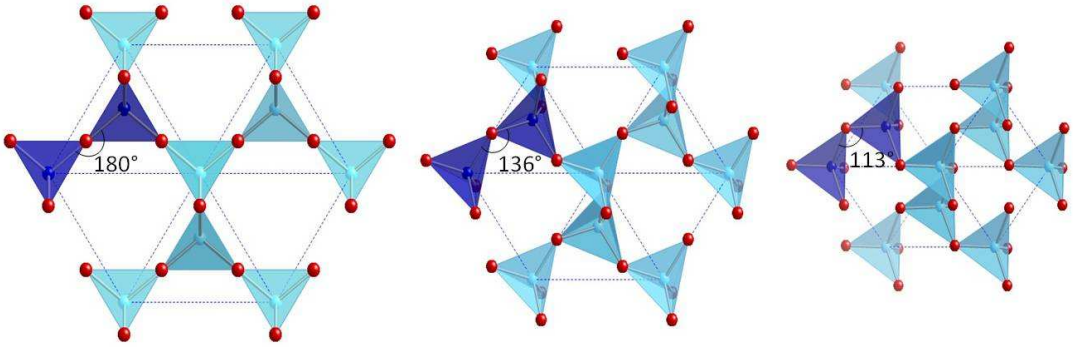

Figure 5.1: The progression of the symmetry-preserving fold for *I*-42*d* cristobalite used for the VASP calculation of the energy dependence of the T-O-T angle. The T-O-T angle between the two darker tetrahedral units is labeled. Cristobalite can maintain perfectly regular tetrahedra over the entire range of T-O-T angles in this symmetry. Each structure is viewed from in the [1 1 1] direction.

framework collapses on itself – that is, every tetrahedron overlaps. The T-O-T angle depends explicitly on the *x* coordinate of the single unique oxygen atom according to the formula $\theta = \cos^{-1}(\frac{16x^2-3}{48x^2+3})$.[81] All other coordinate values are fixed by the symmetry, i.e. $\overrightarrow{\mathbf{r_O}} = (\mathrm{x}, \frac{1}{4}, \frac{1}{8})$ and $\overrightarrow{\mathbf{r_T}} = (0, 0, 0)$. The ratio of the cell lengths is also dictated by *x* i.e. $\frac{c}{a} = \sqrt{2 + 32x^2}$ and the distance between intra-tetrahedral oxygen atoms is $\alpha = \sqrt{4x^2 + 1/4}$.[81] The T-O bond distance d is related to α by a multiplicative factor dictated by the tetrahedral geometry i.e. $d = \sqrt{\frac{3}{8}}\alpha$. Thus, given a chosen bond length, the T-O-T angle is the single degree of freedom in the system. Figure 5.1 shows several configurations along the *I*-42*d* symmetry-preserving fold for cristobalite.

The **SOD** framework of sodalite can be similarly represented in *I*-43*m* symmetry where the T-O-T angle $\theta = \cos^{-1}(\frac{48x^2-24x+2}{48x^2-24x+3})$ and the coordinates of the unique atoms given by $\overrightarrow{\mathbf{r_O}} = (\mathrm{x}, \mathrm{x}, 1 - \sqrt{\mathrm{x}^2 - 1/8})$ and $\overrightarrow{\mathbf{r_T}} = (\frac{1}{2}, \frac{1}{4}, 0)$. The cell edge length a fixes the

T-O bond distance by $a = \sqrt{\frac{16}{3}}\frac{d}{4x-1}$. The tetrahedra remain perfectly regular through $\theta = 160.529^o$ where $= \frac{1}{\sqrt{8}}$. Larger values of x result in a non-realizable structure where the z coordinate of the oxygen atom is an imaginary number.

Three additional topologies (quartz in $P3_221$, tridymite in *Ama*2 and **BCT** in *Imm*2) can be realized with regular tetrahedra over a smaller range of T-O-T angles. **SOD** and **BCT** contain 4-membered rings in addition to 6-membered rings which are present exclusively in the cristobalite, quartz and tridymite frameworks. For these three framework types, configurations with regular tetrahedra and a fixed T-O-T angle were found by placing harmonic constraints on the T-O-T angle in the ideal zeolite cost function (enforcing regular tetrahedra) to force all the T-O-T angles to a single value. The study of diverse framework types allows us to determine whether or not important features of the energy profile of the T-O-T angle vary for different ring distributions and topologies.

Ab initio calculations on the T-O-T angle

Energy calculations were performed in the Vienna Ab-initio Simulation Package (VASP)[82] using a potential form based on the generalized gradient approximation (GGA) with the projector-augmented wave (PAW) method. Additional calculations using the local-density approximation (LDA) and ultrasoft pseudopotential (USP) methods were also performed. The *I*-42*d* cristobalite structure was optimized in each potential (with all parameters allowed to vary, ISIF=3) to obtain a preferred bond length. Idealized structures with this bond length were then generated over a wide spectrum of T-O-T

angles, ranging from 114° up to 180°. Using these structures, the energy dependence of the T-O-T angle was probed by two methods: (1) single point calculations of energy for each fixed T-O-T angle (i.e. the electron energy was optimized, but all other degrees of freedom, including the ion positions were held fixed) and (2) allowing relaxation with fixed fractional coordinates (ISIF=6), thus holding the T-O-T angle approximately constant.

The flatness and turbulent nature of the energy landscape (as returned by VASP) for both silica and germania cristobalite appeared to thwart standard minimization routines in VASP i.e. optimizations from different starting points invariably resulted in different final configurations, even when all structural parameters were allowed to vary. We observed that starting configurations with larger bond lengths tended to result in final configurations of lower energy, although there was a critical point where inflation of the initial structure became counterproductive. Ultimately, we found that there was little qualitative difference in the normalized energy curves whether the structures underwent optimization (with fixed coordinates) or the energy was obtained by a single point calculation (see Appendix B). Similarly, the use of different potentials appears to have only a small effect on the shape of the energy curves, and the results presented are those obtained from the GGA-PAW potentials. Additional details of the energy calculation may be found in Appendix B.

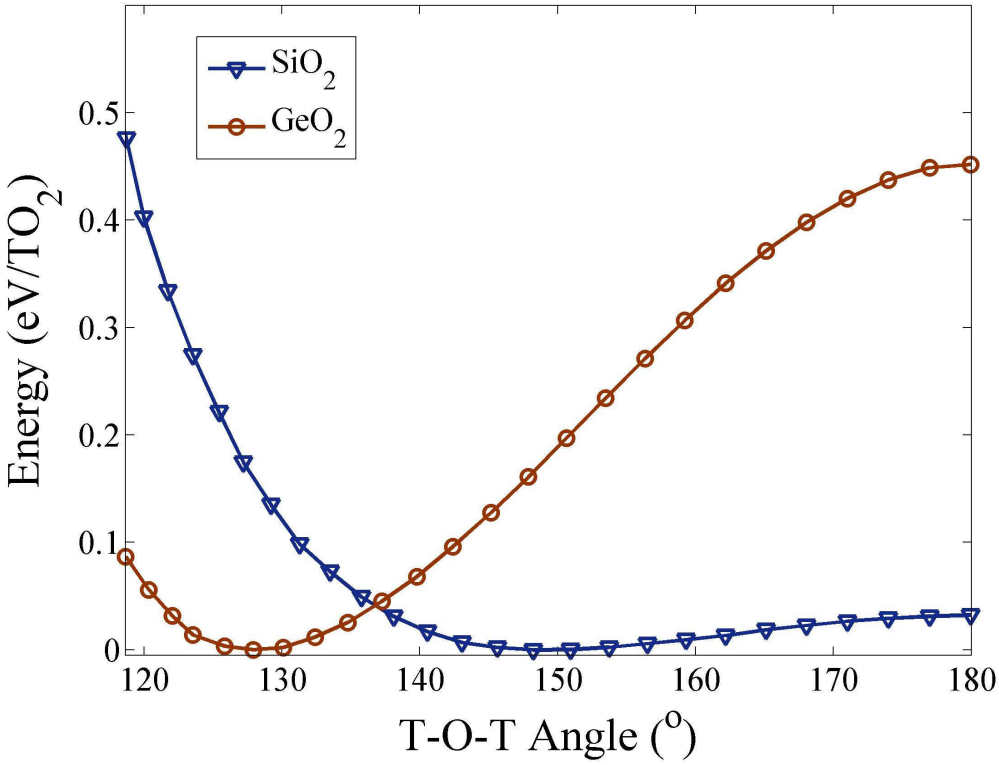

Figure 5.2: Energy dependence of the T-O-T angle for *I*-42*d* cristobalite as silica (triangles) and germania (circles). The curve for germania was obtained by incrementally increasing the initial bond length in VASP until the minimum final energy was found. The curve for silica was obtained by feeding in initial coordinates with a bond length of 1.92Å. Silica displays a much wider range of feasible angles although the range for germania extends to much lower values. The narrow range of feasible angles may explain the dearth of germania materials as compared to silica.

The energy dependence of the T-O-T angle differs dramatically for silica and germania cristobalite as shown in Figure 5.2. There is a steep energy penalty for angles greater than ~145° in germania whereas the curve for silica remains relatively flat over this range. In fact, we find a much greater energy penalty for large angles in germania when compared with earlier calculations performed on cluster models. This is

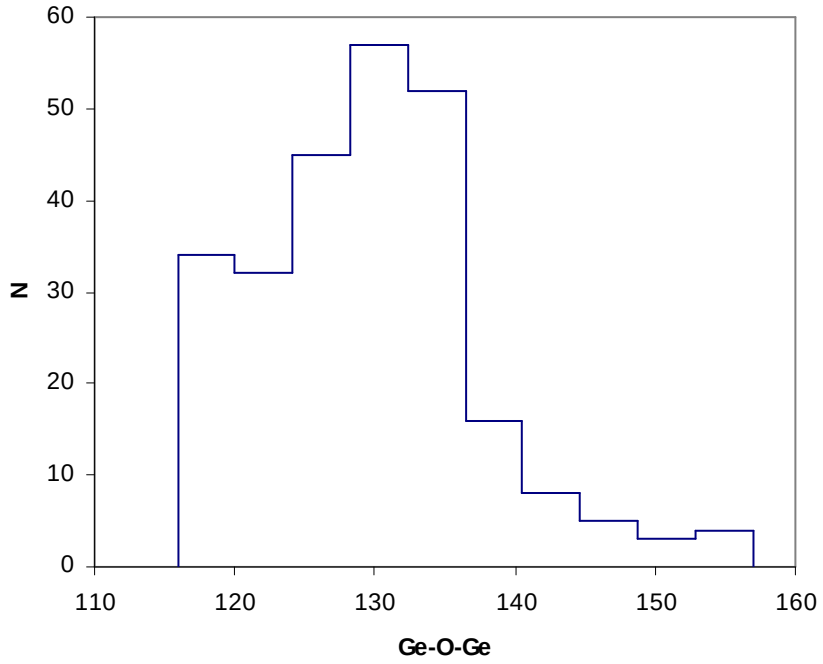

Figure 5.3: Distribution of Ge-O-Ge angles for a wide range of germania materials, including some that contain T-atoms other than germanium. There is a sharp drop-off in angles larger than ~137°, corresponding with the strong energy penalty observed for larger angles in germania. Figure courtesy of Rebeca Sanchez-Smith.

presumably due to additional constraints imposed by the full lattice model as compared to the loosely constrained clusters and is consistent with the distribution of Ge-O-Ge angles in real germania materials as shown in Figure 5.3. The histogram shows a sharp decline in angles greater than ~135° and no angles greater than 157°, consistent with a steeper curve.

Figures 5.4 and 5.5 show a comparison of energy vs T-O-T curves for the various framework types for which all T-O-T angles can be made equal over an appreciable range without tetrahedral distortion. All energies were obtained by single point calculations on structures with regular tetrahedra and a fixed bond length ($d_{Ge-O} = 1.785$ Å and

$d_{Si-O} = 1.622$ Å). There is strong overlap between the various energy curves for both silica and germania, although both forms of quartz show a steeper onset of the energy

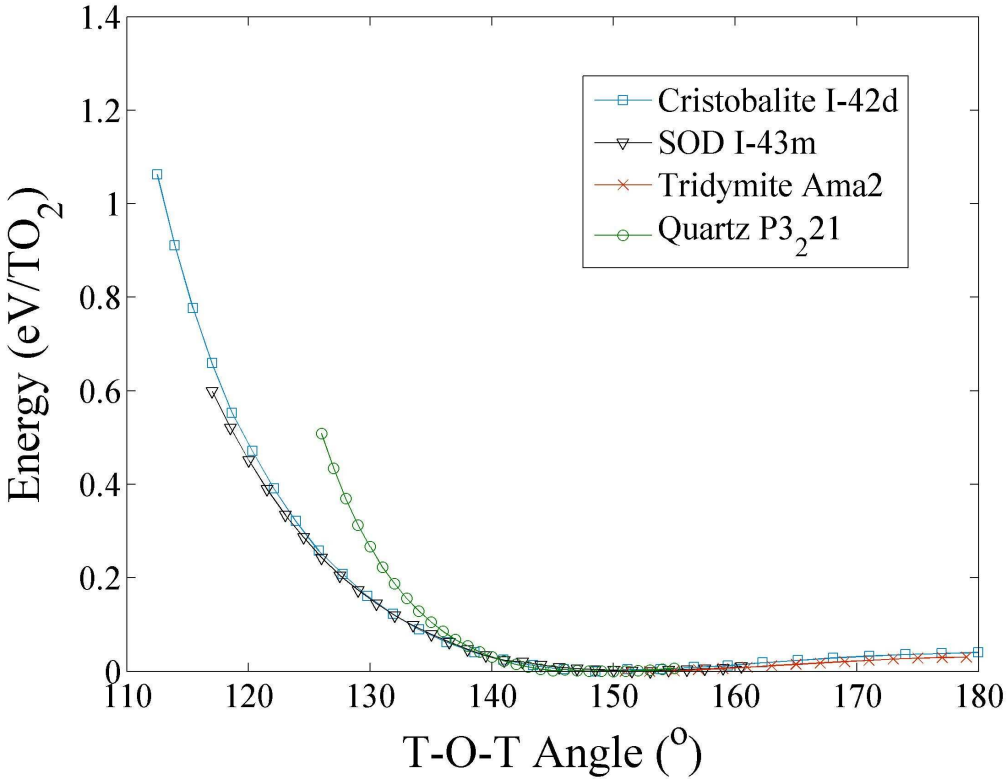

Figure 5.4: Energy dependence of the T-O-T angle for several framework types (represented as silica) in which all T-O-T angles can be fixed to a single value over a wide range. Each data point represents a single point energy calculation for structures with perfectly regular tetrahedra and an Si-O bond distance of $d_{Si-O} = 1.622$ Å .

penalty at low angles. This is likely due to coulombic repulsion [83] which becomes significant for the higher densities at which quartz exists. The agreement between the energy curves for different framework types demonstrates that the energy dependence of the T-O-T angle is relatively independent of other structural constraints.

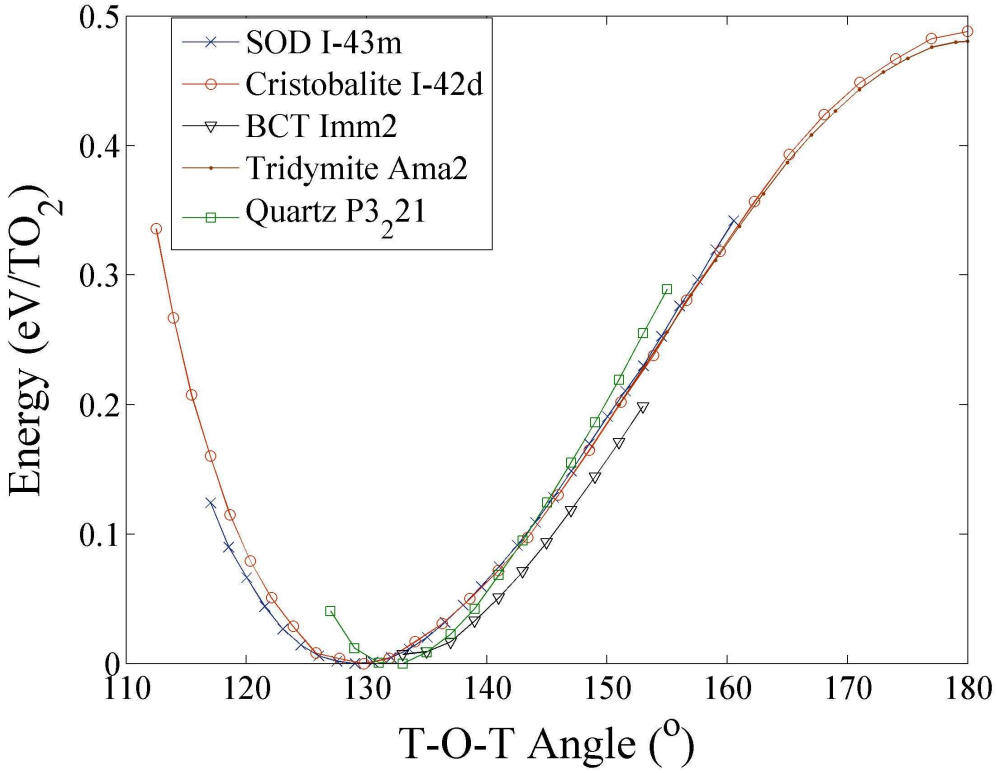

Figure 5.5: Energy dependence of the T-O-T angle for several framework types (represented as germania) in which all T-O-T angles can be fixed to a single value over a wide range. Each data point represents a single point energy calculation for structures with perfectly regular tetrahedra and a Ge-O bond distance of $d_{Ge-O} = 1.785$ Å .

Tridymite in *Ima*2

It is reasonable to assume that silicates adopt a structure that maximizes symmetry while maintaining Si-O-Si angle preferences as much as the structure allows. However, the material tridymite represents a strange case where the experimentally determined structure seems to thwart both of these assumptions. Low-temperature tridymite is reported to adopt *C*1*c*1 symmetry with Si-O-Si angles ranging from 143.3° to 176.5° (with a mean value of 149.5°).[84] However, a higher symmetry version of tridymite has

been found in orthorhombic *Ima*2 symmetry (also noted by Pryde and Dove),[85] where all the T-O-T angles can be made approximately equal down to the apparent preferred range in silica. It is puzzling that tridymite does not adopt this symmetry considering that the lower energy silica polymorphs quartz and cristobalite both adopt a symmetry where all T-O-T angles can be made equal close to the preferred Si-O-Si angle. The structure of tridymite thus presents an intriguing case that may provide clues about additional factors that drive atomic arrangements in silicates.

Conclusion

It has been shown that the T-O-T angle preference is far more restrictive in germania than in silica. In fact, the wide range of viable T-O-T angles in silica provides additional physical justification for the ideal zeolite model in the proper regime (angles greater than ~135°).

It was in examining T-O-T angle ranges in flexible hypothetical zeolites that structures with astonishingly low densities (but also with viable Si-O-Si angles) were discovered. In the next chapter these materials are characterized and evaluated based on the various feasibility characteristics identified up to this point, thus providing a culminating synthesis of the various ideas and methods presented in this thesis.

Chapter 6

LOW-DENSITY ZEOLITES ASSEMBLED FROM SILICA BI-LAYERS

The search for novel zeolite materials with large pores and corresponding internal volume and surface area is ongoing. While very low-density zeolite materials have been synthesized, most are nonviable on an industrial scale due to low-silica or non-silica compositions. Here we present the lowest density hypothetical zeolites ever discovered that exhibit all known feasibility characteristics for silicates.

In this discussion we use 3-letter *lowercase-bold* codes to represent framework types, following a convention adopted in the *Reticular Chemistry Structure Resource* (RCSR).[86] Although this nomenclature is deliberately similar to the *uppercase-bold* system used by the IZA, it is not a part of that IUPAC nomenclature standard.

Double-layer silicates (DLS)

The two-dimensional analog to tetrahedral frameworks is networks of corner-connected triangles. One such pattern is the honeycomb lattice, which is characterized by six-ring formations. Similar to 2-D zeolites, silica bi-layers are formed by two identical 3-coordinated single layers joined by fourth links to form one double layer. Thus, the basic unit in the bi-layer is two SiO_4 tetrahedra sharing a single vertex along a mirror plane with a T-O-T angle of ~180° (Figure 6.1a). The three remaining vertices bridge to other units to form double-ring structures with mirroring layers (Figure 6.1b). Any in-plane ring distribution is possible provided there is an average ring size of 6.[87] Another layer with glide symmetry is found in hypothetical materials proposed earlier by Smith

and Dytrech,[1] (Figure 6.1c) but has a higher energy than layers containing mirror symmetry (Table 6.1).

Figure 6.2 shows several models of silica bi-layers as viewed into the layer wall. While the lowest-energy bi-layer contains only 6-rings (**hna**, in the RCSR nomenclature system), there are several other bi-layer models containing combinations of 5, 6, and 7 ring formations with only slightly higher energy (Table 6.1). The presence of 3 and 4 rings leads to higher energies, as is evident for **hnb**, **hne**, and **hni**. While only a few models are presented here, the possibilities for crystalline silica bi-layers are theoretically endless.

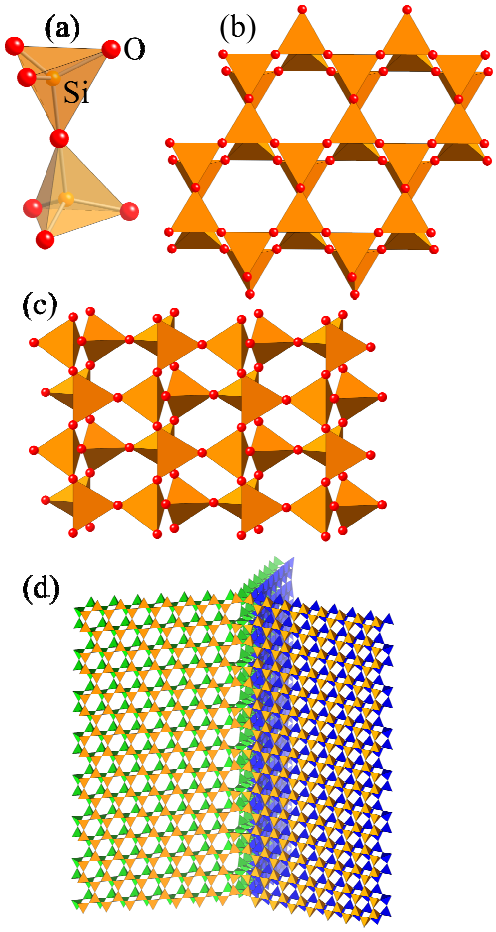

Figure 6.1: (a) The Si_2O_7 unit on which silica bi-layers are based with silicon atoms at the tetrahedral centers and oxygen atoms (small spheres) at the vertices. The T-O-T angle across the connecting oxygen atom is approximately 180°. (b) A double 6-ring formed by connecting six of the units shown in (a). The top and bottom layer are mirror images of each other. Crystalline bi-layers are constructed by connecting series of double ringed units in repeatable patterns. (c) Bi-layers of the type described by Smith and Dytrych [1] where the two halves are related by a glide operation. (d) Illustration of how three bi-layers can be merged seamlessly along a crease (or backbone) to form the beginnings of a 3D channel structure.

Structure	2-D Density (T/nm^2)	Energy (eV/T)	Rings
hna	16.84	0.2204	6^3
hnb	14.35	0.5747	3.9
hnc	16.69	0.2632	$5^4.7^4$
hnd	16.62	0.2408	$5^4.6^2.7^4$
hne	16.29	0.2846	$4^2.7^4$
hnf	16.67	0.3020	$5^4.7^4$
hng	16.37	0.2622	$4^2.5^4.6^4.7^4.8^2$
hnh	16.19	0.2607	$5^4.8^2$
hni	15.39	0.3162	4.8

Table 6.1: Structural information for standing silica bi-layers pictured in Figure 2. Included is a *de facto* two-dimensional framework density, defined as the number of T-atoms per unit area (since the dimension normal to the layer face is arbitrary), the energy (SLC) of the layer relative to that of low quartz, and the ring distribution. As a comparison, the layer of Smith and Dytrych with glide symmetry has an energy of 0.3269 eV/T-atom.

Very low-density structures are constructed by splicing bi-layer walls together (Figure 6.1d) to form large, one-dimensional channel structures. Various types of 'backbone' structures form at the wall intersections where the bi-layer channel edges split, with each half bending to form half of the adjacent edge (Figure 6.1d). In principle, these channels can take almost any shape, but it appears that the lowest-energy varieties have hexagonal pores. Several such structures were analyzed by Bell and Zwijnenburg and were found to be energetically stable.[48]

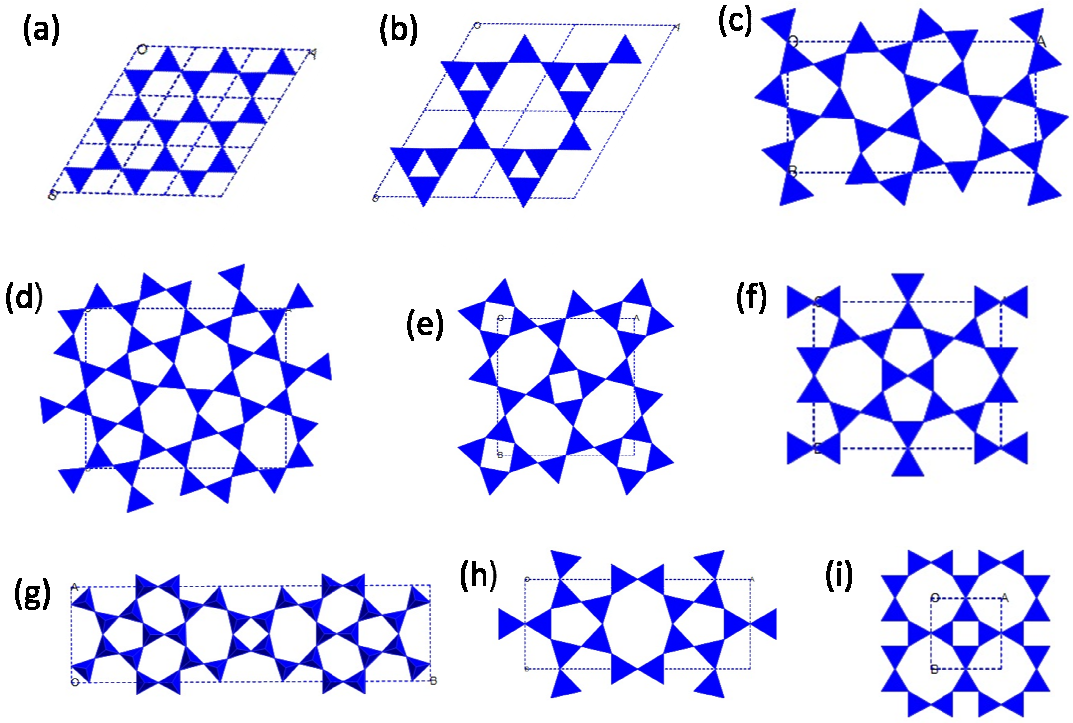

Figure 6.2: Bi-layer models listed in Table 1, including (a) **hna**, (b) **hnb**, (c) **hnc**, (d) **hnd**, (e) **hne**, (f) **hnf**, (g) **hng**, (h) **hnh**, and (i) **hni**. These are some of the possibilities that can act as the interior bi-layer wall structures of low-density DLS zeolites.

DLS-based zeolite families

In the following, several families of closely related structures are presented, each based on a "parent" structure whose pore walls are of the minimum possible width for that particular bi-layer topology. Additional vertices can be added, effectively lengthening the channel edges and in effect, decreasing the framework density.

The first family we analyze is based on the parent structure **fwz**, or191_2_27 (191 is the space group number, 2 is the number of unique T-atoms, and 27 is the somewhat arbitrary graph number used to identify the hypothetical zeolite structure) in the APZS database.[47] Additional members of this family, which occur in space group *P*6/*mmm* can

be formed by extending the repeatable unit in the channel walls, and are assigned the type codes **tdc** (191_3_495, see Figure A.3 in Appendix A), **tdd** (191_4_9370), **tde** (191_5_189679), etc. (Note that, here, the last letter in the 3-letter code has been chosen to indicate the number of crystallographically-unique T-atoms that occur in the framework; thus b=2, e=5, i=9, etc. The first two letters are the same for all members of a given family of frameworks.)

There is a set of structural analogs to this family in space group $P6_3/mmc$, where the connections of the wall to the backbone are counter-aligned from those seen in the original set. Each member of the "**td*** family" thus has a counterpart in $P6_3/mmc$ with the same number of unique T-atoms, but a slightly different structure, e.g. 194_3_189 for **tdc**

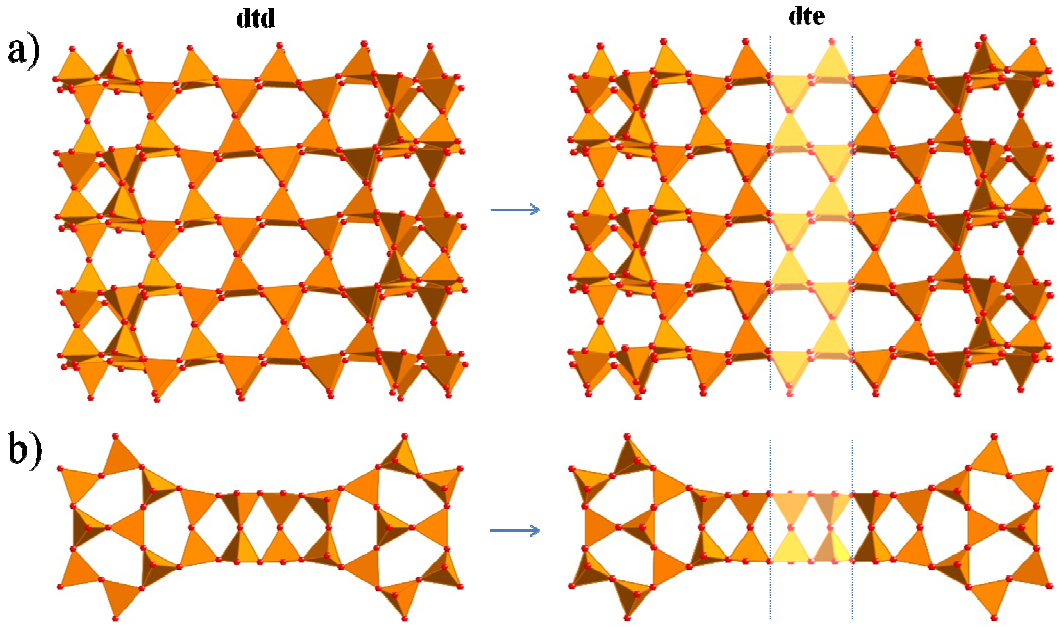

Figure 6.3: (a) An example of wall extension from **dtd** (left) to **dte** (right) as viewed in the [110] direction, facing the bi-silicate wall that forms the channel edges. The interposed section of the repeatable unit is highlighted on the right. (b) The same extension viewed in the [001] direction.

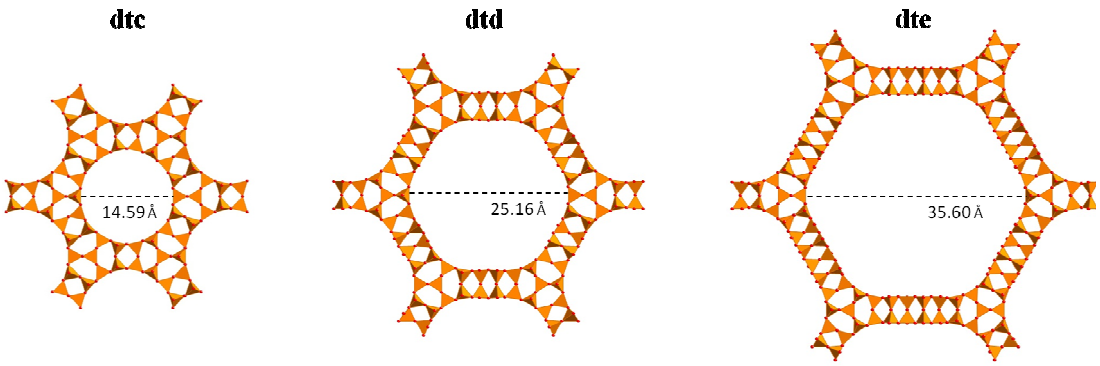

Figure 6.4: The progression in pore size for the **dt*** family as the bi-layer walls forming the cavity edges are extended.

and 194_4_6238 for **tdd**. As expected, the energies of these structures fit along the energy vs density curve for the **td*** family (Figure 6.5).

Another family is based on the parent structure **lon** (194_1_2), which is the framework of tridymite. The first few members of this family are assigned the type codes **dtc** (194_3_2579), **dtd** (194_4_104161, see Figure A.2 in Appendix A), and **dte** (194_5_4713570). Figures 6.3a and 6.3b show how the wall is extended in the progression from **dtd** to **dte**. In principle, this process can be carried out *ad infinitum*, although there are likely limitations in mechanical stability for very low-density structures. As the walls are extended, the pore diameter also increases, as shown in Figure 6.4 for the **dt*** family of frameworks.

There exist several closely related structures with a similar backbone to the **dt*** family, but slightly different patterns in the connections to the wall, including e.g. 191_5_405006, 191_5_405009, and 194_5_4713569. Although structures in the **dt*** family do not exhibit a flexibility window in high symmetry, in lowered *P*1 symmetry,

they are flexible and represent additional low-energy families that compete favorably with the **td*** family (for example, 191_5_405006 in Figure 6.5).

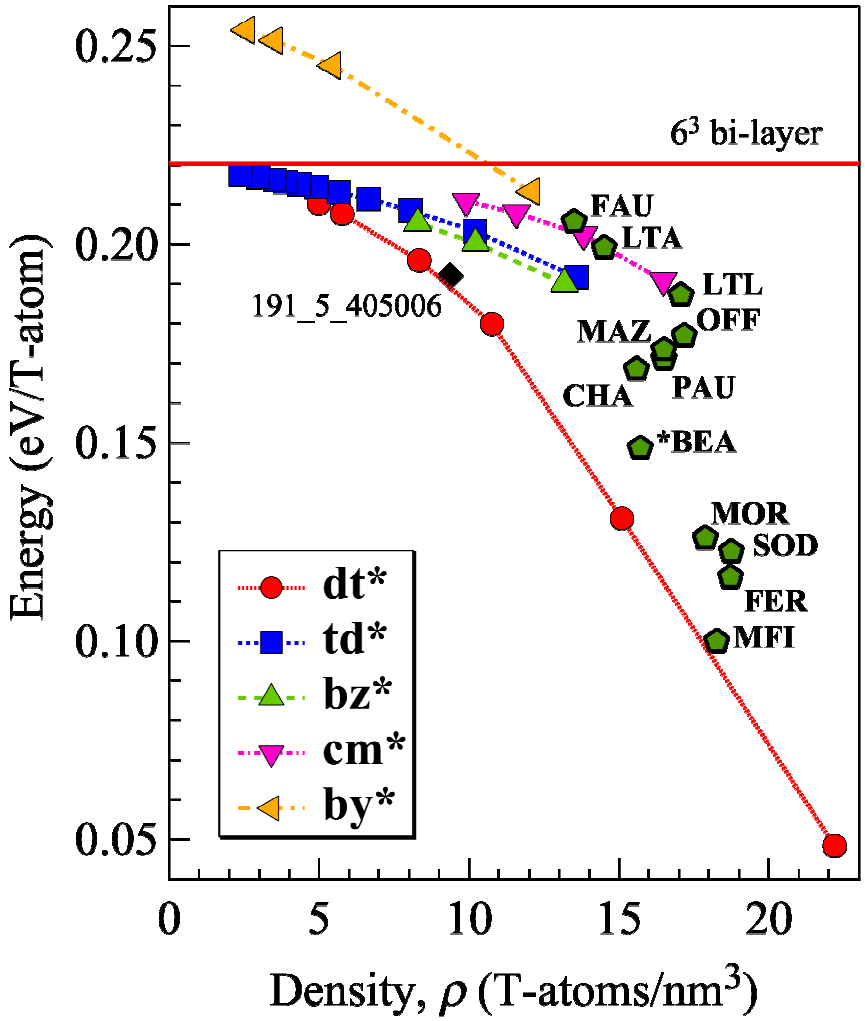

Figure 6.5: Energy per T-atom versus density, ρ, for five families of low-density, layer-based zeolites. Energies are measured relative to quartz using the SLC potential. Since the low-density frameworks are dominated by the bi-layer structure, the incremental energy cost as density decreases is low and the curves flatten out. The energies and densities of several well-known zeolite frameworks (as pure silicates) are given. The horizontal line is the energy of the simple 6^3 bi-layer. All of the mirror-symmetric bilayers tend towards this value, 0.2204 eV/T-atom, at zero density. A point for framework 191_5_405006 from the APZ database is included to show that other DLS topologies can come close to the low-energy/low-density **dt*** line.

In presenting the crystal structure of zeolite L (framework type code **LTL**) Barrer and Villiger proposed several hypothetical structures, one of which contained hexagonal

pores formed by intersecting DLS walls of double 6-rings.[46] This structure is assigned the type code **bbz** in the RCSR database and can also be found in the APZS database as 191_2_37 (see Figure A.4 in Appendix A). Because of the orientation of the 6-ring structures in the bi-layer wall, this family includes only members with even numbers of unique T-atoms. The first member of this family is assigned the type code **bzd** (191_4_29981), corresponding to 4 unique T-atoms. As with the **td*** family, a group of energetically similar structural analogs exists in $P6_3/mmc$, the first of which is 194_3_3784.

It is also possible to conceive structures with square and rectangular shaped pores. One such family in space group $P4/mmm$ is based on **fte** (123_2_13), and maintains square pores as the walls are extended. The first two members of this family are assigned the type codes **cmc** (123_3_232) and **cmd** (123_4_4324). Closely related, low-energy structural analogs with misaligned walls include 139_5_848159 and 131_5_17314206.

While primarily low-energy structures that exhibit a flexibility window have been presented, there are nearly endless possibilities for the formation of layer-based zeolite structures. Another of Barrer and Villiger's hypothetical structures (referred to as **bby** in the RCSR database, and 191_2_13 in the APZS database) is based on DLS walls made up of 8-rings and two 5-rings [46] and the channel walls can be extended to form yet another structural family, the first member being **bye** (191_6_142373). As expected, the **by*** family converges to a marginally higher energy than each of the families with walls made of 6-rings (Figure 6.5).

Channel wall lengths do not need to obey the axial symmetry. In principle ellipsoidal and rectangular channels can be prepared, extending the wealth of

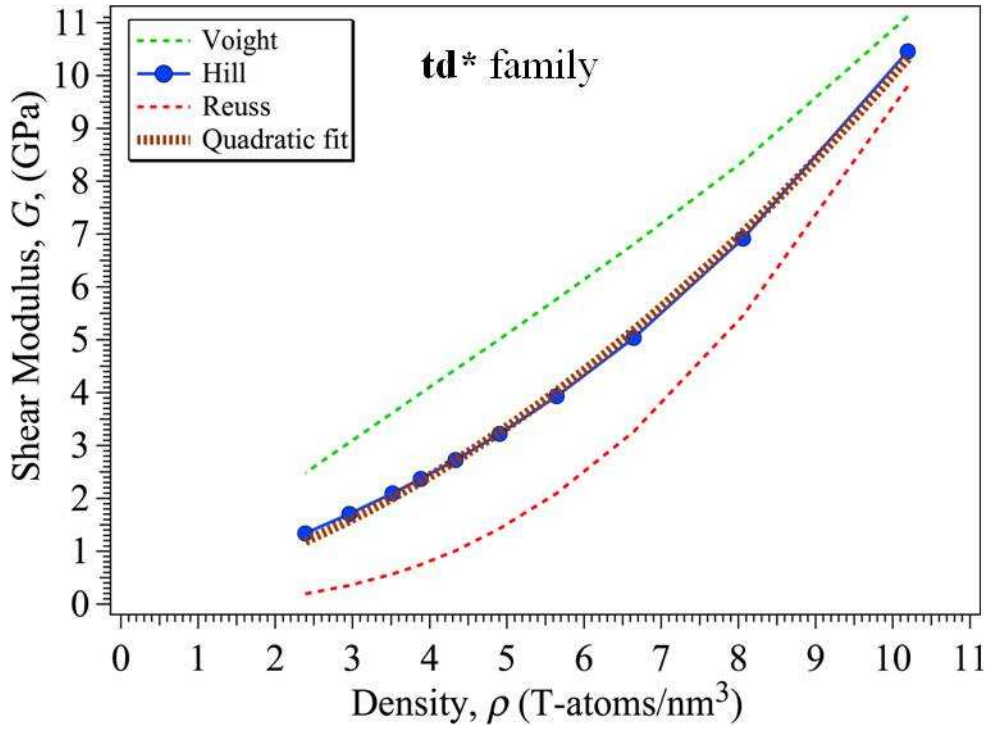

Figure 6.6: Shear modulus, about the c axis, versus framework density for members of the **td*** family. Similar curves are observed for the other families analyzed. The Reuss and Voight conventions represent the lower and upper bounds respectively, whereas the Hill convention is the average of the two. The fit $G \approx \rho(0.34 + 0.066\rho)$ assumes that the shear modulus about the *c* axis is zero at zero

possibilities. As the wall lengths are extended and the energy of the backbone becomes less significant, the lattice energy approaches the expected value of an isolated silica bi-layer with the type of ring pattern observed in the walls (Figure 6.5). As expected, the energy increases with decreasing density, representing the work done in separating charged framework atoms. Asymptotically, the energy converges to that for an isolated bi-layer. There is only a small energy discrepancy between comparable members of various structural families (which vary mostly in the shape of the back bone), particularly at low-density. In practice, a low-density limit will be imposed by the decreasing mechanical stability of the framework. Figure 6.6 shows the evolution of the shear

modulus for the **td*** family as the pore walls are extended as calculated using the Reuss and Voight conventions calculated from the elastic constants using the SLC potential

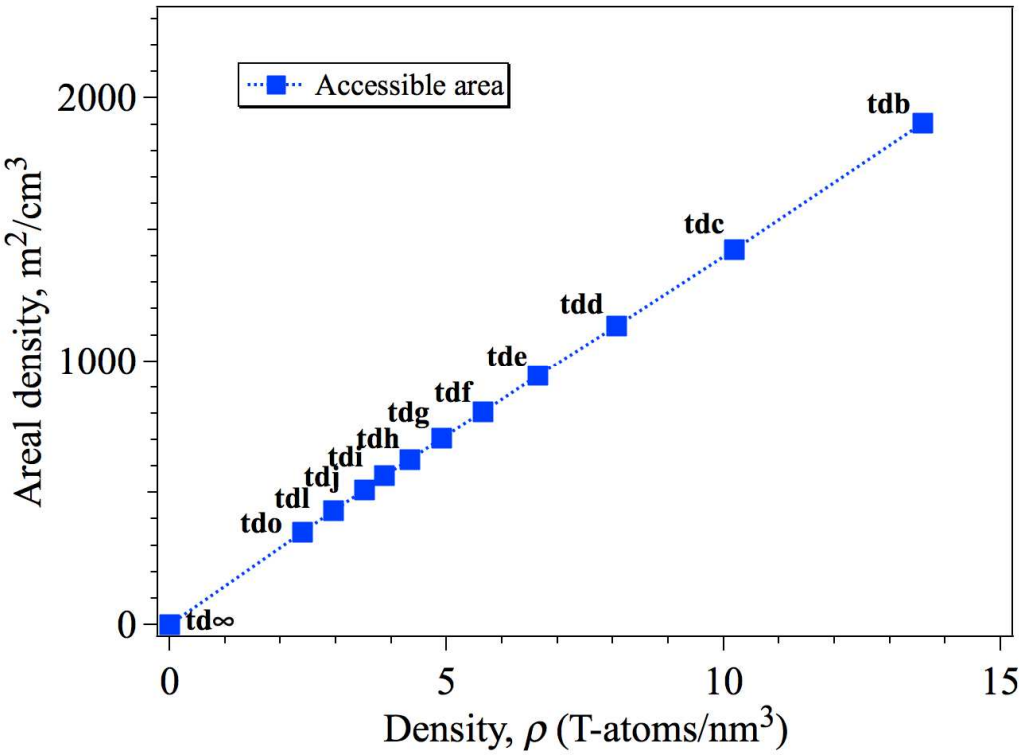

Figure 6.7: Computed accessible area densities (area per unit volume) for the **td*** family of DLS structures. The largest areal density values are for the **tdb** structure, and much of the occupiable area is accessible. This measure is likely more meaningful (for many applications of microporous materials) than the density, which is simply a measure of the proportion of empty space in the material.

(details in GULP manual [53] pages 41-43).

Feasibility characteristics and structural properties

Each of the structures presented exhibits a flexibility window, and all but the **dt*** family, whose starting member **lon** is the tridymite structure, demonstrate extensive growth of flexible modes as with a few select, high symmetry framework types that exist as known zeolites.[88]

Layer-based hypothetical zeolites offer the exciting possibility of materials with very high internal surface area. The planar geometric area for the 6^3 bi-layer is 1190 m^2/g, and the geometric accessible area for a 2.8-Å-diameter probe molecule (i.e. water) increases to 1495 m^2/g when the contributions from the layer corrugations are included. In the **td*** family, the accessible areal density (internal area per unit volume) peaks at the **tdb** structure, 1900 m^2/cm^3 (Figure 6.7), which compares favorably with the best metal-organic framework (MOF) structures, 2200 m^2/cm^3 for MOF-5.[89] Pores can take on many different shapes and sizes, and in theory, could be fine-tuned for a host of useful applications.

Conclusion

We have shown that DLS zeolites meet all known feasibility characteristics, and it is conceivable that materials based on these hypothetical models will someday be synthesized. In fact, the identification of these potentially useful hypothetical zeolites was facilitated by applying known feasibility criteria to the APZS database.

Chapter 7

CONCLUSION

It has been shown that all known zeolite framework types (as well as dense framework silicates) can be represented as comprising perfectly regular tetrahedra. This property has been used to identify potentially realizable zeolite framework types from a set of millions of hypothetical structures. The configuration space over which the constraints corresponding to perfectly regular tetrahedra can be satisfied (termed the *flexibility window*) has been explored and quantified for all known framework types, and additional constraints imposed by T-O-T angle preference have been examined by a first principles calculation. Lastly, an interesting class of hypothetical zeolites assembled from bi-layer sheets have been identified and found to meet all feasibility criteria proposed. There are many possible avenues for future exploration, a few of which will be addressed as follows.

It would be useful to perform additional flexibility calculations on hypothetical zeolite structures using the most advanced relaxation methods outlined in Chapter 2. While earlier calculations imposed isotropic constraints on the unit cell, an unrestricted search would allow full relaxation of both the coordinates and the cell. Also, the study of all symmetry representations for each framework type (rather than just the one yielding the lowest mBGB energy) could identify topologies where the flexibility depends on the choice of unit cell. More advanced searches might include T-atom substitutions (initially over symmetrically unique T-atoms) to examine whether or not framework flexibility is restored for certain structures under a new set of constraints. Such an analysis may help guide synthesis chemists to the optimal gel compositions for producing target structures.

Improved methods of exploring the edges of the flexibility window may include adjustments to the ideal zeolite cost function such as adding a small volume term to deflate the structure to minimum volume (maximum density). Similarly, harmonic constraints placed on the T-O-T angle could be adjusted incrementally to explore the range available for each unique angle. An integration of the ZeNuSpEx null mode following tools and the advanced optimization techniques available in GULP could prove useful for a more systematic exploration of the window. Since the configuration space representing the flexibility window has many dimensions it will remain a difficult problem to quantify and compare the relative flexibility of different framework types, but representations in terms of relevant structural characteristics such as the framework density, unit cell parameters, and T-O-T angle are a useful starting point.

The adaptability of a given framework type under different tetrahedral substitutions can be explored by several approaches. Starting from a relaxed iso-tetrahedral configuration, the preferred T-O bond in a single tetrahedron (either in *P*1 or with symmetry maintained) can be adjusted incrementally to observe whether or not the structure can accommodate a single differently-sized tetrahedron without the onset of tetrahedral deformation. This approach can be built on by moving to multiple tetrahedral substitutions, though the degree of complexity soon increases significantly. Alternatively, the preferred T-O bonds in each tetrahedron can be randomly varied (within a small amplitude) to explore the ability of a framework type to relax with all different tetrahedral sizes. Adaptable framework types are likely to be feasible in a wider array of material compositions.

A comprehensive search over the flexibility of zeolite framework types when represented in realized material compositions is necessary to further evaluate the application of the flexibility approach in predicting T-atom positions. While some zeolites have been found non-relaxable when represented in their experimentally reported compositions, it remains to be seen whether these are the exceptions rather than the rule. Indeed, the flexibility hypothesis is so compelling that it tempts us to consider the possibility that there is an error in the reported compositions in the inconsistent structures. Partial occupancies in experimental coordinates can be impossible to represent in the ideal zeolite model without dropping the symmetry to *P*1. However, when searching for T-atom substitutions that lead to flexibility in a given framework type, the number of possible combinations in *P*1 can be astronomically large. A potential approach to this problem involves iteratively substituting the selected number of T-atoms at random, and progressively counting the percentage of combinations that lead to flexibility. While this approach is inefficient, the vastness of the search space even with additional constraints in place (e.g. Löwenstein's rule) may render the problem otherwise intractable.

The search for new hypothetical zeolite structures is ongoing, and while the number of potential hypothetical structures is theoretically endless, a larger sample set increases the probability that useful new structure types will be discovered. The use of finely tuned filtering criteria will expedite the process of sifting through the enormous number of hypothetical structures to identify candidates for synthesis. These feasibility characteristics can provide clues about the mechanisms that guide zeolite growth and nucleation thus leading toward the ultimate goal of rational design.

References

(1) Smith, J. V.; Dytrych, W. J. *Nature* **1984**, *309*, 607-608.

(2) Levien, L.; Prewitt, C. T.; Weidner, D. J. *American Mineralogist* **1980**, *65*, 920-930.

(3) Kamakoti, P.; Barckholtz, T. A. *Journal of Physical Chemistry C* **2007**, *111*, 3575-3583.

(4) Wright, A. F.; Lehmann, M. S. *Journal of Solid State Chemistry* **1981**, *36*, 371-380.

(5) Sastre, G.; Corma, A. *Journal of Physical Chemistry C* **2010**, *114*, 1667-1673.

(6) Baerlocher, C.; McCusker, L. B.; Olson, D. H. *Atlas of Zeolite Framework Types*; Elsevier: Amsterdam, 2007.

(7) Wragg, D. S.; Morris, R. E.; Burton, A. W. *Chemistry of Materials* **2008**, *20*, 1561-1570.

(8) Treacy, M. M. J.; Rivin, I.; Balkovsky, E.; Randall, K. H.; Foster, M. D. *Microporous Mesoporous Mater.* **2004**, *74*, 121-132.

(9) Earl, D. J.; Deem, M. W. *Ind. Eng. Chem. Res.* **2006**, *45*, 5449-5454.

(10) Pophale, R.; Cheeseman, P. A.; Deem, M. W. *Physical Chemistry Chemical Physics* **2011**, *13*, 12407-12412.

(11) Li, Y.; Yu, J. H.; Liu, D. H.; Yan, W. F.; Xu, R. R.; Xu, Y. *Chemistry of Materials* **2003**, *15*, 2780-2785.

(12) Majda, D.; Paz, F. A. A.; Friedrichs, O. D.; Foster, M. D.; Simperler, A.; Bell, R. G.; Klinowski, J. *The Journal of Physical Chemistry C* **2008**, *112*, 1040-1047.

(13) Deem, M. W.; Pophale, R.; Cheeseman, P. A.; Earl, D. J. *J. Phys. Chem. C* **2009**, *113*, 21353-21360.

(14) Simperler, A.; Foster, M. D.; Friedrichs, O. D.; Bell, R. G.; Paz, F. A. A.; Klinowski, J. *Acta Crystallographica Section B-Structural Science* **2005**, *61*, 263-279.

(15) Li, Y.; Yu, J. H.; Xu, R. R. *Angewandte Chemie-International Edition* **2013**, *52*, 1673-1677.

(16) Sartbaeva, A.; Wells, S. A.; Treacy, M. M. J.; Thorpe, M. F. *Nature Materials* **2006**, *5*, 962-965.

(17) Kapko, V.; Dawson, C.; Treacy, M. M. J.; Thorpe, M. F. *Physical Chemistry Chemical Physics* **2010**, *12*, 8531-8541.

(18) Guest, S. D.; Hutchinson, J. W. *Journal of the Mechanics and Physics of Solids* **2003**, *51*, 383-391.

(19) Kapko, V.; Treacy, M. M. J.; Thorpe, M. F.; Guest, S. D. *Proceedings of the Royal Society a-Mathematical Physical and Engineering Sciences* **2009**, *465*, 3517-3530.

(20) Hammonds, K. D.; Deng, H.; Heine, V.; Dove, M. T. *Physical Review Letters* **1997**, *78*, 3701-3704.

(21) Hammonds, K. D.; Heine, V.; Dove, M. T. *Journal of Physical Chemistry B* **1998**, *102*, 1759-1767.

(22) Thorpe, M. F. *Journal of Non-Crystalline Solids* **1983**, *57*, 355-370.

(23) Hammonds, K. D.; Dove, M. T.; Giddy, A. P.; Heine, V.; Winkler, B. *American Mineralogist* **1996**, *81*, 1057-1079.

(24) Sartbaeva, A.; Gatta, G. D.; Wells, S. A. *EPL* **2008**, *83*, 26002.

(25) Wells, S. A.; Sartbaeva, A.; Gatta, G. D. *EPL* **2011**, *94*, 56001.

(26) Sartbaeva, A.; Haines, J.; Cambon, O.; Santoro, M.; Gorelli, F.; Levelut, C.; Garbarino, G.; Wells, S. A. *Physical Review B* **2012**, *85*,

(27) Garcia-Sanchez, A.; Dubbeldam, D.; Calero, S. *J. Phys. Chem. C* **2010**, *114*, 15068-15074.

(28) Wragg, D. S.; Akporiaye, D.; Fjellvag, H. *Journal of Catalysis* **2011**, *279*, 397-402.

(29) Zokaie, M.; Wragg, D. S.; Gronvold, A.; Fuglerud, T.; Cavka, J. H.; Lillerud, K. P.; Swang, O. *Microporous and Mesoporous Materials* **2013**, *165*, 1-5.

(30) Villaescusa, L. A.; Barrett, P. A.; Camblor, M. A. *Angewandte Chemie-International Edition* **1999**, *38*, 1997-2000.

(31) Rojas, A.; Camblor, M. A. *Angewandte Chemie-International Edition* **2012**, *51*, 3854-3856.

(32) Loewenstein, W. *American Mineralogist* **1954**, *39*, 92-96.

(33) Wells, S. A.; Dove, M. T.; Tucker, M. G. *J. Phys.: Condens. Matt.* **2002**, *14*, 4567−4584.

(34) Kapko, V.; Dawson, C.; Rivin, I.; Treacy, M. M. J. *Phys. Rev. Lett.* **2011**, *107*, 164304.

(35) Pellegrino, S.; Calladine, C. R. *International Journal of Solids and Structures* **1986**, *22*, 409-428.

(36) Hutchinson, R. G.; Fleck, N. A. *Journal of the Mechanics and Physics of Solids* **2006**, *54*, 756-782.

(37) Dawson, C. J.; Kapko, V.; Thorpe, M. F.; Foster, M. D.; Treacy, M. M. J. *Journal of Physical Chemistry C* **2012**, *116*, 16175-16181.

(38) Vanbeest, B. W. H.; Kramer, G. J.; Vansanten, R. A. *Physical Review Letters* **1990**, *64*, 1955-1958.

(39) Gale, J. D. *J. Chem. Soc., Faraday Trans.* **1997**, *93*, 629−637.

(40) Bushuev, Y. G.; Sastre, G. *Journal of Physical Chemistry C* **2010**, *114*, 19157-19168.

(41) Sanders, M. J.; Leslie, M.; Catlow, C. R. A. *Journal of the Chemical Society-Chemical Communications* **1984**, 1271-1273.

(42) Schroder, K. P.; Sauer, J.; Leslie, M.; Catlow, C. R. A.; Thomas, J. M. *Chemical Physics Letters* **1992**, *188*, 320-325.

(43) Henson, N. J.; Cheetham, A. K.; Gale, J. D. *Chemistry of Materials* **1994**, *6*, 1647-1650.

(44) Geisinger, K. L.; Gibbs, G. V.; Navrotsky, A. *Physics and Chemistry of Minerals* **1985**, *11*, 266-283.

(45) Jiang, J. X.; Yu, J. H.; Corma, A. *Angewandte Chemie-International Edition* **2010**, *49*, 3120-3145.

(46) Barrer, R. M.; Villiger, H. *Zeitschrift Fur Kristallographie Kristallgeometrie Kristallphysik Kristallchemie* **1969**, *128*, 352-&.

(47) Treacy, M. M. J.; Rivin, I.; Balkovsky, E.; Randall, K. H.; Foster, M. D. *Microporous and Mesoporous Materials* **2004**, *74*, 121-132.

(48) Zwijnenburg, M. A.; Bell, R. G. *Chemistry of Materials* **2008**, *20*, 3008-3014.

(49) Huang, P. Y.; Kurasch, S.; Srivastava, A.; Skakalova, V.; Kotakoski, J.; Krasheninnikov, A. V.; Hovden, R.; Mao, Q. Y.; Meyer, J. C.; Smet, J.; Muller, D. A.; Kaiser, U. *Nano Letters* **2012**, *12*, 1081-1086.

(50) Lichtenstein, L.; Buchner, C.; Yang, B.; Shaikhutdinov, S.; Heyde, M.; Sierka, M.; Wlodarczyk, R.; Sauer, J.; Freund, H. J. *Angewandte Chemie-International Edition* **2012**, *51*, 404-407.

(51) Lichtenstein, L.; Heyde, M.; Freund, H. J. *Journal of Physical Chemistry C* **2012**, *116*, 20426-20432.

(52) Shanno, D. F. *Mathematics of Computation* **1970**, *24*, 647-&.

(53) Gale J. D. *General Utility Lattice Program, Version 3.4*, https://projects.ivec.org/gulp/help/gulp3.4_manual.pdf (Accessed 3/20/2013).

(54) Banerjee, A.; Adams, N.; Simons, J.; Shepard, R. *Journal of Physical Chemistry* **1985**, *89*, 52-57.

(55) Rajic, N.; Logar, N. Z.; Kaucic, V. *Zeolites* **1995**, *15*, 672-678.

(56) Rouse, R. C.; Peacor, D. R. *American Mineralogist* **1986**, *71*, 1494-1501.

(57) Dorset, D. L.; Strohmaier, K. G.; Kliewer, C. E.; Corma, A.; Diaz-Cabanas, M. J.; Rey, F.; Gilmore, C. J. *Chemistry of Materials* **2008**, *20*, 5325-5331.

(58) Baur, W. H. *American Mineralogist* **1964**, *49*, 697-&.

(59) Corma, A.; Diaz-Cabanas, M. J.; Jorda, J. L.; Rey, F.; Sastre, G.; Strohmaier, K. G. *Journal of the American Chemical Society* **2008**, *130*, 16482-+.

(60) Tang, L. Q.; Shi, L.; Bonneau, C.; Sun, J. L.; Yue, H. J.; Ojuva, A.; Lee, B. L.; Kritikos, M.; Bell, R. G.; Bacsik, Z.; Mink, J.; Zou, X. D. *Nature Materials* **2008**, *7*, 381-385.

(61) McCusker, L. B.; GrosseKunstleve, R. W.; Baerlocher, C.; Yoshikawa, M.; Davis, M. E. *Microporous Materials* **1996**, *6*, 295-309.

(62) Stokes H. T.; Hatch D. M.; Campbell B. J. *ISOTROPY*, stokes.byu.edu/isotropy.html (Accessed 3/20/2013).

(63) Knorr, K.; Depmeier, W. *Acta Crystallographica Section B-Structural Science* **1997**, *53*, 18-24.

(64) Nakagawa, T.; Kihara, K.; Harada, K. *American Mineralogist* **2001**, *86*, 1506-1512.

(65) Briscoe, N. A.; Johnson, D. W.; Shannon, M. D.; Kokotailo, G. T.; McCusker, L. B. *Zeolites* **1988**, *8*, 74-76.

(66) Wells, S. A.; Sartbaeva, A. *Materials* **2012**, *5*, 415-431.

(67) Nocedal, J. *Mathematics of Computation* **1980**, *35*, 773-782.

(68) Pellegrino, S. *International Journal of Solids and Structures* **1993**, *30*, 3025-3035.

(69) Futterer, K.; Depmeier, W.; Altorfer, F.; Behrens, P.; Felsche, J. *Zeitschrift Fur Kristallographie* **1994**, *209*, 517-523.

(70) Richardson, J. W.; Pluth, J. J.; Smith, J. V.; Dytrych, W. J.; Bibby, D. M. *Journal of Physical Chemistry* **1988**, *92*, 243-247.

(71) Dove, M. T.; Giddy, A. P.; Heine, V. *Transactions of the American Crystallographic Association* **1993**, *27*, 65−74.

(72) Corma, A.; Rey, F.; Rius, J.; Sabater, M. J.; Valencia, S. *Nature* **2004**, *431*, 287-290.

(73) Treacy, M. M. J.; Randall, K. H.; Rao, S.; Perry, J. A.; Chadi, D. J. *Zeitschrift Fur Kristallographie* **1997**, *212*, 768-791.

(74) Boisen, M. B.; Gibbs, G. V.; Bukowinski, M. S. T. *Physics and Chemistry of Minerals* **1994**, *21*, 269-284.

(75) Foster, M. D.; Simperler, A.; Bell, R. G.; Friedrichs, O. D.; Paz, F. A. A.; Klinowski, J. *Nature Materials* **2004**, *3*, 234-238.

(76) Blatov, V. A.; Ilyushin, G. D.; Proserpio, D. M. *Chemistry of Materials* **2013**,

(77) Foster, M. D.; Rivin, I.; Treacy, M. M. J.; Friedrichs, O. D. *Microporous Mesoporous Mater.* **2006**, *90*, 32-38.

(78) Lasaga, A. C.; Gibbs, G. V. *Physics and Chemistry of Minerals* **1987**, *14*, 107-117.

(79) Lasaga, A. C.; Gibbs, G. V. *Physics and Chemistry of Minerals* **1988**, *16*, 29-41.

(80) Li, H. L.; Yaghi, O. M. *Journal of the American Chemical Society* **1998**, *120*, 10569-10570.

(81) Okeeffe, M.; Hyde, B. G. *Acta Crystallographica Section B-Structural Science* **1976**, *32*, 2923-2936.

(82) Kresse, G.; Furthmuller, J. *Physical Review B* **1996**, *54*, 11169-11186.

(83) Okeeffe, M. *Acta Crystallographica Section A* **1977**, *33*, 924-927.

(84) Dollase, W. A.; Baur, W. H. *American Mineralogist* **1976**, *61*, 971-978.

(85) Pryde, A. K. A.; Dove, M. T. *Physics and Chemistry of Minerals* **1998**, *26*, 171-179.

(86) O'Keeffe, M.; Peskov, M. A.; Ramsden, S. J.; Yaghi, O. M. *Accounts of Chemical Research* **2008**, *41*, 1782-1789.

(87) O'Keeffe, M. O.; Hyde, B. G. *Crystal Structures I. Patterns and Symmetry*; Mineralogical Society of America: 1996.

(88) Kapko, V.; Dawson, C.; Rivin, I.; Treacy, M. M. J. *Physical Review Letters* **2011**, *107*, 164304.

(89) Furukawa, H.; Ko, N.; Go, Y. B.; Aratani, N.; Choi, S. B.; Choi, E.; Yazaydin, A. O.; Snurr, R. Q.; O'Keeffe, M.; Kim, J.; Yaghi, O. M. *Science* **2010**, *329*, 424-428.

(90) Hohenberg, P.; Kohn, W. *Physical Review B* **1964**, *136*, B864-&.

(91) Kohn, W.; Sham, L. J. *Physical Review* **1965**, *140*, 1133-&.

(92) Ceperley, D. M.; Alder, B. J. *Physical Review Letters* **1980**, *45*, 566-569.

(93) Langreth, D. C.; Mehl, M. J. *Physical Review B* **1983**, *28*, 1809-1834.

APPENDIX A

METHODS

Sanders-Lesle-Catlow (SLC) energy

The Sanders-Leslie-Catlow (SLC) potential splits oxygen atoms into a "shell" and a "core" (separate coordinates and charges for each; $q_{core} = +0.86902e$ and $q_{shell} = -2.86902e$) to account for polarizability. This strategy accounts for the induced mean dipole moment only, and no higher-order spherical harmonics are considered. The silicon atoms are treated as just a "core" ($q_{Si} = +4.0e$). Besides coulomb terms between all atoms, Buckingham terms are included between core-silicon and shell-oxygen atoms (with a cutoff beyond 10.0 Å) and between shell oxygens (with a cutoff of 12.0 Å). A spring term tethers core oxygen atoms to their corresponding shell atom, and a harmonic three-body term is placed on the O-Si-O angle to maintain tetrahedral regularity. The energy function is thus

$$U_{SLC} = \sum_{\text{All atoms}} \frac{q_i q_j}{r_{ij}} + \sum_{\text{Si}_{\text{core}}\text{O}_{\text{shell}}} \left(A_1 e^{-\frac{r_{ij}}{B_1}} + \frac{C_1}{r_{ij}} \right) + \sum_{\text{O}_{\text{shell}}\text{O}_{\text{shell}}} \left(A_2 e^{-\frac{r_{ij}}{B_2}} + \frac{C_2}{r_{ij}} \right) + \sum_{\text{O}_{\text{shell}}\text{O}_{\text{core}}} \frac{1}{2} k_1 {r_{ij}}^2 + \sum_{\angle\text{OSiO}} \frac{1}{2} k_2 (\theta - \theta_0)^2, \quad (A.1)$$

where $A_1 = 1283.907$ eV, $B_1 = 0.32052$ Å, $C_1 = 10.66158$ eV/Å^6, $A_2 = 22764.00$ eV, $B_2 = 0.149$ Å, $C_2 = 27.879$ eV/Å^6, $k_1 = 74.92$ eV/Å^2, $k_2 = 2.09724$ eV/rad^2, and $\theta_0 = 109.47°$.[41,42] Structures were optimized in this potential using the GULP program.[39]

Boisen-Gibbs-Bukowinski (BGB) energy

The Boisen-Gibbs-Bukowinski (BGB) cost function puts harmonic terms on the Si-O-Si angle, O-Si-O angle, and the Si-O bond length. Additional terms are included between intertetrahedral oxygen atoms and a distance along the bond angles. The energy equation is

$$\Delta E = C\left[\frac{1}{2}0.7681\sum_{SiOSi}(L-L_0)^2+\frac{1}{2}0.3452\sum_{OSiO}(\Theta-\Theta_0)^2+\frac{1}{2}0.3951\sum_{SiO}(\mathrm{R}-\mathrm{R}_0)^2 + \frac{1}{2}0.1186\sum_{O}\sum_{Si}(R-R_0)(L-L_0)\right] + \sum[\exp(13.289-4.070d)-2.566\times10^{-8}] \qquad (A.2)$$

where, as quoted from Boisen et. al.[74]

> "ΔE is in atomic units, L is the distance between two points located one Bohr along each of the legs of an Si-O-Si angle, Θ is an O-Si-O angle, R is the Si-O bond length and d is an O-O distance. The parameters are $C = 0.6777$ Hartee, $L_0 = 1.86486b$, $\Theta_0 = 1.91063$ rad and $R_0 = 3.063624b$. The first summation is over all Si-O-Si angles, the second is over all O-Si-O angles, the third is over all Si-O, the fourth is over all O and over the two Si bonded to this O and the fifth is over all non co-dimer O-O distances (cut off at 4 Å) where each summation refers only to the contents of the unit cell."

This expression was modified slightly by Treacy et. al.,[47]when generating their database. In the BGB expression, the SiOSi summation is over all silicon atoms that are within 4 Å of each other. In the Treacy database, the bonding topologies are already defined and so this summation was restricted to the four known links. This allows a significant speed-up in the energy-determining code since the model no longer needs to be searched for the possible encroachment of a fifth (or more) Si atom. For well-relaxed

structures, the final result is nearly always the same, and any differences were small. We refer to this modified algorithm as the mBGB potential.

Flexibility index histogram

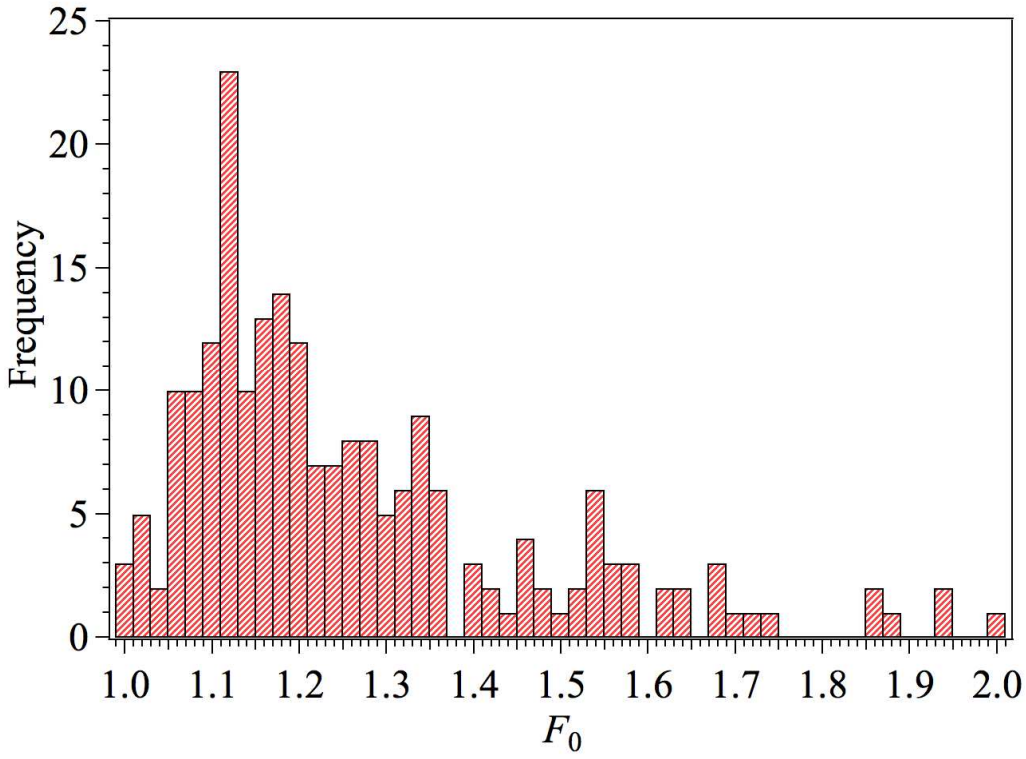

Figure A.1: A histogram of the flexibility indices of all 206 known zeolite framework types as well as seven dense siliscates (quartz, cristobalite, tridymite, moganite, coesite, keatite, and feldspar). The flexibility index F_0 is defined as the ratio of the maximum and minimum densities found within the flexibility window, i.e. ρ_{max}/ρ_{min}.

Rational Function Optimizer (RFO) Hessian update method

In the RFO method, the inverse Hessian matrix is diagonalised to obtain the eigenvalues and eigenvectors. (The Hessian matrix is the square matrix of second-order partial derivatives of the potential with respect to the coordinate degrees of freedom. It describes the local curvature of the potential energy landscape.) From the eigenvalues it is possible to examine whether the matrix has the required characteristics for the stationary point being sought. If the number of negative eigenvalues is incorrect, then the spectrum is level-shifted to correct this and the search direction is reconstructed appropriately. By default, the Hessian modes with the smallest eigenvalues (the 'softest' modes, with the lowest energy) are followed towards the corresponding stationary point. However, eigenvector-following can also be performed in which different modes from the spectrum are selected. Hence the RFO optimiser will, in principle, locate various possible transition states starting from a given position. (Adapted from the manual for the General Utility Lattice Program, Version 3.4, page 37)[53]

Depictions of DLS zeolites

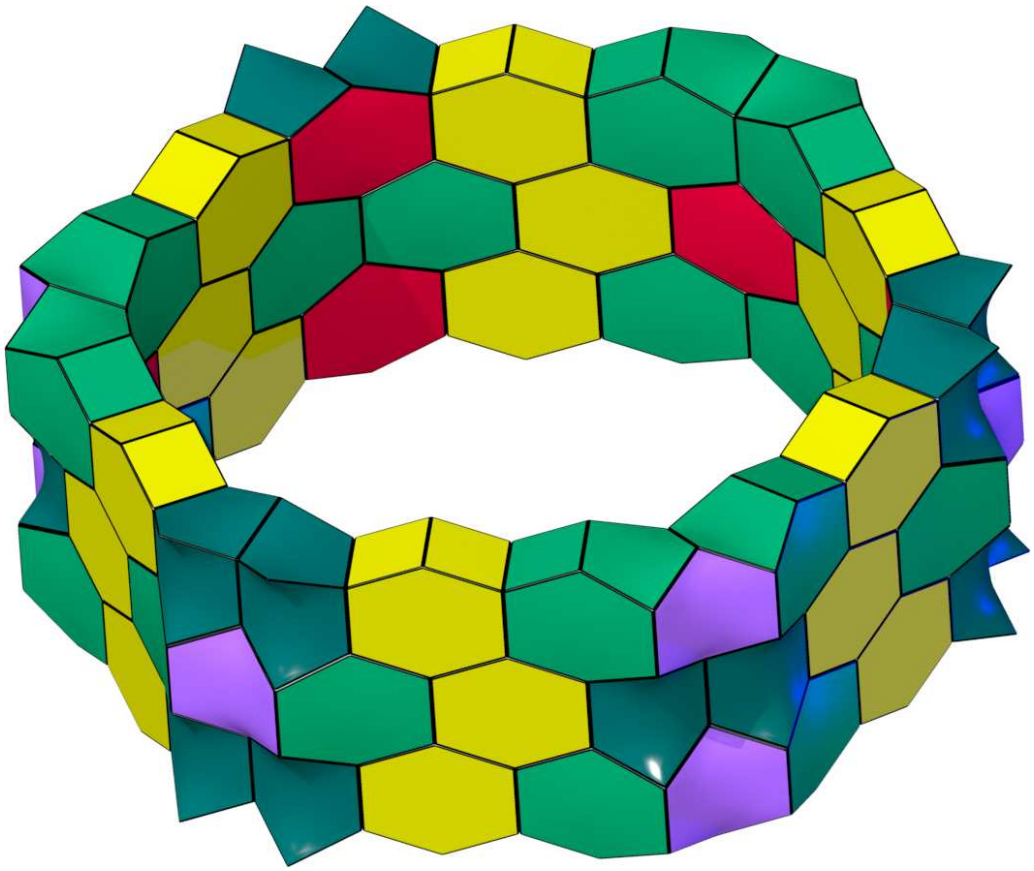

Figure A.2: Depiction of the channel found in the **dtd** structure. Although the exposed channel wall is built entirely from 6-rings, only part of it is formed from 6^3 bi-layers (yellow). The pore size is increased in the **dt*** family by adding more zig-zag rows of 6^3 units (yellow). Figure courtesy of Michael O'Keeffe.

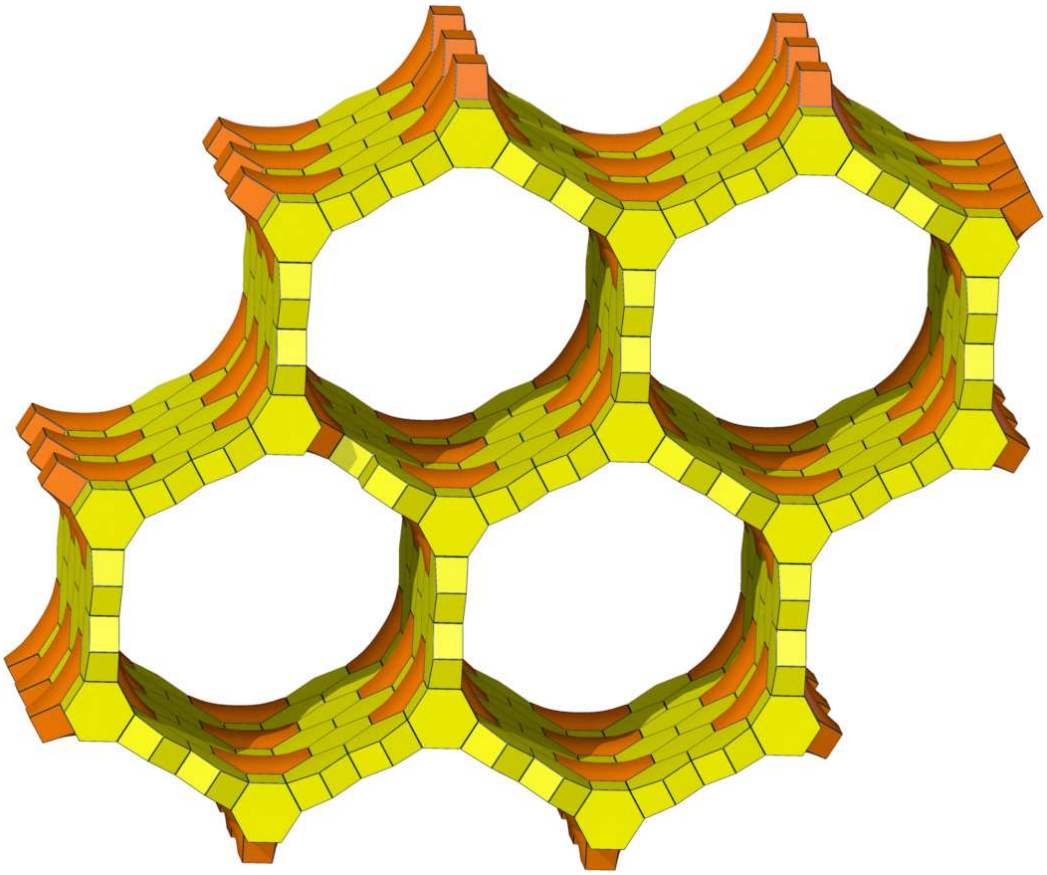

Figure A.3: View down the channel direction of the **tdc** structure showing the spacious 30-ring channels. The channels can be extended further by inserting additional zig-zag rows of 6^3 DLS structure (yellow). The channels structure is impervious to water and so channels are isolated from each other. Figure courtesy of Michael O'Keeffe.

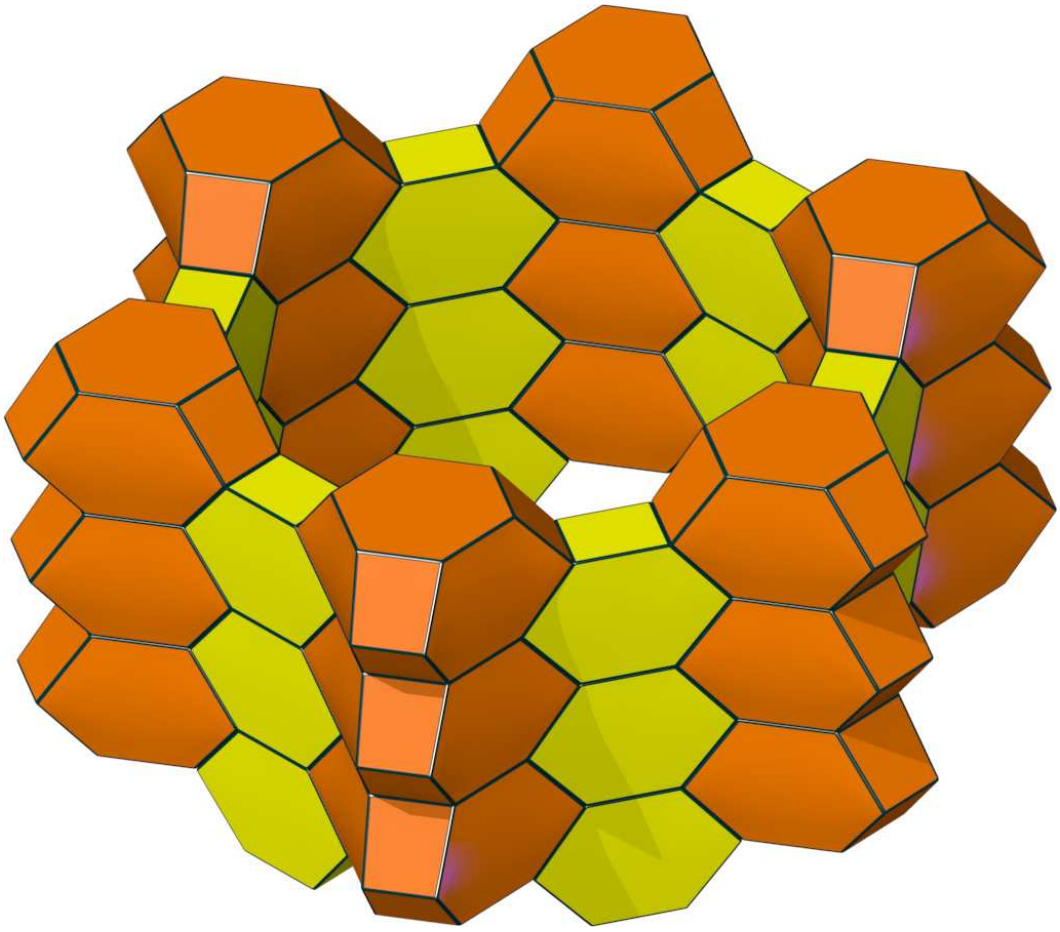

Figure A.4: Depiction of the **bbz** structure that was originally presented by Barrer and Villiger. The channel walls (yellow) contain a single strip of the 6^3 DLS structure, and thus this represenst the second member of the **bb*** family. The first member is where the backbone structures (brown) interconnect directly. The yellow region contracts to a strip of cubes. Figure courtesy of Michael O'Keeffe.

APPENDIX B

DETAILS OF VASP CALCULATION ON T-O-T ANGLE

VASP[82] is based on Density Functional Theory (DFT)[90] which assumes (as demonstrated by Kohn and Sham)[91] that ground state properties of the exchange and correlation energies are a functional of the electron density. The local density approximation (LDA)[92] and the generalized gradient approximation (GGA)[93] offer functional forms for the exchange and correlation energy. Pseudopotentials are used to remove rapid oscillations in the core region.

Ab initio calculations were carried out with the ion positions fixed (ISIM=6 in VASP) in order to maintain the T-O-T angle with some degree of precision. However, the formula that gives the T-O-T angle as a function of the oxygen coordinate is only valid for regular tetrahedra, and small tetrahedral distortion often occurs during optimization, causing the T-O-T angle to vary somewhat from the initial configuration. The cell parameters and cell shape were allowed to vary in accordance with the symmetry. A conjugate gradient algorithm was used for the refinement (IBRION=2 in VASP) with 25 ionic steps (NSW=25) and a strict convergence requirement (EDIFF=-1e-4).

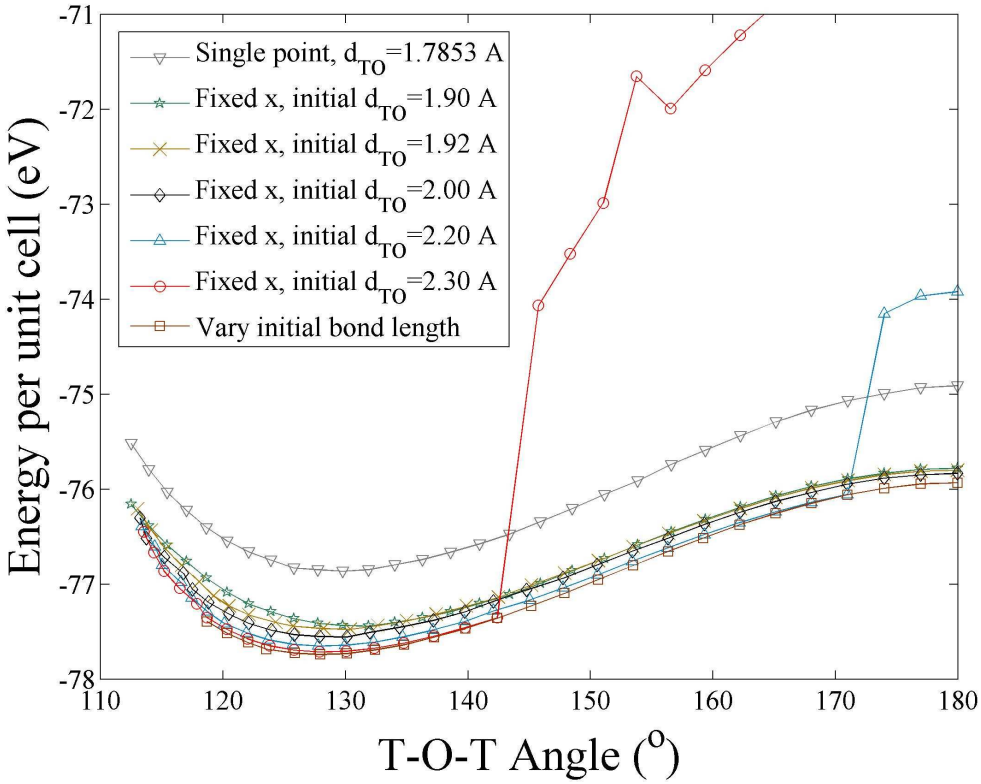

Figure B.1: Improvements in the VASP optimization with increasingly larger initial bond length. At the critical initial bond length for a given T-O-T angle, the structure is no longer able to optimize to a reasonable energy value. The reasons for this numerical phenomenon in VASP have not been completely explored by the author. The lowest energy curve was obtained by fixed coordinate optimization while incrementally increasing the initial bond length until the lowest possible final energy was reached.

It was found empirically during this study that increasing the initial bond lengths, to values much larger than the known equilibrium values, by inflating the structure, resulted in lower final energies at each point. However, for each T-O-T angle, there was a critical bond length at which the optimization failed to find a lower energy. Since the optimization tools in VASP failed to consistently relax the coordinates based on the

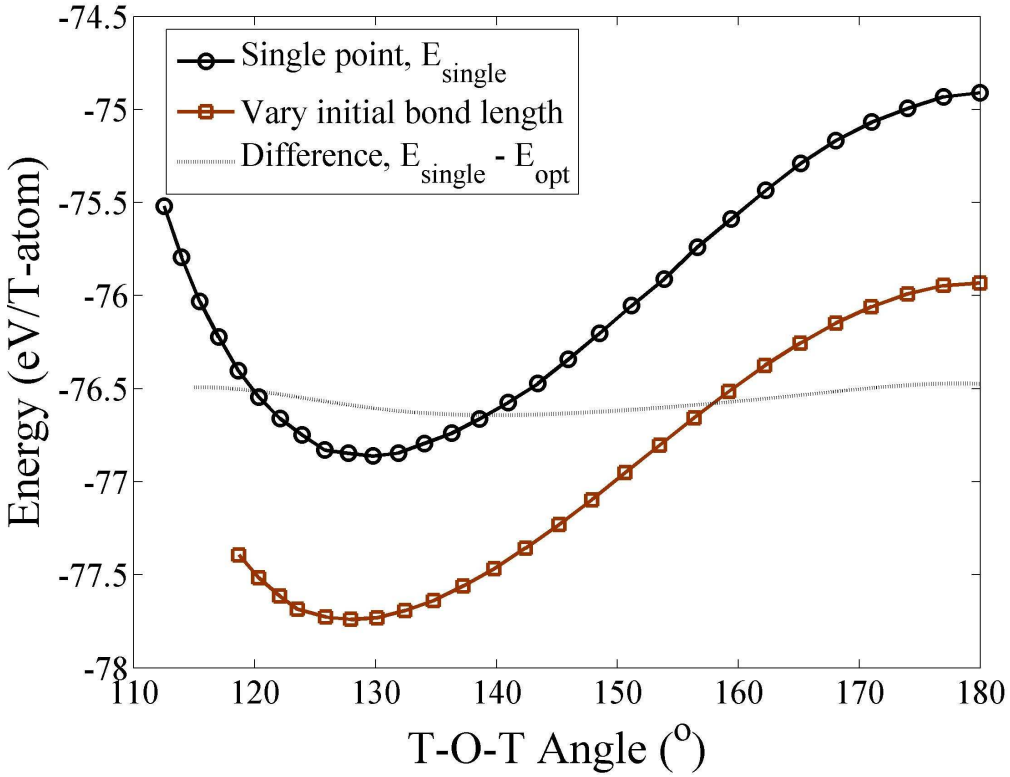

Figure B.2: Comparison between energy curves obtained by a single point calculation with a fixed Ge-O bond length of 1.785Å (circles) and by full optimization (squares). The dotted line represents the difference between the two curves offset by -77.5eV for comparison. The difference between the two curves is approximately constant on the scale of the curves themselves.

input, the inflation strategy was the only known method of finding lower energies at each T-O-T angle. Figure B.1 shows the evolution of the final energy curve as the initial bond length is increased for germania cristobalite. Larger initial bond lengths generally result in lower energies up to a certain point for each T-O-T angle. For example, for angles close to ~143º, an initial bond length above about 2.29Å results in a much higher final energy. For angles close to 171º, the critical initial bond length is about 2.19Å. This effect is probably a numerical artifact of the optimization method in VASP. It appears

that the optimization tools in VASP are more conveniently used for searching for a global minimum rather than subspaces of an energy surface. While the search for lower energies at each T-O-T angle lacked some degree of finality, it is worthwhile to note that there was little difference in the shape of the energy curve whether obtained through optimization or by a single point calculation with regular tetrahedra.

Figure B.2 shows a comparison of the energy curves calculated using both methods. Also plotted is the difference between a cubic spline fit of each curve with a constant offset added for comparison with the energy curves themselves. The amplitude of the difference is 0.171 eV/SiO_2, which is about two orders of magnitude less than the amplitude of the curves overall. It can be concluded that the curve obtained by a single point calculation resembles that obtained by more arduous methods to a good approximation. Since different bond lengths are preferred for different atom densities, the single point calculation could likely be improved by feeding in configurations with bond lengths predicted by fixed coordinate refinements for each T-O-T angle rather than a fixed value.

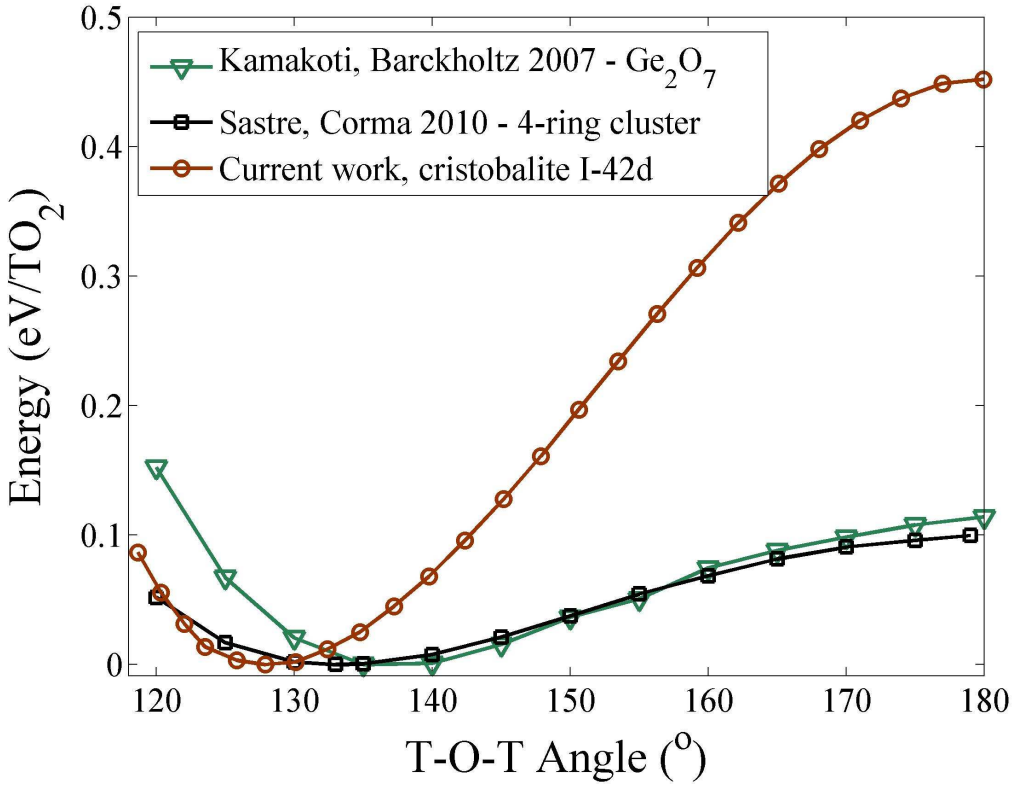

Figure B.3: Comparison between ab-initio energy calculations done on a Ge_2O_7 cluster (triangles),[3] a 4-ring germania cluster (squares), and germania cristobalite in I-42d (circles). The crystalline model gives a much higher energy penalty at high Ge-O-Ge angles than the two previously studied cluster models.

Comparisons with earlier work on cluster models show a much more pronounced difference in the energy dependence on the T-O-T angle for germania than for silica. Figure B.3 shows a superposition of the energy curves of Kamakoti et. al. (calculated on a Ge_2O_7 cluster)[79] and Sastre et. al. (calculated on a 4-ring cluster)[81] as well as the current work. The energy penalty for high Ge-O-Ge angles is at least a factor of four larger for the crystalline model than for the cluster models, possibly due to additional constraints imposed by periodicity. However, it is puzzling that the same effect is not observed for

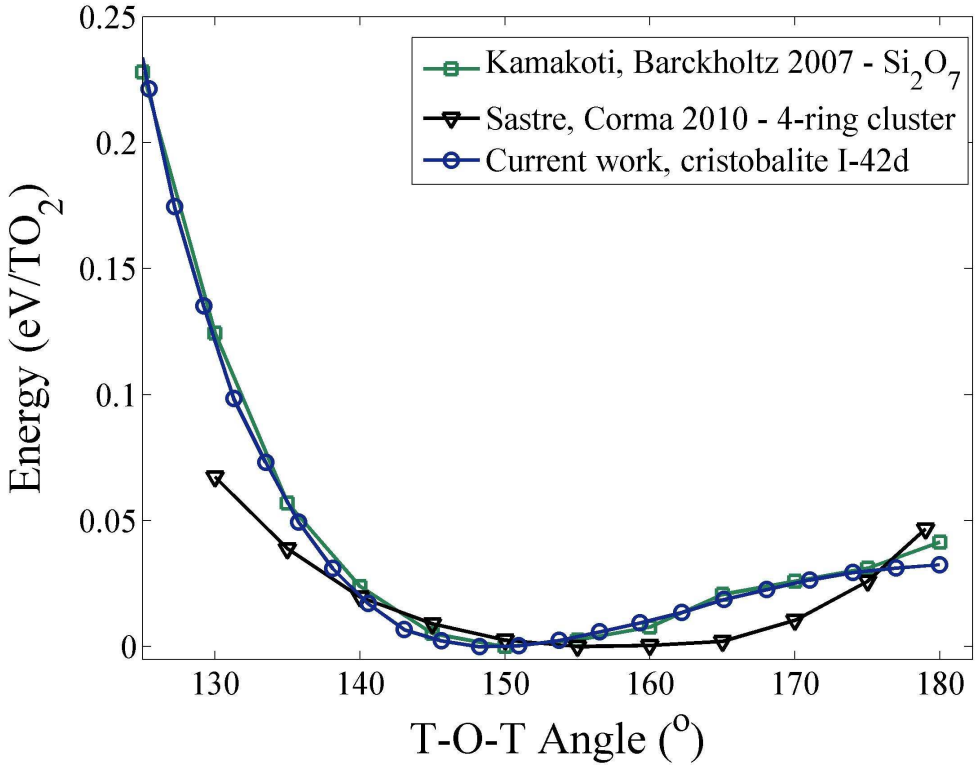

Figure B.4: Comparison between ab initio energy calculations done on a Si_2O_7 cluster (squares),[3] a 4-ring silica cluster (triangles),[5] and germania cristobalite in I-42d (circles). There is close agreement between the curve obtained using the crystalline model and earlier work on the Si_2O_7 cluster.

the Si-O-Si angle, and it is possible that more subtle effects account for this discrepancy. In addition, the minimum energy occurs at lower angles in the current model. There is less discrepancy in the energy curves obtained for silica (Figure B.4).

An additional comparison can be made with the energy curve obtained using the SLC potential in GULP (Figure B.5). The shapes of the curves are similar, although the SLC overestimates the energy penalty at angles away from the minimum. It can be concluded that the SLC potential is useful as a first approximation of the energy landscape in silica.

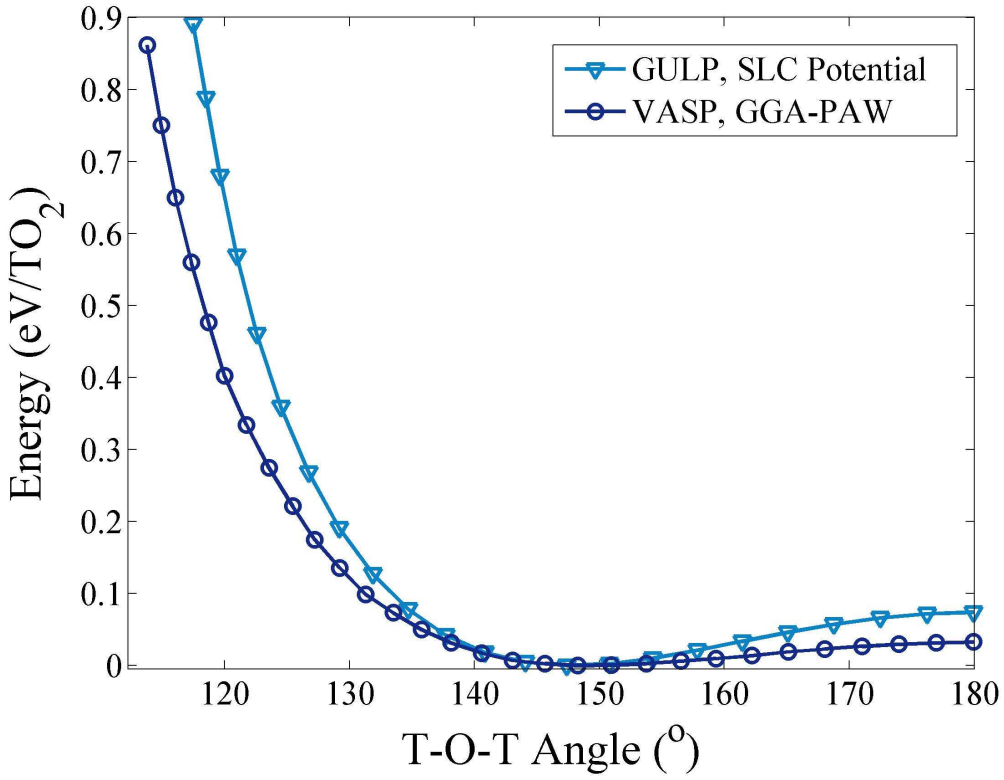

Figure B.5: Comparison between the energy curve obtained by the VASP calculation (circles) and that obtained using the SLC interatomic potential (triangles). The two curves mirror each other closely although the SLC potential overestimates the energy penalty away from the minimum.